Univerzita Karlova v Praze
Matematicko-fyzikální fakulta

BAKALÁŘSKÁ PRÁCE

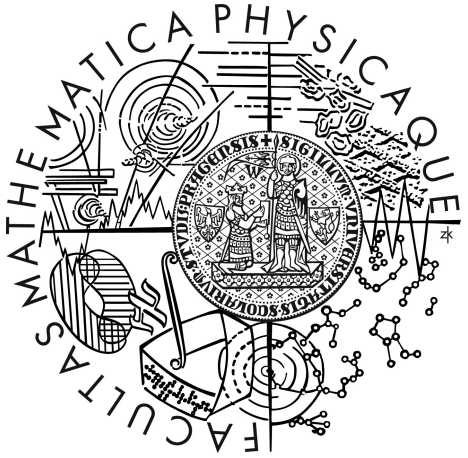

Vojtěch Witzany

Chaos v porušených polích černých děr

Ústav teoretické fyziky

Vedoucí bakalářské práce:	doc. RNDr. Oldřich Semerák, Dr., DSc.
Studijní program:	Fyzika
Studijní obor:	Obecná fyzika

Praha 2013

Charles University in Prague
Faculty of Mathematics and Physics

BACHELOR THESIS

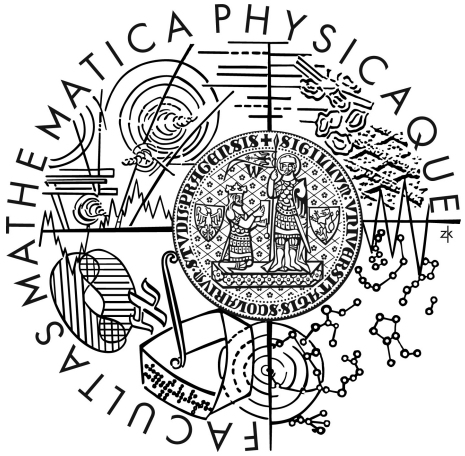

Vojtěch Witzany

Chaos in Perturbed Black-Hole Fields

Institute of Theoretical Physics

Supervisor of the bachelor thesis:	doc. RNDr. Oldřich Semerák, Dr., DSc.
Study program:	Physics
Study specialization:	General Physics

Praha 2013

Rád bych poděkoval především doc. Semerákovi za vedení práce, Mgr. Sukové za četné konzultace a Dr. Heyrovskému za zapůjčení literatury.

The access to computing and storage facilities owned by parties and projects contributing to the National Grid Infrastructure MetaCentrum, provided under the programme "Projects of Large Infrastructure for Research, Development, and Innovations" (LM2010005) is highly appreciated.

I declare that I carried out this bachelor thesis independently, and only with the cited sources, literature and other professional sources.

I understand that my work relates to the rights and obligations under the Act No. 121/2000 Coll., the Copyright Act, as amended, in particular the fact that the Charles University in Prague has the right to conclude a license agreement on the use of this work as a school work pursuant to Section 60 paragraph 1 of the Copyright Act.

In ..... date ..... signature

Název práce: Chaos v porušených polích černých děr

Autor: Vojtěch Witzany

Katedra: Ústav teoretické fyziky

Vedoucí bakalářské práce: doc. RNDr. Oldřich Semerák, Dr., DSc., Ústav teoretické fyziky

Abstrakt: Ztráta úplné geodetické integrability je jeden z důležitých důsledků (a tudíž ukazatelů) odchylek od prostoročasu Kerrova typu. V literatuře bylo vskutku mnohokrát potvrzeno, že i velmi symetrická perturbace Kerrovy nebo Schwarzschildovy metriky může způsobit chaotický pohyb volných testovacích částic. V této bakalářské práci studujeme dynamiku testovacích částic v poli Schwarzschildovy černé díry obklopené tenkým prstencem nebo diskem, používajíce nicméně Newtonovu gravitaci s jednoduchým „pseudo-newtonovským“ potenciálem napodobujícím černou díru. Poincarého řezy ukazují, že studovaný (pseudo-) newtonovský systém je nepatrně více chaotický než obecně-relativistický. Pozorovaný rozdíl se zdá být korelován s větší otevřeností povolených oblastí fázového prostoru k centru v pseudo-newtonovském případě.

Klíčová slova: gravitace, obecná teorie relativity, černé díry, chaos

Title: Chaos in Perturbed Black-hole Fields

Author: Vojtěch Witzany

Department: Institute of Theoretical Physics

Supervisor: doc. RNDr. Oldřich Semerák, Dr., DSc., Institute of Theoretical Physics

Abstract:

The loss of complete geodesic integrability is one of the important consequences (and thus indicators) of deviation from the Kerr-type space-time. Indeed, it has been confirmed many times in the literature that even a highly symmetric perturbation of the Kerr or Schwarzschild metric can make the free test-particle motion chaotic. In this thesis, we study the test-particle dynamics in the field of a Schwarzschild black hole surrounded by a thin disc or ring, using, however, Newton's gravity with a simple "pseudo-Newtonian" potential to mimic the black hole. The Poincaré sections show that the (pseudo-)Newtonian system is slightly more chaotic than the general relativistic one. The difference seems to be correlated with the phase-space allowed region being more open towards the center in the pseudo-Newtonian case.

Keywords: gravitation, general theory of relativity, black holes, chaos

Contents

Prologue

Weak mortals, chained to the earth, creatures of clay as frail as the foliage of the woods, you unfortunate race, whose life is but darkness, as unreal as a shadow, the illusion of a dream, hearken to us, who are immortal beings, ethereal, ever young and occupied with eternal thoughts, for we shall teach you about all celestial matters; you shall know thoroughly what is the nature of the birds, what the origin of the gods, of the rivers, of Erebus, and Chaos; thanks to us, even Prodicus will envy you your knowledge.

At the beginning there was only Chaos, Night, dark Erebus, and deep Tartarus. Earth, the air and heaven had no existence. Firstly, blackwinged Night laid a germless egg in the bosom of the infinite deeps of Erebus, and from this, after the revolution of long ages, sprang the graceful Eros with his glittering golden wings, swift as the whirlwinds of the tempest. He mated in deep Tartarus with dark Chaos, winged like himself, and thus hatched forth our race, which was the first to see the light.

- The Leader of the Chorus in Aristophanes' *Birds* (O'Neill, 1938).

The arousal of interest in the phenomenon of *deterministic chaos* is strongly connected with the work on weather prediction by Edward Lorenz (Lorenz, 1963) at the beginning of the sixties of the twentieth century. However, the latent knowledge of the phenomenon is rooted deeper in the history of classical physics.

The known universe - *κόσμος* of bounded physical systems during the nineteenth century was composed of asymptotically static, periodic, or quasi-periodic motions[1]. Yet before the end of the nineteenth century there is a limited number of physicists and mathematician, who are known or assumed to have been aware of a different type of motion.

For example James Clerk Maxwell, having developed notably the statistical approach to the theory of gasses, opposed the fully deterministic cause of Pierre Simon Laplace and others in his *Essay on Science and Free Will* (Campbell & Garnett, 2010): *"It appears then that in our own nature there are more singular points – where prediction, except from absolutely perfect data, and guided by the omniscience of contingency, becomes impossible – than there are in any lower organisation."*

In the essay Maxwell however supported his statement by examples of systems with unstable equilibria or at least "singular events" such as a stone on an

[1] Ironically, this was also a paradigm Lorenz had to confront once presenting his results, since his colleagues were utterly convinced that a dissipative system must converge to stationary or static motion.

infinitely sharp tip of a mountain or a ray refracting very close to the axis of a biaxial crystal. Thus he immediately softens the tone of his former sentence with the latter: *"But singular points are by their very nature isolated, and form no appreciable fraction of the continuous course of our existence."* He then concludes that the study of such instabilities and singularities may change the view of the "intelligent public" on the matter of strict determinism.

Therefore, by the end of the 19th century the instability of a trajectory was more or less still imprisoned in isolated "bifurcations" of points and events of zero measure and awaited to be unleashed to devour whole portions of phase space. Nevertheless, even in the time of Maxwell the worm of global chaos already awaited to be discovered in the apple least expected – the motion of celestial bodies.

The irony of the development was not only in the fact that the foremost example of regularity – the solar system – actually bore small seeds of stochasticity, but also in the fact that the chaotization of the "*musica universalis*" of the heavenly spheres is assisted by resonances – a perfectly rational proportion of the periods of motion.

It was furthermore the most ardent guardian of determinism, Pierre Simon Laplace, who unconsciously began the route to the discovery of the problem of "small divisors" by first employing the classical perturbation theory with his colleague Joseph Louis Lagrange. The whole history of the perturbation theory and of the problem of "small divisors" hiding in the shades would amount to a full thesis if it was to be treated in detail.

Let us thus jump to year 1885, when King Oscar II offered a prize to anyone who would establish the stability of the solar system. This would require proving the existence of solution for a large set of Newton's equations of motion and the assessment whether they are bound in space. A 31 year old mathematician Jules Henri Poincaré did not feel up to the full challenge but first concentrated on a very simple model - the restricted planar three body problem.

In this problem the first two bodies move on perfect Keplerian orbits in accordance with the solution of a two body problem and the third particle moves strictly in the plane of the orbits and has "infinitely small mass" (it does not perturb the motion of the first bodies). Poincaré, in his intuitively visual approach, found not only that even this problem cannot be resolved analytically but also that some of the initial conditions must lead to strikingly complex movement now known as "chaotic".

The heritage of Poincaré was of course continued to be silently developed by mathematicians such as George Birkhoff or Andrei Kolmogorov. The still persistent fascination by the contrast of $\kappa\acute{o}\sigma\mu o\varsigma$ and $\chi\acute{a}o\varsigma$ then needed only one thing to be triggered - large scale computer simulations and visualization of the acquired results.

The "rediscovery" of chaos by Edward Lorenz illustrates perhaps the best the frail illusion of applied mathematicians and physicists beginning from the times of the inventors of calculus, Isaac Newton and Gottfried Wilhelm Leibniz. It

is the unsubstantiated and mostly tacit faith that small corrections in the input of physical problems, apart from isolated ill-conditioned cases, create small corrections to the output.

Lorenz, in this faith, reset a numerical simulation of a simplified model of the Earth's atmosphere, submitting the initial data with a smaller number of digits after the decimal point, to find to his astonishment that the output of the simulation was completely different from the results of the previous run. For the studied system, the stated response to change of initial data was even found to apply globally.

The belief of small error of a result caused by small error in the initial data is perhaps in tight correspondence with the belief of *analyticity* or at least smoothness in the relations of a dynamical system. In practice, the implicit assumption is even stronger – the Taylor expansions of the characteristic relations of the problem are assumed to converge so fast that, when taking just a few first terms, the rest of the expansion sums up to a contribution of much smaller orders of magnitude.

Nonetheless, chaos responds in it's own fashion – the relations are found not to be only non-analytic but also non-smooth in any possible meaning of smoothness. Almost every boundary between areas of initial conditions leading to different evolutions is fractal-like, i.e., continuous and often nowhere-smooth with an infinitely fine structure of edges and cusps.

A necessary condition for determining a chaotic motion completely is an infinitely precise set of initial data or a countable-infinite set of integer-like data about the motion (such as finite precision states of the system at an infinite number of times). This is true even for regular motion, but for a chaotic trajectory the reliability of a prediction based on finite data decays roughly exponentially, whereas in the regular case the decay is at most linear.

However, as only finite precision and finite data is in practice available to our unfortunate human race, our knowledge of the chaotic state almost completely dissolves after a certain time. From an anthropocentric point of view, the system tends for us to fall again and again into a certain dark, primordial and shapeless state – a state an Ancient Greek would most probably call $\chi\acute{\alpha}o\varsigma$.

First relativity overhauled the paradigm of the very fundamental objects of European natural philosophy, and then quantum mechanics in the Copenhagen interpretation even tampered with realistic ontology itself. Relativity and quantum mechanics are, however, theories which can be omitted in a number of fields of science and engineering.

Chaos, on the contrary, is ubiquitous in every non-linear dynamical science, thus almost exclusively defining the interdisciplinary theory of dynamical systems. The clash of the former tradition of theoretical physics, golden-winged with analyticity, with chaos, dark-winged mainly with the numerical "shadowing trajectories", lead some popular authors to even predict the discovery of chaos to define a completely "new science" (e.g., the title of Gleick, 1997).

Introduction and Outline

Accretion discs are flattened astronomical objects made of rapidly rotating gas which slowly spirals onto a central gravitating body. The physics of accretion are governed by a non-linear combination of a number of physical interactions and phenomena, including gravity, hydrodynamics, viscosity, radiation and magnetic fields. The basic idea of accretion discs was proposed soon after the confirmation of quasars[2], and it's classical picture established at the beginning of the 1970s. The classical models of accretion discs such as those of Shakura & Sunyaev (1973); Novikov & Thorne (1973)[3] however neglected the self-gravitation of the disc itself, considering the disc only as test matter either in a field of a Newtonian monopole or in a Kerr metric.

Nevertheless, it has been proven that in a number of cases the complete geodesic integrability in the Kerr or Schwarzschild metric breaks down under various perturbations[4], thus changing some of the very qualitative properties of the respective test motion. The chaotization of disturbed black-hole fields is thus an astrophysically motivated subject of study with possible observational consequences.

The history of the so called *pseudo-Newtonian potentials* is intertwined with the history of accretion disc modeling, since they are often used and invented as a tool facilitating relativistic effects in otherwise non-relativistic dynamics of the disc. Paczyński & Wiita (1980) introduced the first pseudo-Newtonian potential mimicking the black-hole horizon along with an accretion disc model in it's field, the model nowadays called the *Polish donut* disc.

The Paczyński-Wiita potential was later shown to formally reproduce a number of properties of the Schwarzschild black-hole very well (Artemova, Björnsson & Novikov, 1996, see chapt. 2 of the current thesis for further reference) and is still very popular for it's simplicity.

Following the mentioned astrophysical motivation, the onset of chaos in non-Kerr metrics has also been studied by Suková (2009); Semerák & Suková (2010, 2012) in static, axially symmetric space-times consisting of a Schwarzschild black hole surrounded by a thin disc or ring as the "perturbation". In the current thesis, we study and compare analogous situations to those of Semerák and Suková

[2]Very distant quasi-stellar objects brightly shining in the radio spectrum later identified as active galaxies with supermassive black holes at their centres.

[3]The so-called α-model is sometimes even called the *standard* model of accretion discs (Montesinos Armijo, 2012).

[4]See chapter 2 of the current thesis for references to some examples, or introduction of Semerák & Suková (2010) for a more thorough overview.

in a pseudo-Newtonian approach. I.e., we simulate the test-motion in Newtonian gravitational potentials of the discs and rings with the Paczyńsky-Wiita potential in the center instead of the Schwarzschild black hole.

The comparison of the respective dynamics via Poincaré surfaces of section can be a possible indicator of the usefulness of the pseudo-Newtonian approximation for the study of long-term behavior in the mentioned fields. Nonetheless, the model can also be of interest as a peculiar Hamiltonian system, where for example the line between regularity and chaoticity of a trajectory in many cases decides whether the trajectory is bound (orbits eternally) or unbound (falls in the black hole).

The outline of this work and the aims of individual chapters are the following: First, the exploration of basic terms and facts about the phenomenon of deterministic chaos is undertaken in the chapter *Hamiltonian chaos*. Second, some basic results in the study of static, axially symmetric relativistic space-times are described in the chapter *Chaos Around Black Holes* along with the comparison of Newtonian vs. relativistic integrability of motions and a short overview of "relativistically" modified potentials – the pseudo-Newtonian potentials.

Third, in the chapter *Simulation of Test Particle Motion* the outline of the realization of the original work of this thesis is given. The original, fully relativistic studies of static axially symmetric space-times by Semerák & Suková (2010, 2012); Suková (2009) are mentioned and their chosen pseudo-Newtonian counterpart is presented along with a brief comment on the technical realization of the numerical study.

Fourth, in the final chapter *Results of the Simulation* the output of the conducted free particle simulations is presented via Poincaré surfaces of section. The plots are then compared with the surfaces of section of the original relativistic problem.

Chapter 1

Hamiltonian Chaos

The history of chaos theory especially from the perspective of celestial, i.e., autonomous Hamiltonian mechanics was informally introduced in the Prologue. Dropping most of the informality, we shall continue in the spirit of Henri Poincaré and his geometrical image of dynamics to describe a minimal portion of chaos theory and of chaos in Hamiltonian systems with two degrees of freedom.

The reader should also understand that this is *not* a completely instructive introduction to the subject, mostly presenting the used nomenclature and notation and some non-trivial facts on the matter.

1.1 Elementary chaos theory

1.1.1 Basic definitions

In the oncoming section, the basic construction of differential geometry as developed for example in Helgason (1962) is assumed. For the sake of brevity, we shall introduce less general definitions and theorems relevant particularly to chaos in continuous-time autonomous dynamical systems and especially non time-dependent Hamiltonian systems. Unless stated otherwise, all the mentioned objects are presumed to be of class C^∞ even though for this subsection C^1 objects would suffice.

Definition 1.1. Let $\mathcal{M}$ be a manifold and $\Phi_t : \mathcal{M} \to \mathcal{M}$ a Lie group of automorphisms with the real parameter t with the condition $\Phi_0 = Id$. Then the set $\mathcal{M}_t = (\mathcal{M}, \Phi_t, t)$ is called a *continuous-time dynamical system* (in short *dynamical system* in further text) where the set of automorphisms is usually called the *time flow* and the parameter the *time-parameter*. The generator of the time flow $\frac{\mathrm{d}}{\mathrm{d}t}$ shall be denoted as the *time derivative vector field*. The manifold $\mathcal{M}$ shall often be called the *phase space*.

Definition 1.2. Let $\mathcal{M}_t$ be a dynamical system. Then we define the following equivalence relation $\sim$ on the manifold: $m, n \in \mathcal{M}, m \sim n \Leftrightarrow \exists t : \Phi_t(m) = n$. A *trajectory* γ of a point $m \in \mathcal{M}$ is its $\sim$ equivalence class in $\mathcal{M}$. (We shall also often talk about a trajectory without specifying it's "initial" point.)

A trajectory has a natural structure of a submanifold parametrized by a privileged

parameter t which has however no preferred choice of the origin.

Definition 1.3. Let $\mathcal{M}_t$ be a dynamical system with an affine connection ∇. Then we define the *variation space* $\mathcal{V}(\mathcal{M}_t)$ as the space of vector fields $X \in \mathcal{X}(\mathcal{M})$ satisfying the condition

$$\nabla_{\frac{\mathrm{d}}{\mathrm{d}t}} X = \pounds_X \frac{\mathrm{d}}{\mathrm{d}t}, \tag{1.1}$$

where the symbol $\pounds$ denotes, as per usual, the Lie derivative. The intuitive meaning of the condition (1.1) is that the field varies along the trajectory (left hand side) proportionally to the change of the time derivative vector field in the direction of the vector X (right hand side). It can be shown that the field thus varies along a single trajectory as the "distance" between the observed trajectory and an infinitely close different trajectory. The variation space is still rather large for practical work and the "evolved" vector fields on separate trajectories are independent up to smoothness, it is hence imminent to define the following.

Definition 1.4. We say that two vector fields are equivalent on γ iff their difference vanishes on the points of the trajectory γ. We define the *variation space* $\mathcal{V}_\gamma$ of a trajectory γ in $\mathcal{M}_t$ as the set of all classes of vector fields from $\mathcal{V}(\mathcal{M}_t)$ equivalent on γ.

For *ultralocal* operations on the perturbation space and operations local only up to the trajectory[1], the class can thus be represented by any of it's members.

Theorem 1.1. *If $\mathcal{V}_\gamma$ is non-trivial, it has the same dimension as the ambient manifold $\mathcal{M}$.*

The proof is obvious from the fact that by giving a vector at an arbitrary point the field along the trajectory is completely determined by the first order differential equation (1.1). The non-triviality condition is added due to possibly degenerate flows.

Definition 1.5. Let $(\mathcal{M}_t)$ be a dynamical system with a vector norm $\|\bullet\|$, affine conection ∇ and γ a trajectory in it. Then the *Lyapunov exponents* λ_k are all the existing limits

$$\lambda_k = \limsup_{t\to\infty} \frac{1}{t}\, ln \frac{\|X(\Phi_t(m))\|}{\|X(m)\|},\ m \in \gamma,\ X \in \mathcal{P}_\gamma.$$

Apart from degenerate points of the time derivative vector field, the exponent for a given X are independent[2] of the point m (and thus often points placed in $t \to -\infty$) . It should be also noted that according to Smale (1967), the *sign* of the Lyapunov exponents is independent of the used norm.

[1]That is, depending only on the "immediate components" of the vector fields and on the components' derivatives in the direction of the trajectory.

[2]Usual definitions often state that the Lyapunov exponents are "coordinate dependent". As can be seen, this is true only under the assumption of a coordinate based connection (often trivial) or metric (often "euclidean").

We shall now mention a theorem useful in our case of Hamiltonian flows.

Theorem 1.2. *(Oseledets, 2008) For a μ-measure preserving*[3] *dynamical system of dimension m, there exist m Lyapunov exponents (some of them multiple) for μ-almost every trajectory.*

Definition 1.6. A trajectory is called *bounded* iff it is mappable by a finite number of maps of the manifolds and each of these maps is finite.

All the important definitions have now been prepared to finally define a chaotic trajectory.

Definition 1.7. A *chaotic trajectory* is a bounded trajectory that isn't quasiperiodic, asymptotically quasiperiodic and has at least one positive Lyapunov exponent.

This definition is due to Alligood, Sauer & Yorke (1996) and is rather inelegant, yet perhaps the most practical. There are however various other definitions of chaos (summarized e.g. in Haller (1999)) involving the notion of instability in regard to initial conditions, as portrayed by the Lyapunov exponents in the case of our definition, and also topological transitivity with possible further requirements.

As pointed out in Haller (1999), there is nonetheless a general consent on the chaoticity of the dynamical systems called the Bernoulli shift map and the Smale horseshoe map by all the usual definitions. Furthermore, since chaos in Hamiltonian systems is always associated with a homoclinic tangle which is topologically conjugate to the horseshoe dynamics (see subsect. 1.3.2), the discussed cases will involve chaotic portions of phase space by any of these definitions. Further arguments shall be discussed in section 1.4.

1.1.2 Methods of diagnosis

There exists a variety of tests and theoretical results which aid the classification and analysis of chaoticity of experimental data (see e.g. Ott, Sauer & Yorke (1994)). The methods include phase-space reconstruction from time series, recurrence methods and other more sophisticated indicators. In some cases, surprisingly detailed reports of the system structure can be retrieved from a single time-series, such as the fractal dimension of the attractor[4] of the dynamical system or an estimate of the Lyapunov exponents.

Anyhow, an even larger set of methods can be employed in the case of diagnosis of a given mathematical model. What is important, the *whole* geometric structure of the flow is observable with rather less effort. Fractal boundaries between areas of certain "fate" of trajectories can be found as an indicator of chaos. In dissipative dynamical systems, the "fates" can be the asymptotic falls on the different attractors of the system (e.g. Grebogi et al., 1987), in the unbounded case of chaotic scattering the angle of escape from the system into infinity and in general relativity, the shunless destiny of the trajectory may be the fall into a black hole or a singularity (e.g. Dettmann, Frankel & Cornish, 1995; Podolský &

[3]The affine connection must also preserve the respective volume form.

[4]Attracting sets on the phase space in the case of a dissipative system.

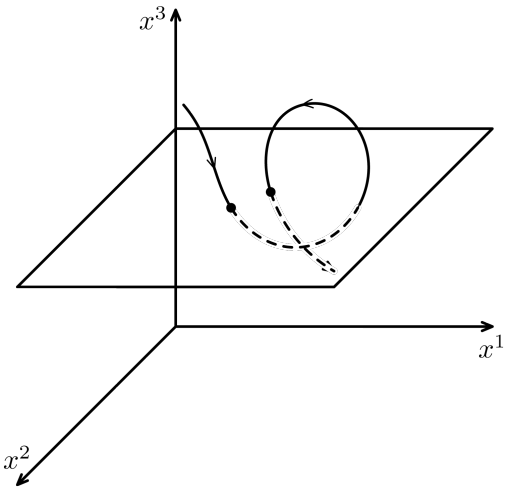

Figure 1.1: Illustration of a Poincaré surface of section in three dimensions, taken from Suková (2009)

Kofroň, 2007).

In the case of Hamiltonian systems the qualitative analysis of certain projections called the *Poincaré surfaces of section* is often employed in a very similar fashion as has been originally proposed by Poincaré himself (Poincaré, 1899, chapt. 33).

In the works of Poincaré and subsequently of Birkhoff (1917), the surface was defined only for systems of two degrees of freedom[5] such as the restricted three-body problem. The original notion requested the surface of section to be a surface (2-dimensional submanifold) which is crossed infinite times by every trajectory in the possible phase space of the considered motion (see fig. 1.1). Along these lines, the sequence of points of intersection define a map of the surface for which area preservation can be proved (Poincaré, 1899, loc. cit.).

For a well defined map and a system with two degrees of freedom (4 dimensions), two other coordinates *of the position* of the surface must be specified apart from the two coordinates *on* the submanifold. A very frequent choice of the surface definition is a fixed value of one of the canonical coordinates and a fixed energy level[6] sometimes with a further specification due to non-monotony of the Hamiltonian function.

Examples of surfaces of section can be found at the end of the last chapter of this thesis.

Occasionally, the plot of coordinates (or a certain projection) of a point under discrete τ-timeshifts Φ_τ is exploited for dynamics understanding instead of surfaces of section. The timeshift approach is frugal especially in the families of integrable systems "kicked" periodically by a δ-pulse for which the time-shift maps are almost always explicit (a brief survey can be found in Zaslavskii (2007,

[5]Half of the dimension of the Hamiltonian dynamical system, see def. 1.9.

[6]Even this choice may often be stated to be "planar", the surface is almost always curved in the sense of canonical coordinates since it is formed by an intersection with the $H = \text{const.}$ submanifold.

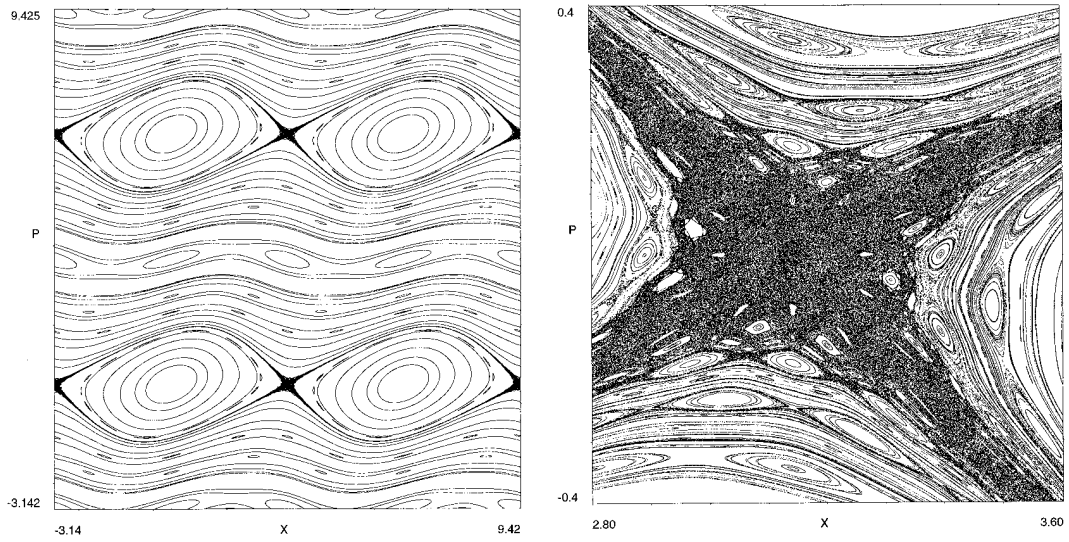

Figure 1.2: The so called Standard map modeling the kicked oscillator - a global view of a 2×2 period of phase space (left) and a close-up of the stochastic layer near the separatrix (right). Taken from Zaslavskii (2007).

chapt. 1)). An example of such a timeshift map can be found in figure 1.2. The similarity or even equivalence to Poincaré surfaces of sections is readily justified by a formal extension of the phase space by a periodic time coordinate and a conjugate momentum (Arnol'd, Kozlov & Neishtadt, 1993).

1.2 Hamiltonian systems

If not stated otherwise, the results brought in this section can be found e.g. in Arnol'd (1989).

Definition 1.8. If on an even-dimensional manifold $\mathcal{M}$ there exists a differential 2-form $\boldsymbol{\omega}$ which is closed and non-degenerate, then the pair $(\mathcal{M}, \boldsymbol{\omega})$ is called a *symplectic manifold* and the form is called *symplectic*.

For a manifold of dimension $2N$ a natural volume-form is defined with the use of the exterior product $\wedge$,

$$\boldsymbol{\omega}^{\wedge N} = \boldsymbol{\omega} \wedge \ldots_{N-times} \wedge \boldsymbol{\omega}. \tag{1.2}$$

As the form $\boldsymbol{\omega}$ is also non-degenerate, it can be used for the so-called "musical isomorphisms" or "index lowering" and "raising" quite similarly to the analogous operations in relativity and riemannian geometry

$$\boldsymbol{\omega}^\flat X \equiv \iota_X \boldsymbol{\omega},\ \boldsymbol{\omega}^\flat(\boldsymbol{\omega}^\sharp \alpha) = \alpha, \tag{1.3}$$

where X is a vector field,α a one-form on the manifold and ι_X denotes contraction with X. The "sharp" mapping is implicitly defined as the inverse of $\boldsymbol{\omega}^\flat$ which is well defined due to it's non-degeneracy.

Definition 1.9. If a $2n$-dimensional symplectic manifold $(\mathcal{M}, \boldsymbol{\omega})$ is also a dy-

namical system, and the time flow Φ_t is a flow of a vector field of the form

$$\frac{\mathrm{d}}{\mathrm{d}t} = \boldsymbol{\omega}^\sharp dH \tag{1.4}$$

for some function H on the manifold $\mathcal{M}$, then the dynamical system is called *Hamiltonian* (similarly the vector field, it's flow and the function H). The number n is then called the *number of degrees of freedom (dof).*

It is not surprising that the local coordinates on the manifold can always be chosen so that $\boldsymbol{\omega} = \mathrm{d}\boldsymbol{p} \wedge \mathrm{d}\boldsymbol{q}$ and the hamilton's equations (1.4) gain the usual canonical form

$$\dot{\boldsymbol{p}} = -\frac{\partial H}{\partial \boldsymbol{q}},\ \dot{\boldsymbol{q}} = \frac{\partial H}{\partial \boldsymbol{p}}. \tag{1.5}$$

The classical result of Hamiltonian (energy) preservation is also inferable from the equation (1.4).

Theorem 1.3. *The Hamiltonian flow preserves the symplectic structure, i.e.*

$$\Phi_t^* \boldsymbol{\omega} = \boldsymbol{\omega}.$$

As a consequence, any $\wedge$-power of $\boldsymbol{\omega}$ is invariant under the flow corresponding to integral Poincaré invariants, the highest being the mentioned volume form (1.2) corresponding to the phase space volume.

The symmetry of the flow has further consequences for eigenvalues of linearizations around trajectories and fixed points (Cvitanović et al., 2012, chapt.7). A rough behavior of a very close trajectory from a fixed point ($dH = 0$) can be described by finding the eigendirections and eigenvalues of the jacobian of the flow. The distance of a trajectory very close to the fixed point in an eigendirection of an eigenvalue λ can be estimated as $\exp(\Re(\lambda)t)$ and $\Im(\lambda)$ determines the rotation (orbiting) of the trajectory around the point (where $\Re$, $\Im$ denote the real and imaginary part of the eigenvalue respectively).

In the Hamiltonian case in canonical coordinates, the eigenvalues of jacobians however always come come in quartets – $\lambda, -\lambda, \lambda^*, -\lambda^*$. E.g. in one dof (2-dimensional) systems, a fixed point *must* be either hyperbolic ($\Im(\lambda) = 0$) or elliptic $\Re(\lambda) = 0$.

A special case where the eigenvalues can be defined for the trajectory as a whole are periodic trajectories. In that case, there is a linear operator of evolution of very close trajectories around one loop called the *monodromy* operator. The monodromy operator can be also shown to have analogous eigenvalue quartets as mentioned in the previous paragraph.

Considering systems of two degrees of freedom and isoenergetic levels, the resulting submanifold is only three dimensional. For the monodromy operators on these spaces one eigenvalue is always 0 corresponding to the direction of the flow and the other two eigenvalues then automatically satisfy either of the conditions $\lambda = \pm\lambda^*$. In this sense, periodic trajectories in 2-dof systems are either stable (elliptic) or unstable (hyperbolic).

For an isoenergetic Poincaré surface of section of a 2-dof system, there will thus be only elliptic[7] or hyperbolic fixed points and periodic orbits.

In conclusion of this section, we would also like to point out the consequences of the mentioned facts about Hamiltonian systems for Lyapunov exponents. As the phase space volume is conserved by the flow, the Oseledets theorem 1.2 is applicable and almost every trajectory has thus got a complete set of Lyapunov exponents.

From the relations between the eigenvalues, it can be shown[8] that the Lyapunov exponents in Hamiltonian systems come in pairs $\pm\lambda$. An intuitive interpretation of the relation between Lyapunov exponents is that the contraction of the neighboring phase-space roughly proportional to $e^{-\lambda t}$ is compensated by the expansion in another direction $e^{\lambda t}$ thus conserving phase-space volume.

1.3 The homoclinic tangle, KAM theory and beyond

As is fittingly stated in Cvitanović et al. (2012), the flows of $2n$-dimensional Hamiltonian systems are "morally n-dimensional" due to the n integral invariants mentioned in the previous section.

This can be also demonstrated by the truth that a general set of $2n$ ordinary differential equations of first order needs a set of $2n$ first integrals to be integrated. However, it is a well known fact that the $2n$ hamilton's equations (1.4) need only n integrals of motion in involution to be solved by quadrature. Let us develop this statement more formally.

1.3.1 Integrable systems

Definition 1.10. We define the *Poisson brackets* on a symplectic manifold $\mathcal{M}, \boldsymbol{\omega}$ of two functions F, G on the manifold consequently

$$\{F, G\} \equiv \boldsymbol{\omega}(\boldsymbol{\omega}^\sharp dF, \boldsymbol{\omega}^\sharp dG).$$

We say that two functions are in *involution* if their Poisson bracket is zero.

Definition 1.11. A function F on a dynamical system is called a first integral iff

$$\frac{\mathrm{d}}{\mathrm{d}t}(F) = 0.$$

It follows that the trajectories are then confined to submanifolds defined by the constant values of the first integrals. The Hamilton's function is also an integral of motion.

[7] Even "circular" in canonical coordinates, as in that case the eigenvalues always have the same norm.

[8] The affine connection on the manifold must be however Levi-Civita with respect to the norm used in definition 1.5 and the norm must be further chosen so that the volume form (1.2) is coincident with the respective metric volume form.

Theorem 1.4. *Let $\boldsymbol{F} = \{F_1, \cdots, F_n\}$ denote the set of n first integrals of a $2n$-dimensional Hamiltonian dynamical system in involution. Let then $\mathcal{N}_{\boldsymbol{F}}(f_1, \cdots, f_n)$ be the invariant manifold of the integrals with values $f_1, \cdots, f_n$ respectively. Then if the differentials dF_i are linearly independent on the invariant manifold:*

- *If $\mathcal{N}_{\boldsymbol{F}}$ is compact and connected, then it is diffeomorphic to $\mathbb{T}^n$.*
- *The motion on the said torus is diffeomorphic to stationary rotations with frequencies dependent solely on the values of the first integrals. I.e. there is a set of local coordinates $\boldsymbol{I} = (I_1, \cdots, I_n)$, $\boldsymbol{\phi} = (\phi_1, \cdots, \phi_n)$ so that the Hamilton's equations take the form*

$$H = H(\boldsymbol{I}),\ \dot{\boldsymbol{I}} = -\frac{\partial H}{\partial \boldsymbol{\phi}} = 0,\ \dot{\boldsymbol{\phi}} = \frac{\partial H}{\partial \boldsymbol{I}} = \boldsymbol{\nu}(\boldsymbol{I},) \tag{1.6}$$

  where $\boldsymbol{\nu} = (\nu_1, \cdots, \nu_n)$ is a vector constant in time called the frequency vector *and the respective coordinates are called* action-angle.

- *The equations (1.4) can be solved by quadratures.*

We call such a Hamiltonian system an *integrable system*[9] in further text. If the integral submanifolds $\mathcal{N}_{\boldsymbol{F}}$ are non-compact, the manifolds are diffeomorphic to Cartesian products of the real line and the unit circle with similarly regular motion. Secondly, if the invariant manifolds $\mathcal{N}_{\boldsymbol{F}}$ aren't connected, the differentiable components satisfy relations analogous to the theorem. Usually, mutually diffeomorphic invariant manifolds foliate whole portions of phase space changing their differentiable structure only in association with points where the differentials of integrals of motion aren't independent.

The degeneracy of the integrals is often due to a hyperbolic fixed point ($dH = 0$) of the Hamiltonian, or in a mechanical interpretation an "unstable equilibrium of forces", with a stable and unstable manifold separating qualitatively different modes of motion. An example of such foliation of phase space is the non-linearized mathematical pendulum in figure 1.3.

1.3.2 Homoclinic tangle

The hyperbolic points are not only important in the change of foliation of the phase space, but also as "seeds of chaos" as is notoriously stated in literature (e.g. Zaslavskii (2007) or Alligood, Sauer & Yorke (1996)). The latter alias of hyperbolic points is due to the phenomenon of a "homoclinic tangle" near the separatrices of the hyperbolic points discovered by Poincaré (1899). We shall introduce a few definitions to discuss the problem in a rigorous fashion.

Definition 1.12. For a fixed point or periodic trajectory we define the *stable* (*unstable*) manifold as the maximal manifold of which every point converges to the fixed point or periodic trajectory for $t \to +\infty$ ($t \to -\infty$).

Obviously, two manifolds of the same stability family cannot intersect as the points on the intersection would have to be asymptotic to two different objects,

[9]Even though this is not strictly correct, we shall leave out the epithet "bounded" for the purposes of this thesis.

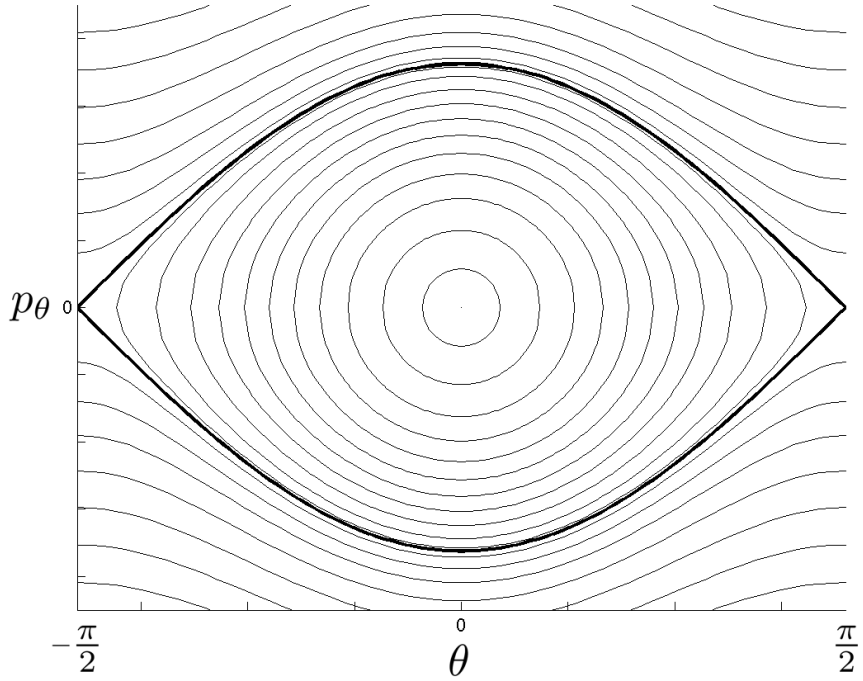

Figure 1.3: Phase space portrait of a mathematical pendulum - the phase space foliated by circular rotations and linear librations is divided by a separatrix - a singular trajectory (bold) spanning from the hyperbolic fixed point in $\theta = \pm\frac{\pi}{2}$. (taken from Wikipedia (2013))

"Cela est encore absurde" as Poincaré stated. Intersections of manifolds of different stability are however possible.

Definition 1.13. The intersection of a stable and an unstable manifold of a single fixed point or trajectory is called a *homoclinic* manifold.

Definition 1.14. An intersection of two submanifolds $\mathcal{M}$ and $\mathcal{N}$ is called *transverse* when for every point m of the intersection the following equality is satisfied

$$dim(T_m\mathcal{M} \oplus T_m\mathcal{N}) = dim(\mathcal{M}) + dim(\mathcal{N}), \tag{1.7}$$

where $T_m\mathcal{M}$, $T_m\mathcal{M}$ are the tangent spaces of the respective submanifolds at m and the direct sum is executed in the sense of the tangent space of the ambient manifold.

The intuitive meaning of definition 1.14 is that the submanifolds do not tangentially touch but they cross, i.e. their tangent spaces don't coincide in any direction and their immersion spans the whole $T_m\mathcal{M}$.

The stable and unstable manifolds form invariant sets of the flow and so does consequently a homoclinic manifold. The statement now stands: if the homoclinic manifold is formed by a transverse intersection, the structure of the stable and unstable manifolds gets infinitely complicated so that *"On serra frappé de la complexité de cette figure, que je ne cherche même pas à tracer."*[10] - *"One will be struck by the complexity of this figure, which I shall not even attempt to draw."*

[10]Poincaré (1899, chapt.33, p.389)

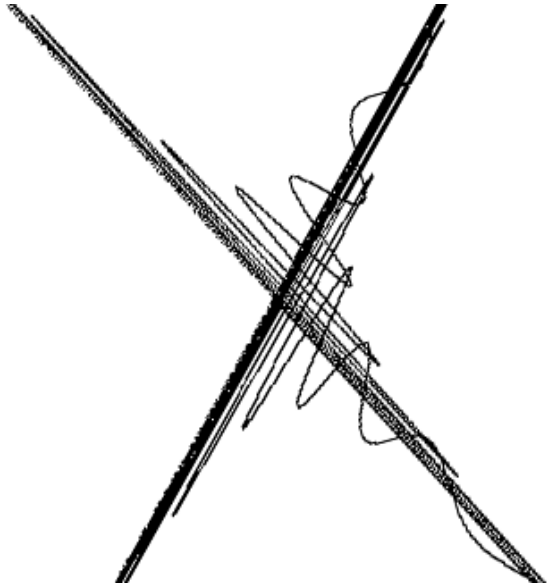

Figure 1.4: An approximate picture of the homoclinic tangle in the Standard Map. The lobes of the stable and unstable manifolds intersect more and more frequently approaching the hyperbolic point at the centre of the picture forming the so-called "tangle".

Howeve,r unlike Poincaré, we will give a rough illustration of the situation in fig. 1.4 which has been gained by numerical computation. Constructive arguments justifying the provided picture were given by Melnikov or Smale (Guckenheimer & Holmes, 1990; Smale, 1967).

The situation in the homoclinic tangle can be described as follows. Suppose we have a Poincaré map on an isoenergetical level in 2-dof intersecting transversally a hyperbolic trajectory. As has been mentioned in subsection 1.2 the periodic trajectory is then represented by a hyperbolic fixed point with lines as the stable and unstable manifolds. The transversal intersection is then also represented by a point but as it's homoclinicity is invariant under the flow and the map, there has to be an infinity of other intersections (points) at both the forward and backward iterates of the Poincaré map.

Following the lines of Poincaré, Smale (1967) proved the following theorem through topological conjugacy to a model diffeomorphism of the plane now known as the Smale horseshoe:

Theorem 1.5. *Suppose x is a transversal homoclinic point of an auto-diffeomorphism f of a manifold $\mathcal{N}$. Then there is a Cantor set $\Lambda \in \mathcal{N}$, $x \in \Lambda$, and $n \in \mathbb{Z}^+$ such that $f^n(\Lambda) = \Lambda$ and f^n restricted to Λ is topologically a shift automorphism.*

A shift automorphism is for example the Bernoulli shift - a formal shift to the result of another coin flip in the sequence of such - and it can be proven to have positive Lyapunov exponents (e.g. Alligood, Sauer & Yorke, 1996). The transversal homoclinic intersection thus implies chaos in a portion of phase space which is however of zero measure. As Contopoulos (2010) states, there is ample evidence of chaos in larger non-integrable regions of the phase-space neighboring the homoclinic tangle, but there does not seem to be an analytical result guaranteeing

chaos in non-zero measure regions due to the homoclinic tangle.

1.3.3 Stability of the invariant structures

There is a rich perturbation theory assessing the persistence of order in integrable systems under non-integrable influences developed since the onset of classical mechanics, as has been mentioned in the Prologue. The collection of results developed through fifties and sixties concerning themselves with persistence of the invariant tori under non-integrable perturbations of the Hamiltonian function is called the *Kolmogorov-Arnold-Moser theory* (KAM theory) according to it's main contributors. We shall introduce here only one main theorem and a qualitative discussion of more general cases and extensions as discussed in Arnol'd, Kozlov & Neishtadt (1993), Zaslavskii (2007) and Haller (1999).

Definition 1.15. We say that a torus of an integrable system is *resonant* iff the trajectories on the torus compact[11].

The invariant structure of the torus is then further foliated into $\mathcal{S}^1$ invariant manifolds - the periodic trajectories. In the action-angle coordinates, this condition can be alternatively expressed in terms of integer ratios between the frequencies on the torus i.e.: $(\boldsymbol{k}, \boldsymbol{\nu}) = \sum_i k_i \nu_i = 0$, $\boldsymbol{k} \in \mathbb{Z}^n$.

Definition 1.16. A Hamiltonian system is called *nondegenerate* if the lie bracket $\left[\frac{\mathrm{d}}{\mathrm{d}t}, \bullet\right]$ is non-vanishing (even locally) on at least n vector fields of a commuting set of $2n$ vector fields.

In the case of an integrable system, the non-vanishing set is also at most n and the degenerate case corresponds to "too much integrals of motion" (sometimes only in a local sense).

Definition 1.17. A Hamiltonian system is called isoenergetically nondegenerate iff the flow is nondegenerate on every submanifold of constant H (with sets of $2n-1$ commuting vector fields on the submanifold) and $dH \neq 0$.

In a nondegenerate integrable system, resonant tori form a dense subset of the phase space of zero measure, whereas the tori with irrational frequency vectors form a dense subset with nonzero measure. For an isoenergetically nondegenerate integrable system, this is true even for every isoenergetic (H =const.) submanifold.

Theorem 1.6. *Suppose the Hamiltonian of an integrable system is analytic*[12] *and the system is nondegenerate or isoenergetically nondegenerate. Then if the Hamiltonian is subject to a sufficiently small perturbation term of order ϵ and of class C^r, where $r > 2n$*[13]*, then a majority of the nonresonant invariant tori survive the perturbation with slight deformations and unchanged frequencies. These tori are called* Kolmogorov tori *and their union is the* Kolmogorov set*. The statement can be developed more formally:*

[11] This definition, however non-standard, seems to be the most elegant coordinate-free way to express the fact that the trajectory closes after a finite number of loops.

[12] For the term "analytic" to have a good meaning, the manifold has to be analytic as well.

[13] r can be considered a non-integer, thus allowing C^r to be a Hölder space.

1. *For a given number* $\mu : n - 1 < \mu < \frac{r}{2} - 1$ *the frequencies of motion on the Kolmogorov tori form the following set:*

$$\Omega_\kappa = \{\boldsymbol{\xi} : \boldsymbol{\xi} \in \Omega - \kappa, |(\boldsymbol{k}, \boldsymbol{\xi})| < \kappa |\boldsymbol{k}|^\mu \ \forall \boldsymbol{k} \in \mathbb{Z}^n\},$$

   where Ω *is the unperturbed set of frequencies* $\boldsymbol{\nu}(\boldsymbol{I})$*,* $\Omega - \kappa$ *the set of points whose* κ *neighborhood is contained in* Ω*, and* κ *is a quantity of order* $\sqrt{\epsilon}$*.*

2. *The measure of tori destroyed by the perturbation does not exceed a quantity of order* $\sqrt{\epsilon}$*. If the frequency on the torus belongs to* Ω_δ *with* $\delta > \kappa$*, the deformation of the torus does not exceed a quantity of order* ϵ/δ *(and hence of order* $\sqrt{\epsilon}$*).*

The proof is described e.g. in Arnol'd, Kozlov & Neishtadt (1993) and is based on an iterative series of canonical coordinate transformations based on modified methods of averaging theory. The series converges quadratically in ϵ to a set of new action-angle coordinates on the Kolmogorov set.

Obviously, the theorem does not address the "strength" of the perturbation term apart from a moderately smooth behaviour. Hence the strict applicability of the theorem is very limited without further analytical investigations.

For specific perturbations, analytic estimates of the development of invariant structure can be obtained using the mentioned averaging methods. As pointed out in Contopoulos (2010, see p. 71 for a complete set of references), the estimates of perturbation strengths for which the Kolmogorov tori may be destroyed were usually found to be much smaller than "critical" strengths of perturbation found by numerical simulations.

1.4 The onset of chaos in two degrees of freedom

The situation of 2-dof systems is special in a number of aspects. Firstly, it follows from Poincaré-Bendixson theorem (Haller, 1999) that a 2-dof system is the simplest autonomous Hamiltonian system with the possibility of chaos.

Secondly, on isoenergetical levels of a weakly perturbed integrable system, the 3-dimensional flow is divided by 2-dimensional tori. The nonintegrable flow is hence confined to small separate regions of phase space effectively close to the original system. In higher degrees of freedom, the tori do not provide a division of phase space letting the trajectories wander as illustrated in fig. 1.5. This process of seemingly random wandering of trajectories in unconfined phase-space is often called "Arnold diffusion".

The last but not least important aspect of 2-dof systems again connected to the fact that the flow is 3-dimensional is that the isoenergetical levels have almost always Poincaré surfaces of section. The integrability of 2-dof systems can thus be qualitatively studied just by straightforward examination of the surfaces of section without an urgent need for time-series analysis and other techniques.

Let us now qualitatively describe the "evolution" of the perturbed 2-dof system under the perturbation parameter ϵ in the language of Poincaré surfaces of section as portrayed by Zaslavskii (2007) and Guckenheimer & Holmes (1990).

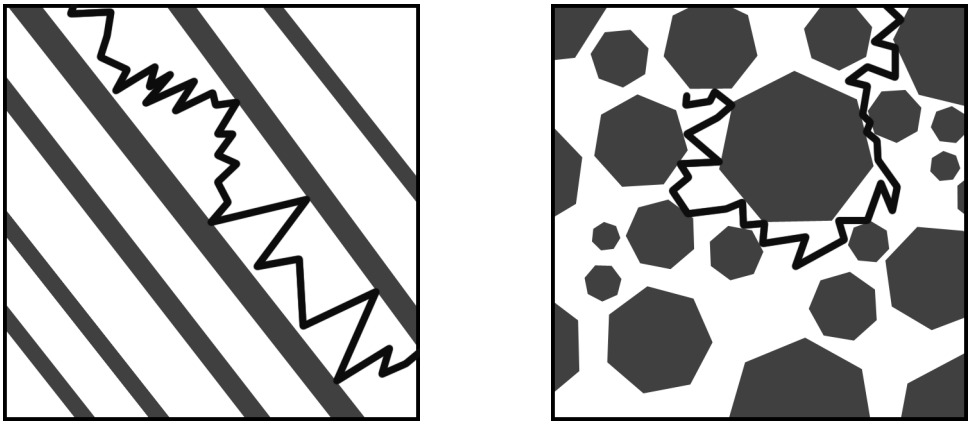

Figure 1.5: Illustration of confinement and diffusion in weakly nonintegrable systems. On the left is a situation analogous to 2-dof systems - unpredicatble trajectories are well separated by lines. Whereas on the right a situation analogous to higher dof systems is illustrated - "random" trajectories in different parts of phase-space may visit arbitrary nonintegrable regions only "scattering" from invariant points or dots.

1.4.1 Chains of islands and their bifurcations

The periodic trajectories, represented by n-periodic points on the surfaces of section, are affected most by the perturbation as they bifurcate into $2k$ n-periodic trajectories represented as $2kn$ points alternating between hyperbolic and elliptic. This sequence is often called a *chain of resonance islands* as the stable elliptic points naturally forms a set of width of order $\sqrt{\epsilon}$ of invariant tori separated from the Kolmogorov set by the separatrices of the hyperbolic points (fig. 1.6). The separatrices however often form a homoclinic tangle for even very small perturbations and thus stable elliptic "islands" are almost always plunged in a layer of a chaotic "sea".

The generation of the resonance islands does not however terminate at the primary tori of the original integrable system. Resonant tori of the unfolded elliptic islands can be destroyed as well, forming secondary chains of islands and this sequence can reach to chains of islands of arbitrary order to form fractal-like structures often encountered in surfaces of section.

As the perturbation parameter grows, further doubling bifurcations may occur with a roughly geometrically growing frequency as has been found in a number of 2D area preserving maps (Benettin, Galgani & Giorgilli, 1980) and some Poincaré surfaces of section (Contopoulos, 2010).

By reviewing the results presented e.g. in Contopoulos (2010), the general bifurcation scheme for Poincaré surfaces of section does not seem to be established as various different behaviours have been found. A passing from a bifurcating phase to a "joining" phase has been numerically observed forming "infinite bubbles" and also a combination of switches between stability and instability has been observed in a different model then evolving into "infinite gaps". There is thus no complete understanding of universality in conservative systems so far (Gaidashev, Johnson & Martens, 2012).

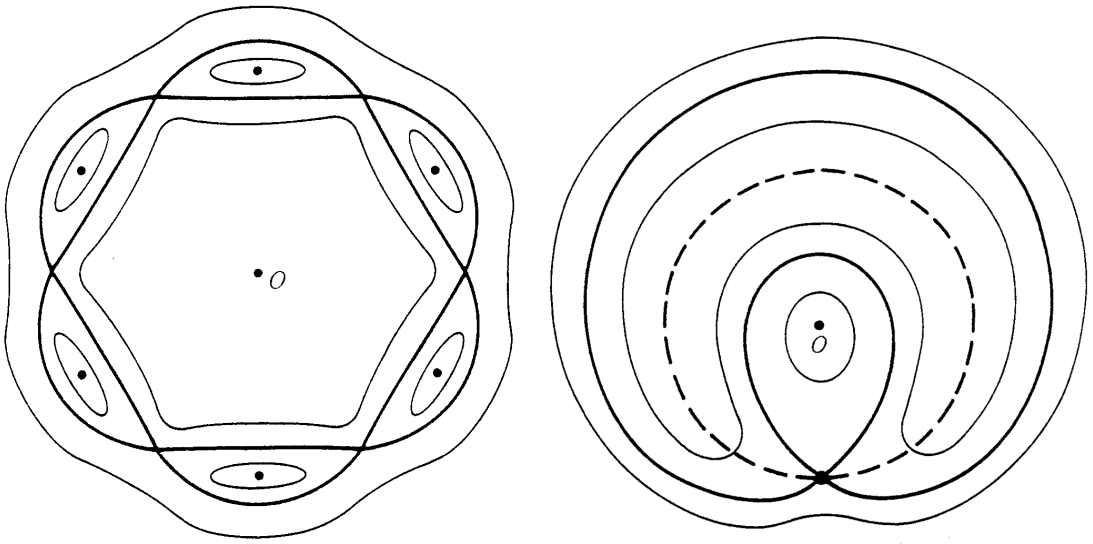

Figure 1.6: A chain of resonance islands of period 6 and 1. Taken from Zaslavskii (2007).

1.4.2 Resonance overlap and heteroclinic intersection

The conventional distinction of "strong chaos" as opposed to "weak chaos" which we have been describing to this moment, is the resonance overlap. The resonance overlap occurs when $\sqrt{\epsilon}$ is of order of the width between the primary resonances and the chaotic layers get connected allowing for a widespread diffusion of irregular trajectories.

However, the distinction isn't only conventional, as the resonance overlap is the first moment when a *heteroclinic intersection* of two different resonances usually occurs. I.e., the stable and unstable manifolds of *different* hyperbolic points intersect transversally to generate chaos in a similar mechanism as descibed in section 1.3.2.

1.4.3 Cantori and stickiness

By the analysis of the so called 2D twist maps it can be shown (Arnol'd, Kozlov & Neishtadt, 1993) that apart from continuous tori, the area preserving maps can have invariant sets called *cantori*. The subsequent mappings of the points on the cantorus can be shown to have a one-to-one correspondence with rotations on a circle. Nevertheless, this one-to-one mapping is homeomorphic only up to a countable infinity of points of discontinuity. Hence the name of the cantorus - it then forms a cantor set (of zero length (MacKay, 1987)) in the original 2D space.

The cantori on the Poincaré surfaces of sections have been observed in a heft of numerical simulations (see e.g Contopoulos (2010), sect. 2.7.3, for a complete set of references). The corresponding objects in the full phase space are obviously twisting dicontinuous surfaces which however do not confine the trajectories in between, presenting only partial barrier to the trajectory diffusion. Another partial barrier considered e.g. by Zaslavskii (2007) is the self-similar structure of remnant islands around a main island.

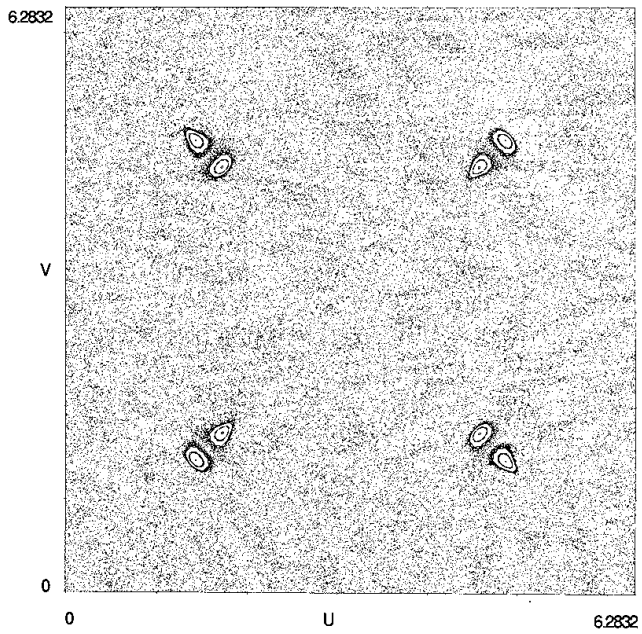

Figure 1.7: A set of eight sticky islands from the standard map. Taken from Zaslavskii (2007).

The mentioned structures are generally considered to be the main actors in the phenomenon of "stickiness", the tendency of certain trajectories to spend very long times in the neighborhood of stable islands even though they are not confined by an invariant surface (i.e. escapes from the region are observed).

Stickiness of an island is observable as a "darker" region around the respective island as seen in fig. 1.7. The statistics of irregular trajectories in chaotic seas present rather curious behaviour often denoted as "fat tails" usually interpreted as power laws.

For example, the mean escape time for a trajectory from a sticky region may even amount to infinity (Zaslavskii, 2007). That is caused by the fact that the probability density $\rho(\tau)$ of escape after a time τ is proportional to $\tau^{-\beta}$ with $\beta < 2$ for τ sufficiently large. Thus the designation "fat tail" of a probability distribution which causes certain momenta of the distribution to diverge.

As has been noted in MacKay, Meiss & Percival (1984), the stated behaviour can be acquired for example as a superposition of a countable set of exponential decays with the right behaviour of coefficients in result of an infinitely delicate structure in the neighborhood of the island. The set of decays could however also be finite but very large and the phenomenon of a fat tail may fall of into a "regular" exponential decay for very long times. Such times may however not be accessible numerically.

We would like to conclude this subsection by noting that there is a rich variety of results concerning stickiness and in general transport in Hamiltonian systems, consequences for recurrence and statistical physics, as well as semi-analytical approaches to the problems. A complete review would however be way beyond the scope of this thesis and thus we point the reader to the already cited Contopoulos (2010, loc. cit.), Zaslavskii (2007), MacKay, Meiss & Percival (1984) and also to

Meiss (1992) for a detailed review of the problems.

Chapter 2

Chaos Around Black Holes

In the first section we will present an overview of differences of relativistic dynamics in comparison with the Newtonian case and in the second section a minimal introduction to Weyl space-times is outlined. Finally, in the last section the pseudo-Newtonian approach is introduced along with an only partially complete review of literature concerning itself with development and applications of non-relativistic approximations of relativistic features.

2.1 Nonintegrability in relativistic geodesic flows

It would be a turn of tables if the relativistic motions were found to be completely integrable in contrast to for example Poincaré's three body problem, but this is not the case. In some problems such as the geodesic flow in the field of two fixed black holes Contopoulos (2010, sect. 4.2) a flow completely integrable in the Newtonian case has been found to be even completely chaotic (for null-geodesics). A review of chaos in relativity can be found e.g. in the introduction of Semerák & Suková (2010).

Arguments can be developed which explain volatility of an integrable relativistic motion being subject to perturbation versus the volatility of it's Newtonian counterpart. Such is for example the Schwarzschild spacetime containing an unstable periodic trajectory which immediately after perturbation generates chaos. Since a vast majority of local (i.e. non-cosmological) astrophysically relevant relativistic models involve a black hole with it's unstable periodic orbit, chaos is often found to be stronger in the relativistic case (see subsection 2.3.2 for examples).

Nonetheless, there is no universal argument for the observed relativistic-Newtonian non-integrability correspondence, since the formalism is comparable only asymptotically and thus even the simplest integrable settings often differ in qualitative tendencies of evolution.

2.1.1 Motion of a test particle as a Hamiltonian flow

The equation of geodesic[1] in a relativistic space-time does possess a Hamiltonian formulation

$$H = \frac{1}{2m} g^{\mu\nu} p_\mu p_\nu, \tag{2.1}$$

with $p_\mu = m\dot{x}_\mu$ the canonical momentum conjugate to x^μ, m the rest mass of the particle, and the dot denotes covariant differentiation with respect to it's proper time τ. The Hamilton's equations with the canonical symplectic form $\boldsymbol{\omega} = \mathrm{d}p_\mu \wedge \mathrm{d}x^\mu$ then stand without any modifications. The Hamiltonian has quite obviously got a constant value of $-1/2m$ corresponding to the four-velocity normalization.

All the results of the previous chapter apply with the phase space being the cotangent bundle of the 4-dimensional space-time. It would seem that the test motion in relativity has more degrees of freedom than in the Newtonian case. The dependency of the Hamiltonian (2.1) on the fourth "extra" coordinate however corresponds to a time dependency of the gravitational field in the Newtonian case. The four-velocity normalization then corresponds to $\dot{t} = 1$.

Hence the main formal difference between the Einstein and Newton gravity as to the respective Hamiltonian dynamical system of a free particle is the fact that the Newtonian case is always expressible in a set of coordinates in which the configuration-space-independent kinetic energy $T(\boldsymbol{p})$ is separate from the gravitational potential $V(\boldsymbol{q})$, on the contrary dependent only on the values of configuration coordinates. On the other hand, the formally elegant relativistic case has the whole dynamics tucked into a configuration-space dependent quadratic form of the momenta.

The integrability and non-integrability of the relativistic geodesic flow is however a strongly geometric property (in a not strictly local sense) of the spacetime expressible in terms of symmetries of the metric. Namely, a continuous isometry group or equivalently a Killing vector field always corresponds to a linear momentum integral of motion and a Killing tensor of second order corresponds to a quadratic integral of momenta. A brief overview of the link between Killing tensors and their generalizations to integrability of geodesics can be found in Stephani et al. (2003, sect. 35.3).

2.1.2 Relativistic specialties

The Killing vectors have a Newtonian analogue - symmetries of the mass distributions and thus also of the gravitational potential. Anyhow, the topological non-triviality of certain space-times cannot be dubbed by the Newtonian case. There exists a number of results concerning topological obstructions to geodesic integrability on *Riemannian* manifolds (Bolsinov & Jovanovic, 2003). For example, it has been proven that if the fundamental group of the manifold has

[1] Strictly speaking, the described flow is a *cogeodesic* flow since it involves the whole cotangent bundle of the manifold.

exponential growth [2] (as is the case with spaces with negative curvature), the *topological entropy* of the geodesic flow must be positive. Furthermore, the positivity of topological entropy is proven to imply nonexistence of analytic integrability of the flow. On the other hand, counterexamples have been found which have positive topological entropy with *smooth but non-analytic* first integrals of the flow.

Omitting the fact that the thin line between analyticity and smoothness of the integrals is usually beyond the scope of a physicist's interest, the mentioned results consider only Riemannian metrics and the pseudo-Riemann case isn't thoroughly discussed in the literature. Additionally, the results concerning topological obstructions to integrability do not seem to have stirred wide physical interest as general theorems associate non-trivial topology with physical singularities, controversial closed time-like curves or censorship of the occurring phenomena for a distant observer (see introduction of Silva, 2010).

The other specific phenomenon of relativity are gravitational waves. These can either be used to perturb the background leading to chaos (Bombelli & Calzetta, 1992; Letelier & Vieira, 1997) or possibly to analyze the wave-emitting chaotic motion from far away (Kiuchi, Koyama & Maeda, 2007).

The last but not least special feature of General Relativity is the fact that the background itself is governed by non-linear equations – even in a dynamical sense. The matter is however delicate, since there is most often no preferred choice of the time parameter, as has been a crucial historical argument in the discussion of chaos in the Bianchi IX (Mixmaster) cosmological model.

According to Contopoulos (2010, sect. 4.3), most of the classical cosmological models include some degree of chaoticity at least in the sense of chaotic scattering as seems to be the case of the Bianchi IX model (see introduction of Semerák & Suková, 2010, for a recent list of contributions). Yet for example in the Bianchi IX model most of the chaotic oscillations occur before Planck time where the classical description is most probably invalid.

2.2 Weyl space-times

The metric describing static axisymmetric vacuum solutions of Einstein equations was first devised by Weyl (2012, first published 1917) with a nowadays surprising motivation to attempt to elucidate the inner workings of an atom. Weyl himself admits by the end of the article that the result cannot be perhaps used in the stated way, yet the metric has found use in the description of idealized astrophysical models. In Weyl's canonical coordinates utilizing geometrized units $c = G = 1$ and the $(-+++)$ signature, the metric reads.

$$\mathrm{d}s^2 = -e^{2\nu(\rho.z)}\mathrm{d}t^2 + \rho^2 e^{-2\nu(\rho,z)}\mathrm{d}\phi^2 + e^{2(\lambda(\rho,z)-\nu(\rho,z))}(\mathrm{d}\rho^2 + \mathrm{d}z^2). \tag{2.2}$$

[2] The *fundamental group* is the group of homotopy-equivalent classes of loops passing through a certain point. If the manifold is path-wise connected, the fundamental group is independent of the respective point. *Growth rate* of the group is the rough dependency of the number of nonequivalent loops generated by a fixed number of joinings of a generating set of loops.

Einstein's equations in vacuum impose the following conditions on the functions ν and λ:

$$\frac{\partial^2\nu}{\partial\rho^2}+\frac{1}{\rho}\frac{\partial\nu}{\partial\rho}+\frac{\partial^2\nu}{\partial z^2}=0 \tag{2.3}$$

$$\frac{1}{\rho}\frac{\partial\lambda}{\partial\rho}-\left(\frac{\partial\nu}{\partial\rho}\right)^2+\left(\frac{\partial\nu}{\partial z}\right)^2=0 \tag{2.4}$$

$$\frac{1}{\rho}\frac{\partial\lambda}{\partial z}-2\frac{\partial\nu}{\partial\rho}\frac{\partial\nu}{\partial z}=0 \tag{2.5}$$

Equation 2.3 is the Laplace equation in cylindrical coordinates ρ, z. Furthermore, analysis of the Einstein equations shows that ν is actually the Newtonian potential of a mass distribution $w(\rho, z)$ with respect to cylindrical coordinates ρ, z in Galilean space-time.

Equations 2.4, 2.5 can be reformulated into the quadrature

$$\lambda(\rho,z)=\int_{\text{axis}}^{(\rho,z)}\rho\left(\left(\left(\frac{\partial\nu}{\partial\rho}\right)^2-\left(\frac{\partial\nu}{\partial z}\right)^2\right)\mathrm{d}\rho+2\frac{\partial\nu}{\partial\rho}\frac{\partial\nu}{\partial z}\mathrm{d}z\right), \tag{2.6}$$

where the lower bound is anywhere on the axis of symmetry and the integration trajectory lays in vacuum entirely. The potentials ν of different sources superpose linearly, but the function λ has to be almost always recalculated from eq. (2.6).

If the source of the field is an infinitely thin annular disc in the equatorial plane with mass density $w(\rho)$, the Poisson integral for ν leads to (Semerák, 2004)

$$\nu(\rho,z)=-4\int_b^\infty\frac{w(\rho')\rho'}{\sqrt{(\rho'+\rho)^2+z^2}}K\left(\frac{2\sqrt{\rho'\rho}}{\sqrt{(\rho'+\rho)^2}}\right)\mathrm{d}\rho', \tag{2.7}$$

where b is the Weyl inner radius of the disc[3] and $K(k)$ the complete elliptic integral of the first kind.

Due to the singular behavior of $K(k)$ around $k\to1^+$, ν has got as much finite derivatives as is the number of derivatives of $w(\rho)$ which vanish as $\rho\to b^+$. The non-analyticity of the potential ν around the inner radius of the disc proved to be important in our numerical study, since the function cannot then be expanded in it's proximity.

2.2.1 Schwarzschild black hole in Weyl coordinates

The Schwarzschild spherical coordinates are related to the Weyl coordinates by the following relations

$$\rho=\sqrt{r(r-2M)}\sin\theta,\ z=(r-M)\cos\theta, \tag{2.8}$$

where M could be any feasible constant, in this case the mass of the black hole. The respective potentials of the Schwarzschild black hole then read

[3]Simply the first ρ, where the disc "starts".

$$2\nu_{\text{schw}} = \ln\left(1 - \frac{2M}{r}\right), \tag{2.9}$$

$$2\lambda_{\text{schw}} = \ln\frac{r(r-2M)}{(r-M)^2 - M^2\cos^2(\theta)}. \tag{2.10}$$

From the transformation rules (2.8) it can be seen that the black hole horizon is transformed into a mere segment of the axis ranging from $z = -M$ to $+M$.

2.2.2 The Bach-Weyl ring and the first inverted Morgan-Morgan disc

Considering an infinitely thin ring of Weyl radius b and total mass $\mathcal{M}$ in the meridional plane, Bach & Weyl (2012, first pub. 1922) showed that the potential ν takes the form

$$\nu_{\text{BW}} = -\frac{2\mathcal{M}K(k)}{\pi\sqrt{(\rho+b)^2+z^2}},\ k = \sqrt{\frac{4b\rho}{(\rho+b)^2+z^2}}, \tag{2.11}$$

where $K(k)$ is again the elliptic integral. An explicit formula for λ is to be found in the cited article.

A class of static axi-symmetric solutions of Einstein's equations was published by Morgan & Morgan (1969) describing classes of gravitating infinitely thin discs with mass distributions

$$w^{(m)}_{\text{MM}}(\rho < b) = \frac{(2m+1)\mathcal{M}}{2\pi b^2}\left(1 - \frac{\rho^2}{b^2}\right)^{m-\frac{1}{2}}, \tag{2.12}$$

where $\mathcal{M}$ is the disc mass and b is it's Weyl radius. The discs are often called counter-rotating, since they have no net angular momentum and their stability is explained by particles orbiting back and forth in the disc with the same speed (Saa & Venegeroles, 1999). It is known that the Laplace equation is invariant with respect to Kelvin transformation:

$$\rho \to \frac{b^2\rho}{\rho^2+z^2},\quad z \to \frac{b^2 z}{\rho^2+z^2}, \tag{2.13}$$

rendering the mass distribution

$$w^{(m)}_{\text{iMM}}(\rho > b) = \frac{2^{2m}(m!)^2\mathcal{M}b}{(2m)!\pi^2\rho^3}\left(1 - \frac{b^2}{\rho^2}\right)^{m-\frac{1}{2}}. \tag{2.14}$$

By the transformation the disc is thus inverted from the inside and spread into infinity. The mass distribution however roughly vanishes as $\frac{1}{\rho^3}$ and the disc has a finite mass

$$2\pi\int_b^\infty w^{(m)}_{\text{iMM}}\rho\mathrm{d}\rho = \mathcal{M}. \tag{2.15}$$

The Newtonian potential of the first inverted Morgan-Morgan disc reads

$$\nu^{(1)}_{\mathrm{iMM}} = -\frac{\mathcal{M}}{\pi(\rho^2+z^2)^{3/2}}\left[\left(2\rho^2+2z^2-b^2\frac{\rho^2-2z^2}{\rho^2+z^2}\right)\operatorname{arccot}\sqrt{\frac{\Sigma-(\rho^2-b^2+z^2)}{2(\rho^2+z^2)}}\right.$$
$$\left.-(3\Sigma-3b^2+\rho^2+z^2)\sqrt{\frac{\Sigma-(\rho^2-b^2+z^2)}{8(\rho^2+z^2)}}\right], \tag{2.16}$$

where $\Sigma \equiv \sqrt{(\rho^2+z^2-b^2)-4b^2z^2}$. It is easy to show that for $\rho > b$

$$\lim_{z\to 0^{\pm}} \frac{\partial \nu^{(m)}_{\mathrm{iMM}}}{\partial z} = \pm 2\pi w^{(m)}_{\mathrm{iMM}}. \tag{2.17}$$

2.3 The pseudo-Newtonian approach

As can be seen from eq. (2.6), even very simple (highly symmetric) space-times are often superposed nonlinearly in relativity causing interesting new phenomena, but also technical difficulties. On the contrary, in Newtonian gravitation the effects of mass superpose linearly.

The idea of pseudo[4]-Newtonian potentials (PNP) is to capture or reproduce some of the essential features of motion in a relativistic solution by a suitably chosen potential in flat space.

2.3.1 Potentials for non-rotating black holes

As has been already mentioned in the introduction of this thesis, a pseudo-Newtonian potential was first introduced by Paczyński & Wiita (1980) to study the accretion flows of gas onto non-rotating astrophysical black holes in a simpler Newtonian mode. The potential for a black hole of mass M has the following form in spherical coordinates

$$\Phi_{\mathrm{PW}} = -\frac{M}{r-2M}. \tag{2.18}$$

If the spherical coordinate r is put in correspondence with the Schwarzschild radial coordinate, the potential reproduces a number of salient features of the Schwarzschild space-time. Namely, the marginally stable[5] and marginally bound[6] orbits are reproduced exactly ($r_{\mathrm{ms}} = 6M$, $r_{\mathrm{mb}} = 4M$) and the potential reproduces approximately also other features such as the binding energy and angular momentum of circular orbits (Tejeda & Rosswog, 2013).

Nowak & Wagoner (1991) introduced an alternative potential

$$\Phi_{\mathrm{NW}} = -\frac{M}{r}\left(1-3\frac{M}{r}+12\left(\frac{M}{r}\right)^2\right), \tag{2.19}$$

[4]The pseudo-Newtonian potentials usually *do not* comply to the classical Poisson equation $\Delta\Phi = 4\pi\rho$ in any good sense.

[5]The radius of the smallest stable circular geodesic giving then usually the inner edge of the accretion disc.

[6]The smallest circular geodesic with energy E¡m.

which reproduces exactly the marginally stable orbit with it's angular velocity Ω but fails to reproduce for example the marginally bound orbit by putting $r_{\rm mb} = 3.5M$.

A survey of PNPs has been given by **?** who introduce four new potentials for rotating and non-rotating black holes. They conclude however that the Paczynski-Wiita (PW) potential is most effective for non-rotating holes, rendering the parameters of accretion discs within 10-20% of accuracy. A refined PNP for rotating black holes was proposed by Semerák & Karas (1999).

Another very recent survey was given by Tejeda & Rosswog (2013) also introducing a new generalized potential by identifying it in a low-energy limit of the equations of motion of a test particle in the Schwarzschild space-time. The potential reads

$$\Phi_{\rm G} = -\frac{GM}{r} - \left(\frac{2M}{r-2M}\right)\left[\left(\frac{r-M}{r-2M}\right)\dot{r}^2 + \frac{r^2\dot{\phi}^2}{2}\right]. \qquad (2.20)$$

The low-energy limit is $-u_t \approx 1$ meaning mostly low velocities or weak fields, but not necessarily. The Tejeda-Rosswog potential reproduces exactly a number of traits of the Schwarzschild field such as the marginally bound, marginally stable and circular photon orbits and generally shows excellent behavior of test particles, notably failing only in connection with the coordinate behavior near the horizon. The effective approximation is however taken one step further – to a "generalized" pseudo-Newtonian approach as even a velocity dependence is introduced.

2.3.2 Chaos in Newtonian, pseudo-Newtonian and fully relativistic approaches

In this subsection we present a short review of the works analyzing chaos in fully relativistic and other modes concentrating mainly on the static, axially symmetric configurations with a central black-hole (massive monopole).

Vieira & Letelier (1999) considered a core-shell model describing a neutron star or a black hole with a hollow halo of matter in a Newtonian and relativistic mode. The authors found that even though the models show a similar regularity response to the breaking of reflectional symmetry around the meridional plane, the relativistic case showed much larger portions of phase space devoured by chaos.

The purely Newtonian monopole $1/r$ is thus considered to be an inappropriate approximation in small distances from the horizon. A very similar conclusion was drawn from the study of a superposition of a monopole and an infinite homogeneous thin disc in the relativistic and Newtonian mode conducted by Saa & Venegeroles (1999). The authors also considered a smoothening of the thin disc into a thick one in a purely Newtonian mode, finding the smoothening to suppress chaotic behavior.

In the footsteps of the latter study, Kiuchi, Koyama & Maeda (2007) have further analyzed the monopole–thick-disc system in a semi-classical approach. Even though purely Newtonian motion was considered, the authors have, as already mentioned in this chapter, utilized the quadrupole formula for retrieving possibly

emitted gravitational waves a purely relativistic phenomenon.

In a mission to incorporate the essential relativistic effects in many-body simulations, Guéron & Letelier (2001) tested the fully relativistic, pseudo-Newtonian and Newtonian description of a massive monopole and a dipolar halo. Furthermore, they also compared special-relativistic and Galilean equations of motion for the pseudo-Newtonian case.

The Newtonian case is completely integrable, but by modifying the monopole potential, chaos spurs in the phase space strengthened further by the special-relativistic equations of motion. On the contrary, the relativistic formulation shows through Poincaré surfaces of section a somewhat weaker irregularity than in the motion in the field of the Paczynski-Wiita potential. For one particular set of parameters, the authors have found a larger maximal Lyapunov number in the pseudo-Newtonian case than in the relativistic one and an even larger one for the special-relativistic motion.

As the authors themselves state, in an attempt of a "zeroth step" to incorporate relativistic effects, Steklain & Letelier (2006) investigated the influence of introducing the PW potentials instead of the classical ones in the Hill problem. Due to the nature of the Hill problem, the PNPs did not make a great difference in the physically relevant cases, only slightly changing the stability of the system. By investigation of maximal Lyapunov numbers and escape basin boundaries they even concluded that for a certain finite value of Schwarzschild radius r_s (in $1/(r - r_s)$) the system is *less chaotic* than in the Newtonian case.

Even though PNPs have not been involved in the work of Wu & Zhang (2006), they have quite interestingly found that for a superposition of Weyl space-times of a black hole and a thin disc, omitting the cross terms of (2.6) leads to apparent attenuation of chaos in the geodesic flow. According to the authors, the result suggests that the non-linear superposition may be one of the "mechanisms" of chaos generation in the space time. This conjecture would however require a more stringent investigation.

Chapter 3

Simulation of Test Particle Motion

3.1 Statement of the problem

In Semerák & Suková (2010, 2012); Suková (2009) the dynamics of time-like geodesics in exact static, axially and reflection symmetric space-times has been studied. The fields describe a superposition of a central Schwarzschild black hole with thin discs and rings, namely, the first and fourth disc of the inverted Morgan-Morgan (iMM) family and the Bach-Weyl (BW) ring described in the previous chapter.

The study investigated the influence of parameters of the system on the Poincaré surfaces of section in the equatorial plane and further analysed time series of phase variables by various methods to indicate different degrees of chaos. The varying parameters were specific particle momentum $\ell \equiv \frac{L}{m} = u_\phi$, specific particle energy $\mathcal{E} \equiv \frac{E}{m} = -u_t$, inner disc or ring *Schwarzschild* radius $r_{\rm disc}$ and ring or disc mass $\mathcal{M}$ (see figs 3.1-3.4 for examples).

A variety of responses to the changes of parameters have been found on the Poincaré surfaces of section of which the full set is to be found in Suková (2009).

As described in the previous chapter, pseudo-Newtonian potentials often serve as substitute to a fully relativistic solution in important astrophysical problems. It is an open question how much of the relativistic behavior is actually reproduced by the modified potentials. At least a qualitative correspondence in every aspect of motion should however stand for the pseudo-Newtonian approach to be justified.

Our investigation will thus try this correspondence by numerically simulating test particle dynamics in the mentioned disc/ring and black hole problem with the sole difference of utilizing the pseudo-Newtonian approach instead of the relativistic formulation. The Hamiltonian of the free particle will then take the form

$$H = \frac{1}{2}\boldsymbol{M}^{-1}(\boldsymbol{p},\boldsymbol{p}) + V_{\rm PN} + V_{\rm ext}, \tag{3.1}$$

where $\boldsymbol{p}$ are canonical momenta of the particle, $\boldsymbol{M}$ is the mass form or alterna-

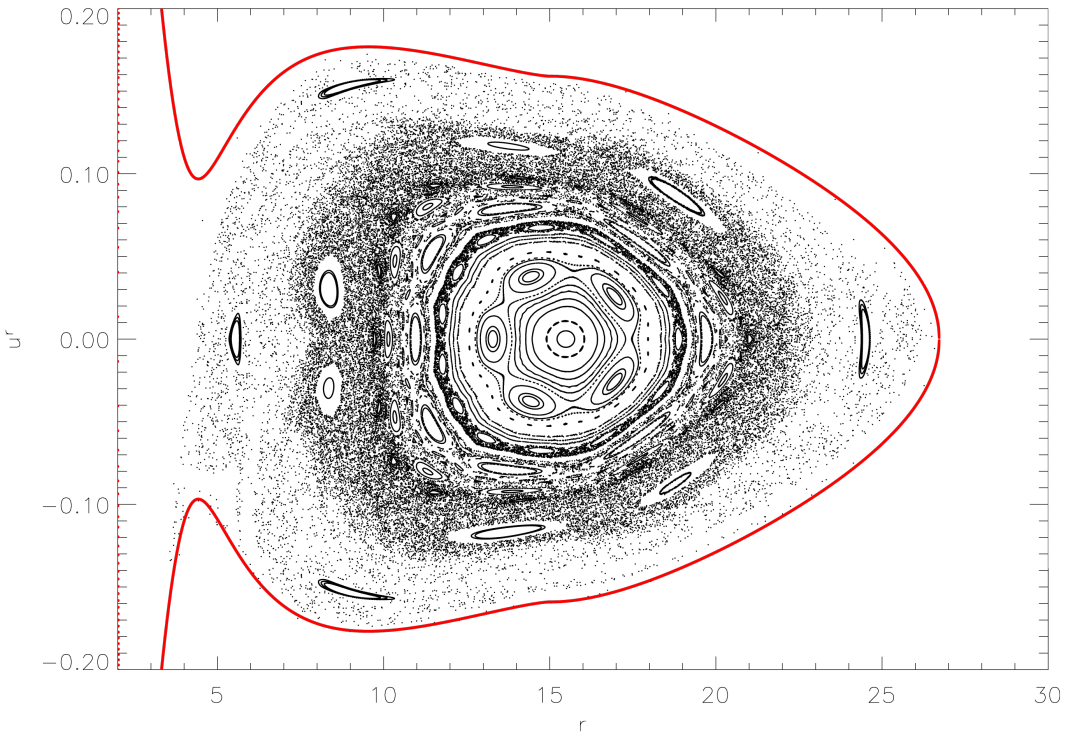

Figure 3.1: Relativistic surface of section for the first iMM disc superposition for the parameter values $r_{\rm disc} = 15M$, $\mathcal{E} = 0.955M$, $\ell = 3.75M$, $\mathcal{M} = 0.5M$ (Suková, 2009)

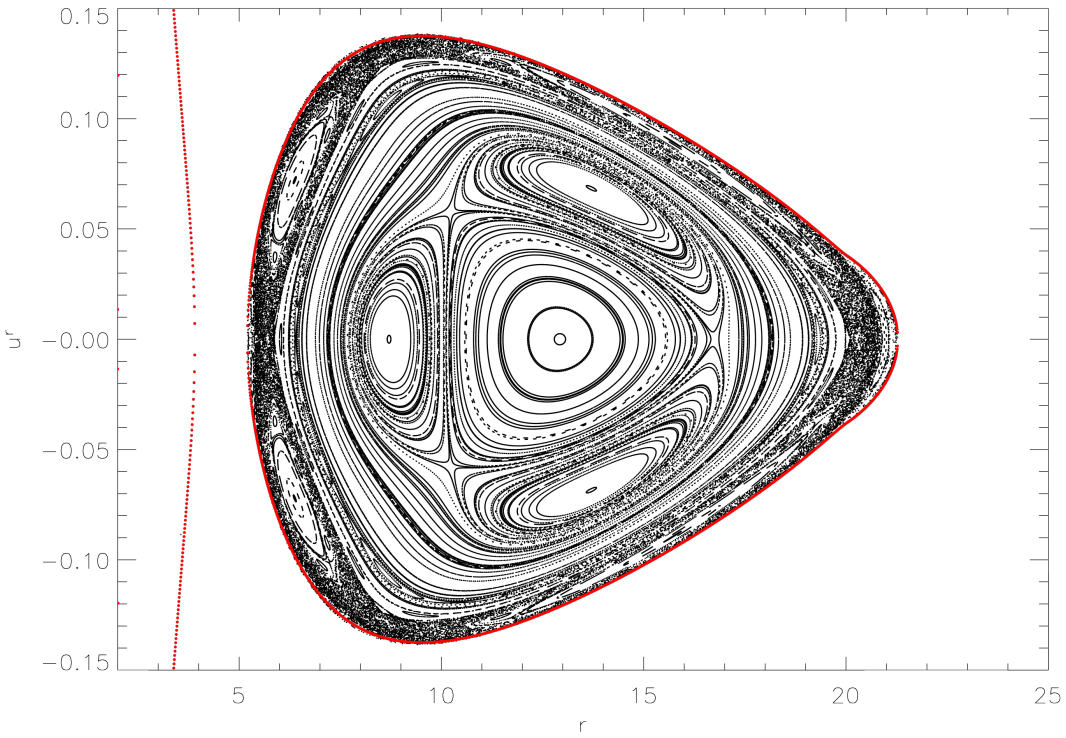

Figure 3.2: Relativistic surface of section for the first iMM disc superposition for the parameter values $r_{\rm disc} = 20M$, $\mathcal{E} = 0.955M$, $\ell = 3.75M$, $\mathcal{M} = 0.42M$ (Suková, 2009)

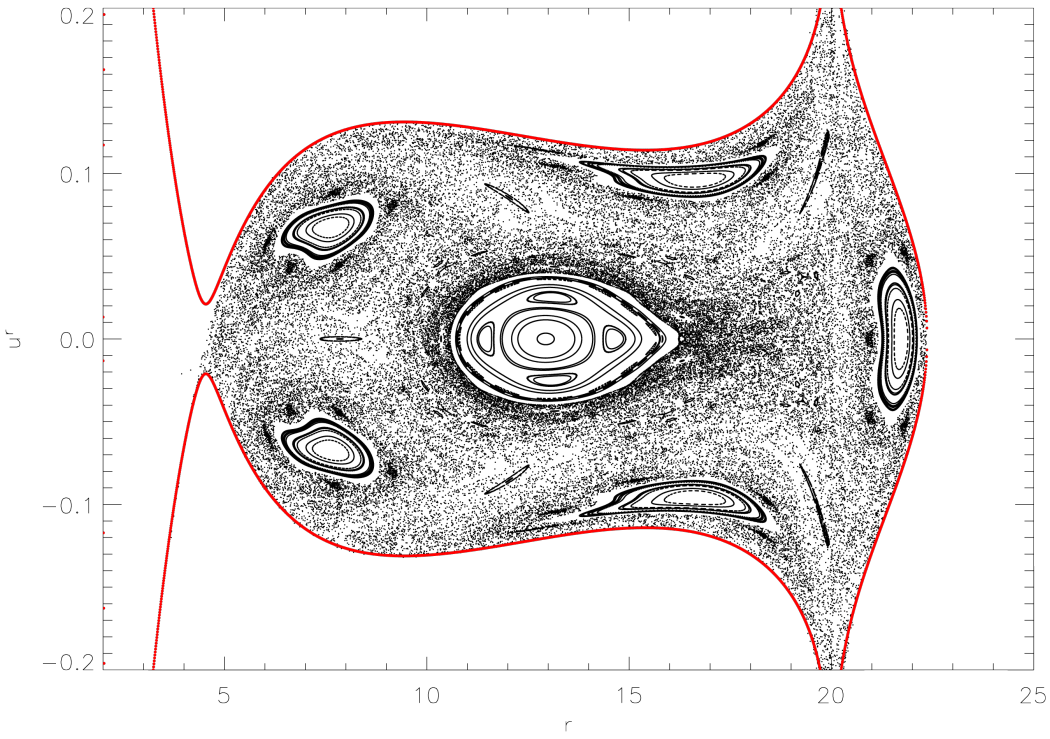

Figure 3.3: Relativistic surface of section for the BW ring superposition for the parameter values $r_{\rm disc} = 20M$, $\mathcal{E} = 0.935M$, $\ell = 3.75M$, $\mathcal{M} = 0.5M$ (Suková, 2009)

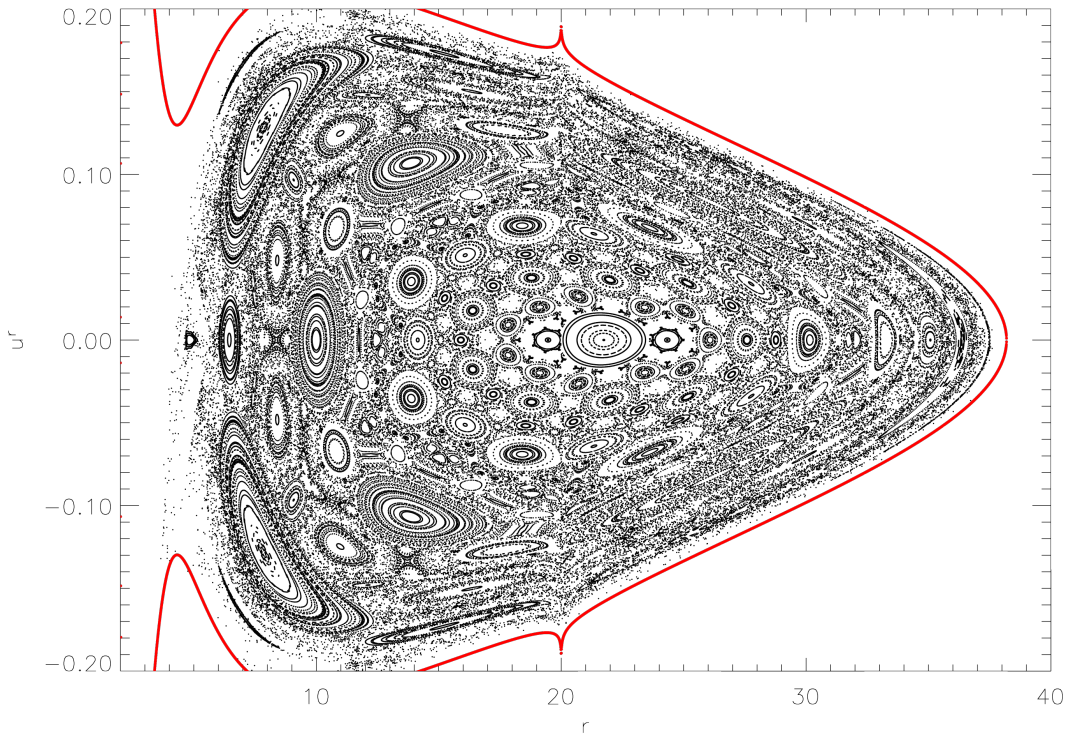

Figure 3.4: Relativistic surface of section for the BW ring superposition for the parameter values $r_{\rm disc} = 20M$, $\mathcal{E} = 0.935M$, $\ell = 3.75M$, $\mathcal{M} = 0.5M$ (Suková, 2009)

tively mass matrix[1] and V_{PN} is the pseudo-Newtonian potential of a black hole and V_{ext} the potential of the external source, namely ring or disc. In our case the mass matrix will be effectively coordinate independent and the potentials will be, on the other hand, momentum independent, thus falling in a class of Hamiltonians commonly called "separable".

In this chapter, we will now present the procedure of testing the pseudo-Newtonian vs. relativistic correspondence and the results.

3.2 Newtonization of the space-times

Firstly, as our PNP we choose the Paczynski-Wiita (PW) potential presented in the last chapter:

$$\Phi_{\mathrm{PW}} = -\frac{M}{r-2M}. \tag{3.2}$$

Secondly, we choose the Bach-Weyl ring and the first Morgan-Morgan disc as the external source perturbing the black hole background.

The last but perhaps the least trivial choice to make is the choice of coordinate equivalence. To narrow the question - *are the Weyl or the Schwarzschild coordinates the "right" Euclidean coordinates*[2] *in which to express the Newtonian motion?* We choose the Weyl coordinates, as in those the external potentials are exactly the Newtonian potentials of identical mass distributions in Euclidean space. We then superpose the field of the external potentials with the PW potential by putting $r = \sqrt{\rho^2 + z^2}$.

The stated choice however does not have any canonical or rigorous meaning. I.e., the PW potential corresponds through the Newtonian Poisson equation to negative mass distributions behind the horizon and a positive mass density vanishing approximately as $\frac{1}{r^4}$ far from the horizon. Furthermore, as has been mentioned in the previous chapter, the Swarzschild black-hole horizon is represented as a bar on the symmetry axis in Weyl coordinates, which obviously isn't the case of our superposition.

The purpose of the relativistic vs. pseudo-Newtonian comparison is to investigate the justification of common practice in astrophysics, which is most usually a fully Newtonian approach only superseding the Newtonian monopole by the pseudo-Newtonian potential. Our selection can thus be understood as an effort to mimic the conventional astrophysical method of modeling the situation without the use of relativity.

3.3 Numerical realization

Numerical integration reproduces a trajectory of a dynamical system through discrete steps h with an accumulated error of order h^r. The global error of the trajectory, usually hidden behind the symbol $\mathcal{O}(h^r)$, is however a complicated perturbation power series which is difficult to investigate, since even the round-off error in every integration step plays an important role in it's creation.

[1] For example in Euclidean coordinates $M_{ij} = m\delta_{ij}$.

[2] In the sense of respective Euclidean space in spherical and cylindrical coordinates.

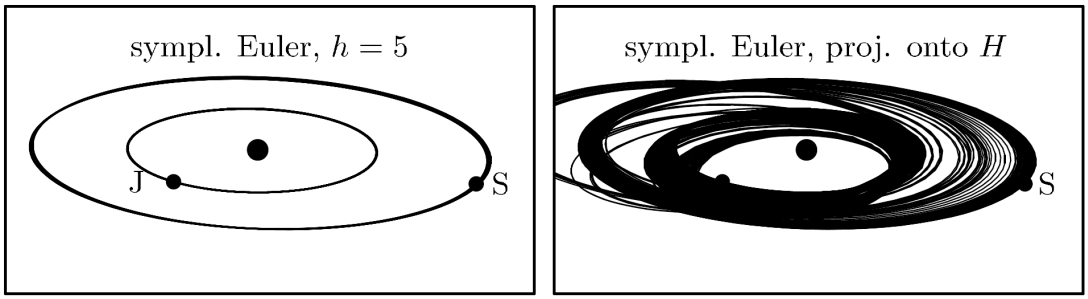

Figure 3.5: Numerical integration of the Sun-Jupiter-Saturn system, image due to Hairer (2006)

A quiet assumption of many applications of numerical integration is the fact that for finite h the perturbation amounts to a reasonable error of an approximate form Ah^r where A is a not too large constant. This is obvously not true in chaotic dynamical systems where an infinitely small perturbation of initial conditions may lead to qualitatively different trajectories and the global error power series will not converge in the stated manner.

The main argument in support of the usage of numerical integration in chaos are thus the Shadowing theorems of which an overview is given by Palmer (2009). The Shadowing theorem for continuous-time dynamical systems states that under certain conditions the errorfull numerically acquired trajectory is shadowed within a certain ϵ-range by an actual trajectory of the dynamical system with slightly different initial conditions.

As has been mentioned in the first chapter about Hamiltonian chaos, one of the main features of Hamiltonian systems is the preservation of the symplectic structure and the Hamiltonian. An overview of approaches to energy conservation has been given e.g. by Hairer (2006) and Hairer, Lubich & Wanner (2006).

As illustrated in figure 3.5, the attempts to conserve energy *exactly* by projections of the trajectory on the energy hypersurface has been proven to be even destructive towards the qualitative properties of the integrated solution. In the following subsection we will present a very brief overview of the methods of tackling energy conservation and of integration methods tailored for Hamiltonian systems and discuss the application to our problem.

3.3.1 Symplectic integration

The most frugal approach to energy conservation has surprisingly come from the exploitation of the symmetries of the dynamical system, namely time-reversal symmetry, reversibility and the mentioned symplecticity. In studies of simple mechanical systems an "accidental" discovery of the properties of symplectic algorithms has been found leading to analytical investigations and a notable result of Benettin, Galgani & Giorgilli (1980). The result basically states that the flow of a symplectic integrator is an exact flow (up to round-off error) of a Hamiltonian system very close to the original one for exponentially long times.

After a few necessary definitions, we shall mention here only a simplified reformulation of the result referring the reader to the cited article for details.

Definition 3.1. Let $\boldsymbol{y}(t)$ be the point of a trajectory at time t in a dynamical system. Then we define an *h-step integrator of order r* as a mapping Ψ_h for which

$$\Psi_h(\boldsymbol{y}(t)) = \boldsymbol{y}(t+h) + \mathcal{O}(h^{r+1}). \tag{3.3}$$

We call the sequence $\{y_n = \Psi_h^n(y(0))\}$ the *pseudo-trajectory*. An integrator is called *symplectic*, if it preserves the symplectic form $\boldsymbol{\omega}$ under differential pull-back[3]. An integrator is called *time-reversal symmetric* when the following condition holds:

$$\Psi_h = \Psi_{-h}^{-1}. \tag{3.4}$$

For a Hamiltonian dynamical system with canonical momenta and coordinates $(\boldsymbol{p}(t), \boldsymbol{q}(t))$ we call the integrator *reversible* if the following holds[4]:

$$\Psi_h(\boldsymbol{p}(t), \boldsymbol{q}(t)) = \Psi_{-h}(-\boldsymbol{p}(t), \boldsymbol{q}(t)). \tag{3.5}$$

Theorem 3.1. *Consider*

- *a Hamiltonian system with an analytic Hamiltonian function H and*
- *a symplectic integrator $\Psi(h)$ of order r.*

As long as the pseudo-trajectory $\{y_n\}$ is bounded, we have, for $h \to 0$,

$$H(y_n) = H(y_0) + \mathcal{O}(h^r) + \mathcal{O}(nhe^{-\gamma/\omega h}), \tag{3.6}$$

where $\gamma > 0$ depends only on the method and ω is related to the Lipschitz-constant[5] (or highest frequency) of the dynamical system.

This formulation is due to Hairer (2006). In numerous situations the third term on the right hand side is exponentially small and thus the energy error of the integration is bounded to very small quantities. In practice the error may only be due to the round-off error with the algorithm faulting only negligibly.

Another property of symplectic algorithms is the result that if a symplectic integrator preserves energy *exactly*, it is the exact flow of the system up to a time reparametrization. Hence if the energy is preserved almost exactly, it is natural to assume the flow almost exact[6].

However, the most palpable drawback of symplectic integrators is the fact that varying the time-step h during evolution breaks the error estimate (3.6) and has been proven numerically to destroy the invariant geometric structures (local integrals/invariant tori) of the problem. Special treatment for varying time-steps and symplecticity is required, the respective integrators are very difficult to construct and usually apply only to a certain class of Hamiltonians.

[3]For conventional reasons the symplecticity of an integrator is very often equivalently defined by push-forward of the symplectic bivector $\boldsymbol{\omega}^{-1}$ or "symplectic matrix" $\boldsymbol{J}$.

[4]There exists a more general definition of a reversible integration method not needed in this thesis.

[5]The maximal slope of a function.

[6]A rigorous proof of this assumption is however difficult to find in literature.

The important class of time-reversal symmetric integrators and their properties will not be developed further in this thesis and the reader is referred to chapter V and XI of Hairer, Lubich & Wanner (2006). We only note that the reversible and time-reversal symmetric integrators have similar properties as the symplectic ones including linear error growth, long-time integral near-conservation and existence of invariant tori.

3.3.2 Ring, horizon and disc singularities

In our case, the Hamiltonian is however *non-analytic*, bearing singularities (on the ring and the horizon) and cusps (on the disc, thus leading to jumps in the time-derivative vector field). Hence in certain parts of the potentials the Lipschitz-constant grows without bounds or is explicitly inifinite, corrupting the error estimate (3.6) and causing energy error growth in the respective areas.

Furthermore, in the proximity of the horizon, the force due to the PW potential is in the form $(\textit{difference of two close floating point numbers})^{-2}$ leading to vast round-off errors. This problem as well as a number of various other encountered problems with numerical evaluation mainly due to floating point arithmetic, could possibly be resolved by higher number representations which are however implementation difficult.

Another violation of the conditions for the estimate (3.6) is the fact that the trajectories falling into the horizon head towards infinite velocities[7] thus actually stopping to be bounded in the phase space. This flux of the phase space of initial conditions into the horizon is reflected by possibly numerical deformations of the observed sticky regions and of the "visited areas" of chaotic trajectories.

We have tried to tackle these issues by choosing a time-reversal symmetric and reversible integrator with a variable time-step called *IGEM* introduced by Seyrich & Lukes-Gerakopoulos (2012) which would then bind the error growth in steep potentials. However a time-reversal symmetric integrator is necessarily implicit, i.e. the evolution is found as an iterative solution of an implicit equation. Even though the convergence of the fixed-point iteration of the implicit equation was cleverly handled by the algorithm for sufficiently smooth potentials, it not so surprisingly failed at the jump in the time-derivative vector field.

Following the iteration convergence difficulties, we have thus switched to an explicit symplectic integrator of sixth order due to Blanes & Moan (2002). The specific method is a partitioned Runge-Kutta-Nyström method (possible only for separable Hamiltonians) denoted by SRKN^b_{11}. For details on and definitions of the mentioned terms the reader is referred to the cited article.

The main advantage of the method is a simple implementation and low computation cost per step, yet without time-step control.

[7] An analogy of the particle passing through coordinate $t = \infty$ by falling into the horizon.

3.4 Poincaré surfaces of section

For the simulation, almost identical sets of parameters of the system with the first Morgan-Morgan disc and the Bach-Weyl ring have been taken as in Suková (2009). Following the lines of the cited thesis, we have conducted simulations producing Poincaré surfaces of section for these system parameters with the geometrized units $G = c = 1$ and the length unit M. Furthermore, the mass of the particle is also taken $m = 1$ in accordance with the fact that the physical trajectory is mass-independent and the canonical momentum is then identical with the particle velocity $\boldsymbol{u}$. Applying all the stated choices, the Hamiltonian in units of M reads

$$H = \frac{1}{2}(u_\rho^2 + u_z^2) + \frac{\ell^2}{2\rho^2} - \frac{1}{r-2} + V_{\mathrm{ext}}(\rho, z). \tag{3.7}$$

For a fixed V_{ext}, the Poincaré surface of section was chosen in the equatorial plane $z = 0$ at a fixed specific energy $\mathcal{E}$ and specific angular momentum ℓ. As a consequence, for a set of initial coordinates ρ, u_ρ the inital size of u_z on the plane is determined. En plus, the Hamiltonian is also reflectionally symmetric with respect to the equatorial plane and thus the sign of initial u_z is irrelevant. The Poincaré surface of section is thus a well defined single-valued discrete map of the ρ, u_ρ plane with all the important symplectic properties presented in the first chapter.

Chapter 4

Results of the Simulation

In this chapter we present the results of the simulations of the problem of the Bach-Weyl (BW) ring and first inverted Morgan-Morgan (iMM) disc superpositions introduced in the previous chapter.

The sets of parameters are not always strictly taken the same as in Suková (2009), yet the series are taken so that a clear comparison can be made. Every series of Poincaré sections depicting a given parameter influence has a first figure (such as 4.2, the first figure of the specific-energy influence series in the iMM superposition) presenting the set of parameter values staying constant. The other figures of the series then only state the changing values of the given influence-parameter (such as $\mathcal{E}$ in figs 4.3-4.6) with reference to the first figure of the series. The units are *always* assumed to be M and are not further mentioned[1].

Almost every surface of section also shows the curve of zero velocity (COZV) in gray - the border of the energetically allowed area - whereas the points of intersection are plotted black. For technical reasons, all the figures with surfaces of sections are placed at the end of the chapter

It should be noted that even though the relativistic surfaces of section from Suková (2009) are often referred and described in this chapter, a full set of the relativistic surfaces of section would expand the present thesis unbearably and would also be mere replicas of those in the cited thesis. The reader may thus rely on the brief and partial description in this chapter or can asses the relativistic vs. pseudo-Newtonian comparison utilizing the original thesis.

When talking about the relativistic vs. pseudo-Newtonian correspondence, we take the Euclidean radius b of the disc or ring equivalent to r_{disc} as well as with all the other parameters (even though this correspondence may be highly flawed).

The velocity coordinate is taken as u_ρ in contrast to the relativistic u^r but in the equatorial plane $z = 0$ the Euclidean interpretation of u^r is the same as u_ρ.

The last difference from Suková (2009) is the energy convention. We adopt the convention common in Newtonian mechanics, i.e. the specific rest energy in zero potential is 0, whereas in relativity the same situation gives specific rest energy 1.

In numerous surfaces of section, the influence of numerical error is discernible. As per usual, there was a typical erroneity associated with a given superposition or

[1]The parameters P can be instead thought of as dimensionless: $\tilde{P} = P/M$

set of parameters since small tweaks and variations were added to the numerical algorithms on the go. Hence, observing phenomena such as invariant structure blurring or COZV crossing might be used as a rule of thumb for assessing the reliability of other phenomena on the entire surface of section.

The relative energy error was however never allowed to cross 10^{-3}, and in the less cumbersome BW ring superposition, relative energy error larger than 10^{-4} was not allowed.

4.1 The first inverted counter-rotating Morgan-Morgan disc

The first iMM disc has a jump in the derivative in the z direction for $\rho > b$. The onset of the jump at the disc inner edge is sudden and non-analytic, causing perhaps the strongest sources of perturbation in it's neighborhood when the particle passes through the disc.

On the other hand, intuitive arguments utilizing for example Gauss's law can show that the field is fairly weak on the inside of the disc. Hence, the disc can be understood as a quite general perturbation when the inner edge is out of the reach of the allowed area.

4.1.1 Influence of the particle energy

The surfaces of section for the test particle specific energy variation were taken with the parameter values $\mathcal{M} = 0.5$, $b = 20$, $\ell = 3.75$ starting from $\mathcal{E} = -0.048$ and are to be found in figs 4.2-4.6.

Right from the lowest energies, the main discrepancy in comparison with the relativistic case is the communication of the allowed area with the horizon. This makes the early pseudo-Newtonian surfaces of section resemble the higher energetic relativistic surfaces of section starting from $\mathcal{E} = -0.044$ (0.956 with the addition of rest energy), where the allowed area also communicates with the horizon with large portions of chaotic phase space and bears a central 1-periodic island wrapped by a large 3-periodic island.

The mentioned characteristic then more or less continues for the sections with growing $\mathcal{E}$ untill $\mathcal{E} = -0.035$ where in both cases the 3-periodic island vanishes and a 5-periodic one appears (discernible as blank spaces in fig. 4.5).

Higher energies $\mathcal{E} = -0.025, -0.02$ (fig. 4.6) then discord in the fact that a 2-periodic island is additionally formed in the pseudo-Newtonian case, whereas the relativistic case displays only the 1-periodic dominant island. The calculation of the highest two energies turned out to be very time-costly so only a rough surface of section is presented in fig. 4.6.

4.1.2 Influence of the angular momentum

The angular momentum influence on the surfaces of section was studied for the parameter values $\mathcal{M} = 0.4$, $\mathcal{E} = -0.4635$, $b = 20$, starting from $\ell = 0.65$ and is depicted in figs. 4.7-4.9. The allowed areas are large and vastly open to the horizon for most values of L, hence the chaotic trajectories usually did not leave

many traces on the section before falling into the black hole. Also for this reason the first three surfaces of section do not have a visible COZV in the plots.

Firstly, the main stable orbit and it's island are visible with only three "ghosts" in the pseudo-Newtonian case where on the other hand the relativistic case displays a robust 3-periodic island. The 3-periodic islands become more robust with growing angular momentum but the pseudo-Newtonian image does not reach the regularity of the relativistic surfaces of section which even close the communication channel with the horizon for $\ell = 3.75$.

The COZVs tend to tighten the channel to the horizon much more in the relativistic case, which seems to be the reason for the greater regularity of the relativistic series.

4.1.3 Influence of the inner radius of the disc

The surfaces of section for small b with $\mathcal{M} = 0.5$, $\ell = 3.75$, $\mathcal{E} = -0.045$ are obviously the most erroneous from the whole set due to the frequent (and sometimes even necessary) passing through the time-derivative field jump on the disc. Most notably the first $b = 3$ is probably outright wrong because fo the COZV and invariant structure crossing.

Even worse than the one-sided-smooth jump is the completely non-analytic ring edge at which we had difficulty in evaluating the time-derivative vector field precisely. This can be seen most explicitly in the haziness introduced when the disc edge coincides with the stable 1-periodic trajectory at $b = 15$ (fig. 4.12).

Apart from the numerical problems, there is accordance with the relativistic case even in the sequence of periodic island layers $1 - 5 - 3$ counting from the central 1-periodic trajectory. The pseudo-Newtonian case then displays the 5-periodic island for slightly higher radii until $b = 17$. Both the cases fully coincide with growing inner disc radii from about $b = 18$ in the tendency of slowly eliminating chaos in the phase space by a growing 1-periodic island with a large 3-periodic layer.

The main dicrepancy is the absence of closing-off of the allowed area from the horizon for higher radii ($b = 20+$ in the relativistic case). Such a closing-off does not occur in the pseudo-Newtonian case even for higher radii than presented in Suková (2009) (fig. 4.15).

4.1.4 Disc mass influence

In the case of the disc mass influence on surfaces of section of the parameter values $\mathcal{E} = -0.045$, $\ell = 3.75, b = 20$ starting from $\mathcal{M} = 0.1$ (figs. 4.16-4.27), the allowed area is again open to the horizon right from the beginning unlike the relativistic case. Consequently, the typical 1-periodic island with a 3-periodic island bracelet is observed even for the initial mass of the disc again in contradiction to the relativistic sections.

In the relativistic case the 3-period island created at $\mathcal{M} = 0.1$ survives up to the perturbation $\mathcal{M} = 0.86$, whereas in the pseudo-Newtonian case the 3-island is destroyed as early as for $\mathcal{M} = 0.7$. In both cases, the 3-island is superseded with a 5-periodic island.

The 5-periodic island, or more precisely it's remnants, survive perhaps until $\mathcal{M} = 1.2$, 1.025 in the relativistic and pseudo-Newtonian case, respectively. The central 1-periodic island transforms into a 2-periodic island at $\mathcal{M} = 1.05$, 0.98 in the relativistic vs. pseudo-Newtonian case, respectively. A first appearance of a new 1-periodic island in between the 2-periodic island occurs at $\mathcal{M} = 1.2$, 1.1, respectively.

The overall qualitative tendency is thus almost identical, yet the spawning and vanishing of islands occurs for slightly weaker perturbations in the pseudo-Newtonian case.

4.2 The Bach-Weyl ring

The Bach-Weyl ring is a more singular and thus in a sense "stronger" gravitating source (a linear singularity) than the first iMM disc. Hence, a larger disagreement of the simulations with the relativistic case is expected. The allowed phase space is also vastly different since the singular ring creates it's own allowed area for an arbitrarily large binding energy no matter whether the area is or is not topologically connected with the original black-hole allowed area in phase space.

The BW ring will play a major role in the formation of any invariant structure in the nearby phase-space and can't thus be strictly regarded as a perturbation to the field. However, once far away enough, similar perturbation effects as for the first iMM disc are also to be expected.

4.2.1 Influence of the particle energy

The initial situation for the surfaces of section at $\ell = 3.75$, $\mathcal{M} = 0.5$, $b = 20$ in figs 4.28-4.34 starting from specific energy $\mathcal{E} = -0.085$ is very similar in the relativistic case – there is a set of two disconnected allowed areas (one near the former stable circular orbit and the next one near the ring) with regular motion and no communication with the horizon.

The situation however quickly changes in the pseudo-Newtonian case as the "ring area" becomes fully chaotic and the area around the stable 1-periodic orbits connects with the horizon at $\mathcal{E} = -0.08$. The two disconnected areas connect as early as at $\mathcal{E} = -0.075$ (fig. 4.29), unlike the relativistic case. However, for higher energies the main characteristics coincide - the allowed area is simply connected and communicating with the horizon with a most notable 1-periodic island and some minor higher periodic islands.

At about $\mathcal{E} = -0.055$ (a tick later in the relativistic case), the 2-periodic island inside the ring appears followed by the appearance of a 2-periodic island oscillating from the around the radius of the ring. At $\mathcal{E} = -0.04$ the inside 2-periodic island disappears and the "oscillatory" island dominates in both cases. A "new" stable 1-periodic orbit appears along with it's island gaining magnitude again in accordance in both cases at $\mathcal{E} = -0.035$. The highest-energy surface of section at $\mathcal{E} = -0.015$ was unreachable numerically with sufficiently small energy error in our case, most probably because of the "almost scattering" nature of the states.

4.2.2 Influence of the ring radius

There is hardly any strong analogy with the relativistic case in the influence of the variation of b on surfaces of section at $\mathcal{E} = 0.94$, $\ell = 3.75$, $\mathcal{M} = 0.5$. There is a discrepancy even in the qualitative properties of the COZVs for $b > 23$. The COZVs in the relativistic case close the escape route to the horizon and as early as at $b = 26$ disconnect the allowed regions into two distinct parts. In the pseudo-Newtonian case the horizon isn't cut off at all and the disconnection occurs at $b = 29$.

Appart from a similar portion of connected chaotic regions and the strong role of the central 1-periodic island with intermittent stickiness, there is perhaps a similarity between two sets of islands of *different periodicity*. Namely a 4-periodic island in the relativistic case and a 3-periodic one in the pseudo-Newtonian grow through $b = 21$ to higher radii and survive the conversion to the less chaotic mode at the highest radii $b = 25+$.

The figures 4.38, 4.39 for $b = 25$, 26, 27, 29 clearly demonstrate the non-linear dependence of the surfaces of section on the radius b since we can observe intermittent connection and disconnection of the separatrix chaos of the 3-periodic island with the chaotic sea.

The apparent discord between the relativistic and pseudo-Newtonian formulation may be caused by the fact that the qualitative properties of the motion are very sensitive to the ring radius and with a finer step of variation, analogies might be found at different but close radii.

4.2.3 Influence of the ring mass

There are two important types of characteristic islands in the "evolution" of the Poincaré surfaces of section in dependence on the mass of the ring $\mathcal{M}$ at $\ell = 3.75$, $\mathcal{E} = -0.023$, $b = 20$ depicted in figs 4.40-4.46. The first island is of the original 1-periodic stable orbit and and the second are islands of a 2-periodic trajectory "oscillating" around the ring.

A straight-forward analysis of the evolution is not easily possible, since for small parameters starting from $\mathcal{M} = 0.001$, uncountable complex structures spur all over the surface of section. This phenomenon is not in contradiction with the KAM-theory which in principle predicts the creation of islands of arbitrary order and periodicity.

The reasons for the realization of such a phenomenon in this case may however be two.Firstly, the singular ring is placed very close to the former stable circular orbit[2] (notice the slightly more complex structures in the case of the iMM disc in fig. 4.13) thus maybe hitting a "weak spot" of the whole island. Secondly, the steep and singular potential may by definition provide a spectrum of perturbations richer in the high-frequency region.

The generic 3-periodic island known from the "low frequency" perturbation modes of the first iMM disc superposition as well as the 2-periodic "oscillation" island are firstly discernible through $\mathcal{M} = 0.02$, 0.04 in accordance with the relativistic

[2]There is exactly one stable circular orbit for a fixed ℓ in the situation unperturbed either by the disc or ring. The circular trajectory is represented as the centre of the dominant 1-periodic island.

case. Even though the complex structures are not easy to analyze, *there are discernible cases of higher periodic islands which do not have a corresponding island in the relativistic case and vice versa.*

The correspondence however fails most notably in the case of the strongest ring field $\mathcal{M} = 1.1$ where apart from the oscillatory island another large 2-periodic island with an unstable periodic trajectory are formed outside the ring from the former 1-periodic island. This is in strong contradiction to the relativistic case where the 1-periodic island grows and does not change it's nature.

4.3 Conclusions

As expected, differences between the surfaces of section in the relativistic and pseudo-Newtonian cases *were* found. However, in some cases the qualitative correspondence for slightly different values as in the case of the iMM disc mass influence was quite impressive, considering the fact that the PW potential is a mere effective *ansatz*.

Apart from a few examples of major periodic islands undubbed in the relativistic surfaces of section such as for the highest perturbation masses of both the ring and the disc, the overall qualitative correspondence in the sense of "roughly same section phenomena at roughly same parameter values" was not gravely violated.

Furthermore, the disc and ring masses raised on the same level as the black-hole mass would for the sake of consistence also require special pseudo-Newtonian modifications as similarly strong gravitating sources. In the case of extreme ring and disc masses, the analogy thus failed beyond the borderlines of it's consistent applicability.

Nonetheless, as the greatest source of discord could be identified the different characteristics of the allowed areas for the surfaces of section. The PW potential was numerically observed to close the areas for smaller sets of parameters which caused the overall image of the pseudo-Newtonian case to be slightly less regular.

The inconsistency of the ring radius influence on the sections may also be caused by the already mentioned "wildness" of the dependence together with consistency problems in the coordinate interpretation. The Weyl ρ and Schwarzschild r are related by $\rho = \sqrt{r(r-2M)}$ in the equatorial plane as can be seen in fig. 4.1. This relation slowly converges to equivalence but always shifts the meaning of the ρ or r coordinate according to which Euclidean interpretation we choose.

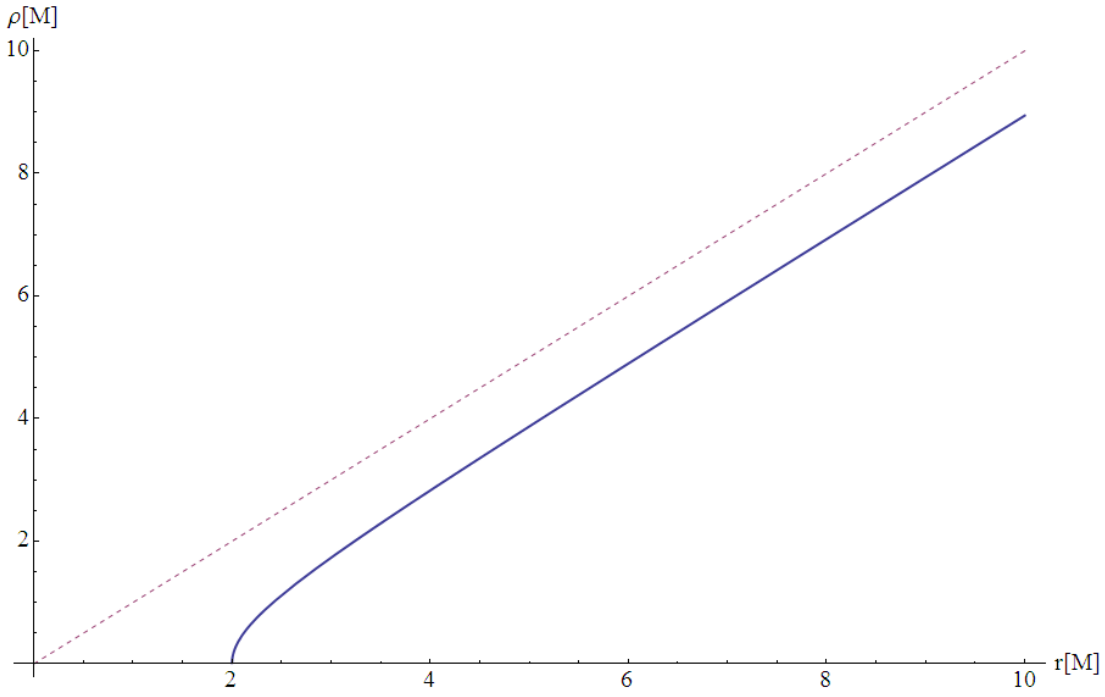

Figure 4.1: The Weyl ρ and Schwarzschild r relation at $z = 0$ or $\theta = \pi/2$. The relation $\rho = \sqrt{r(r-2M)}$ is in blue and the relation $\rho = r$ is dashed.

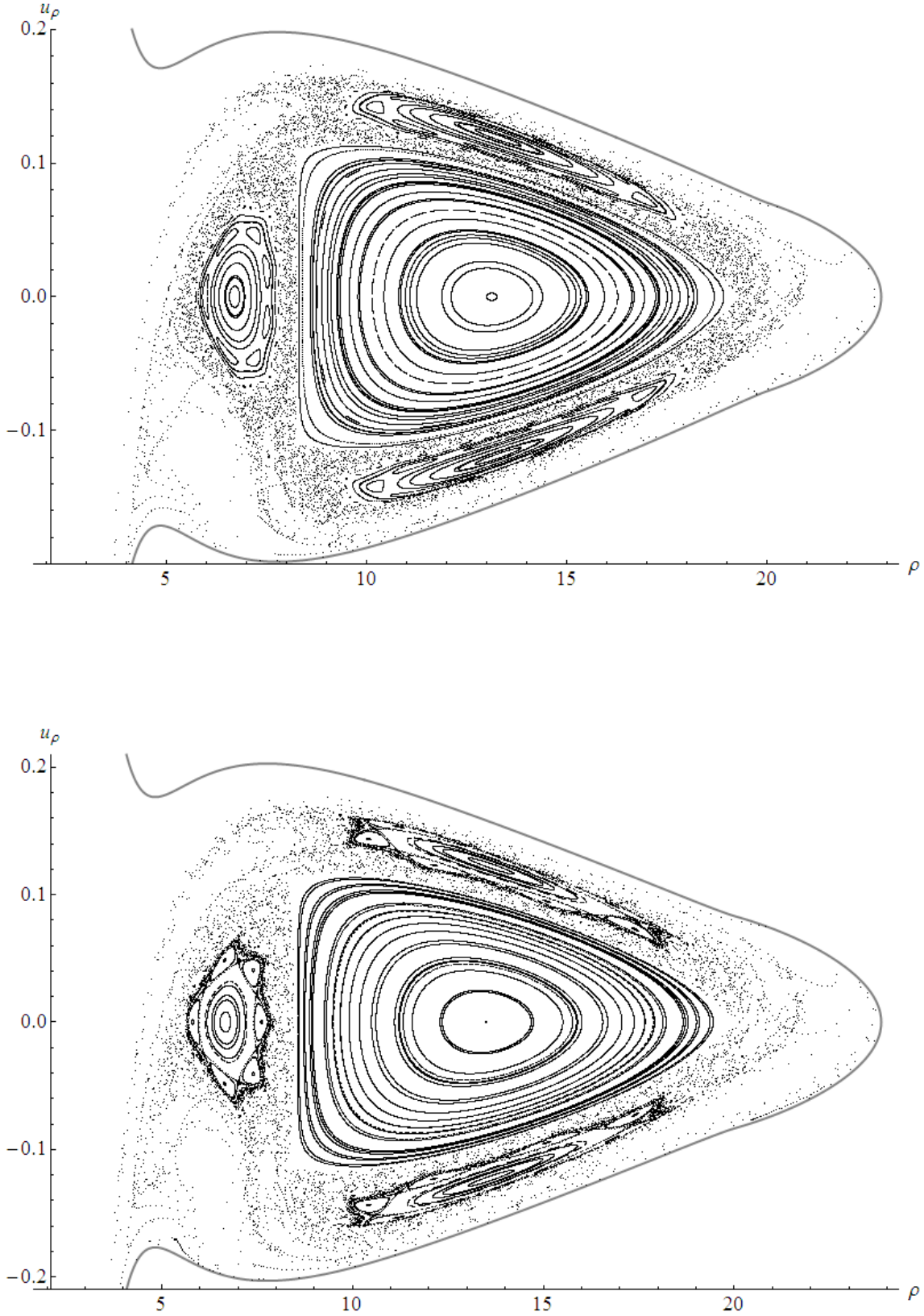

Figure 4.2: Surfaces of section at $z = 0$ for the first iMM disc superposition with parameter values $\mathcal{M} = 0.5$, $b = 20$, $\ell = 3.75$ and $\mathcal{E} = -0.048, -0.047$ respectively.

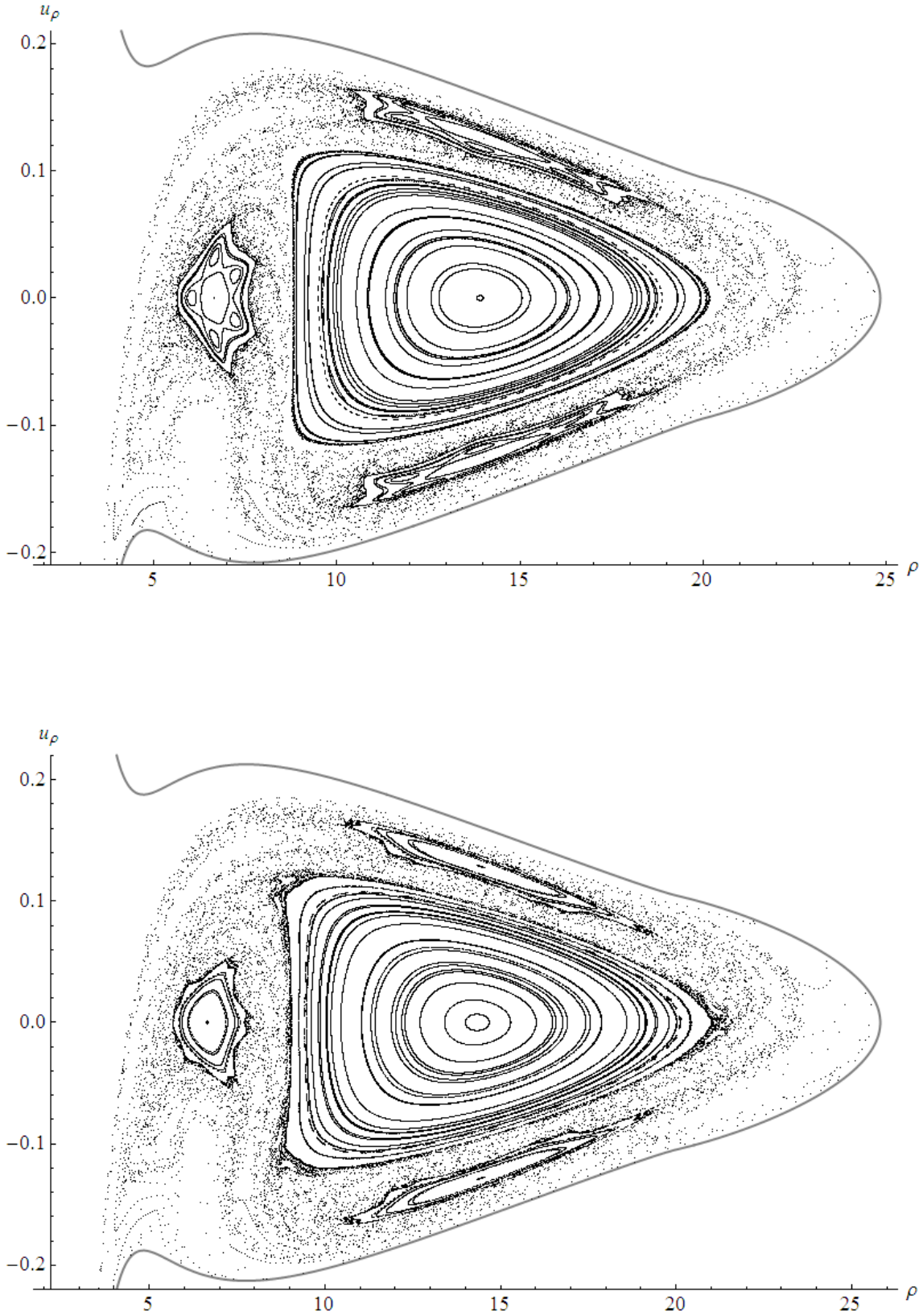

Figure 4.3: Surfaces of section for the first iMM disc superposition as in figure 4.2 for $\mathcal{E} = -0.046, -0.045$ respectively.

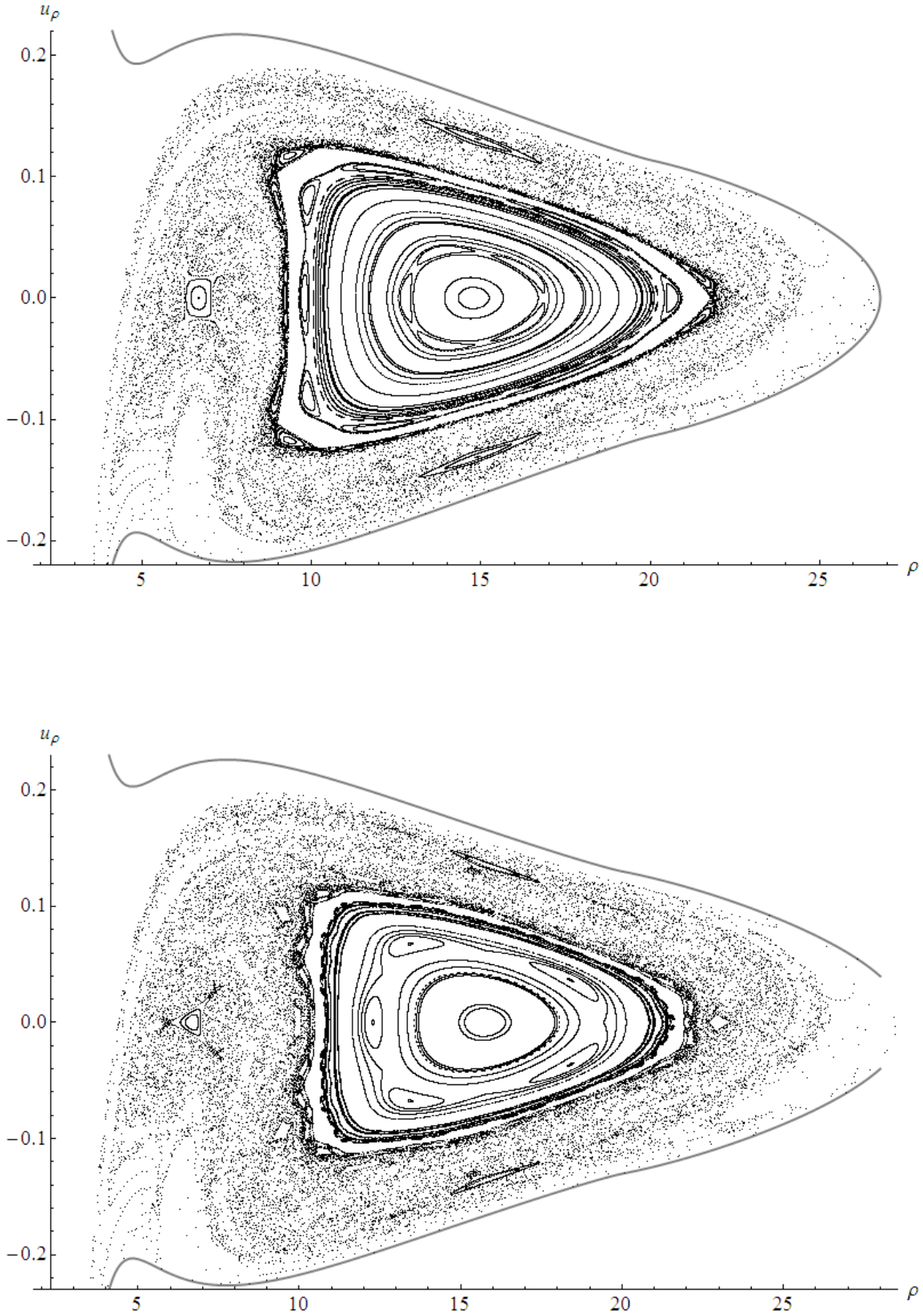

Figure 4.4: Surfaces of section for the first iMM disc superposition as in figure 4.2 for $\mathcal{E} = -0.044, -0.042$ respectively.

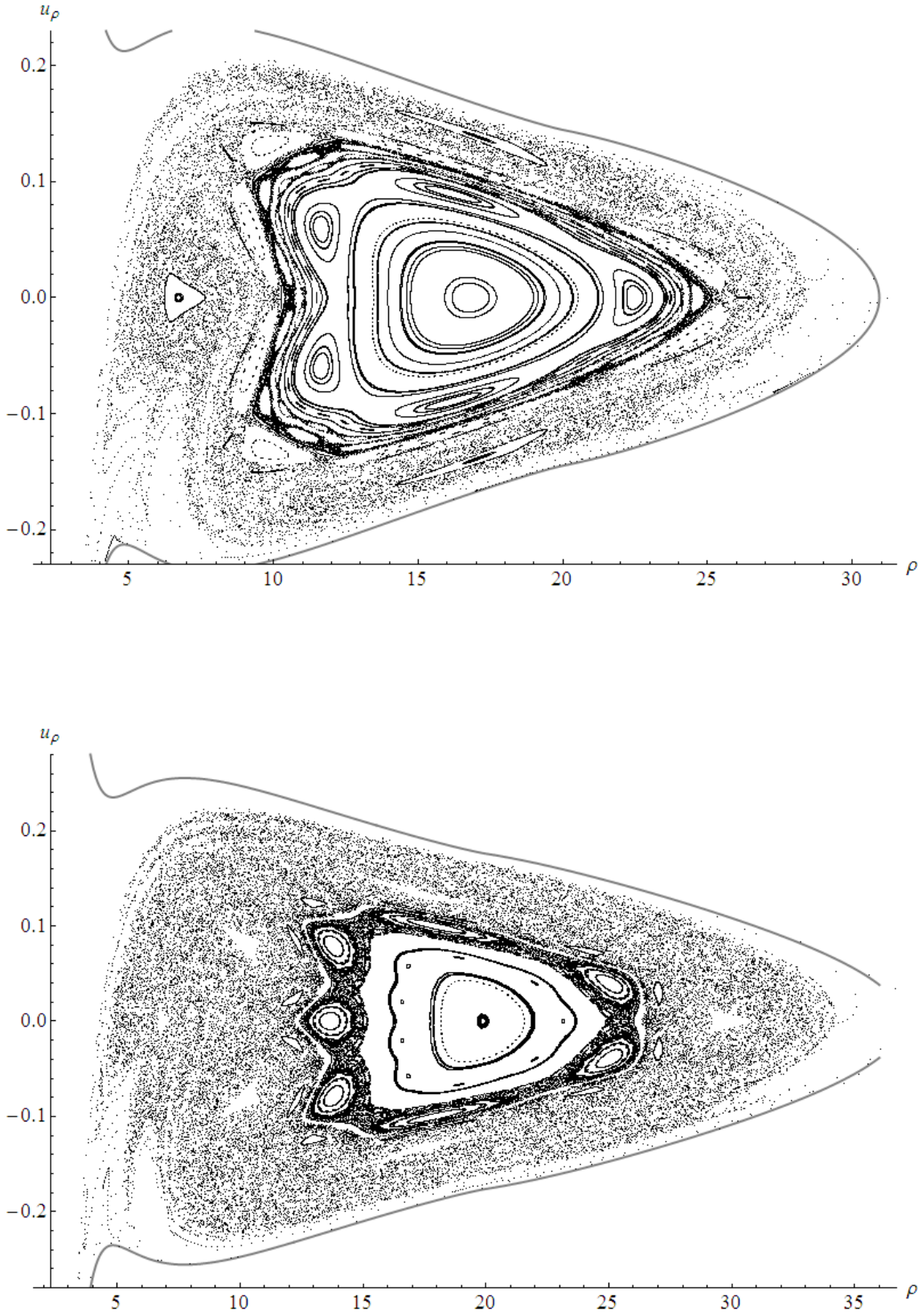

Figure 4.5: Surfaces of section for the first iMM disc superposition as in figure 4.2 for $\mathcal{E} = -0.04, -0,035$ respectively.

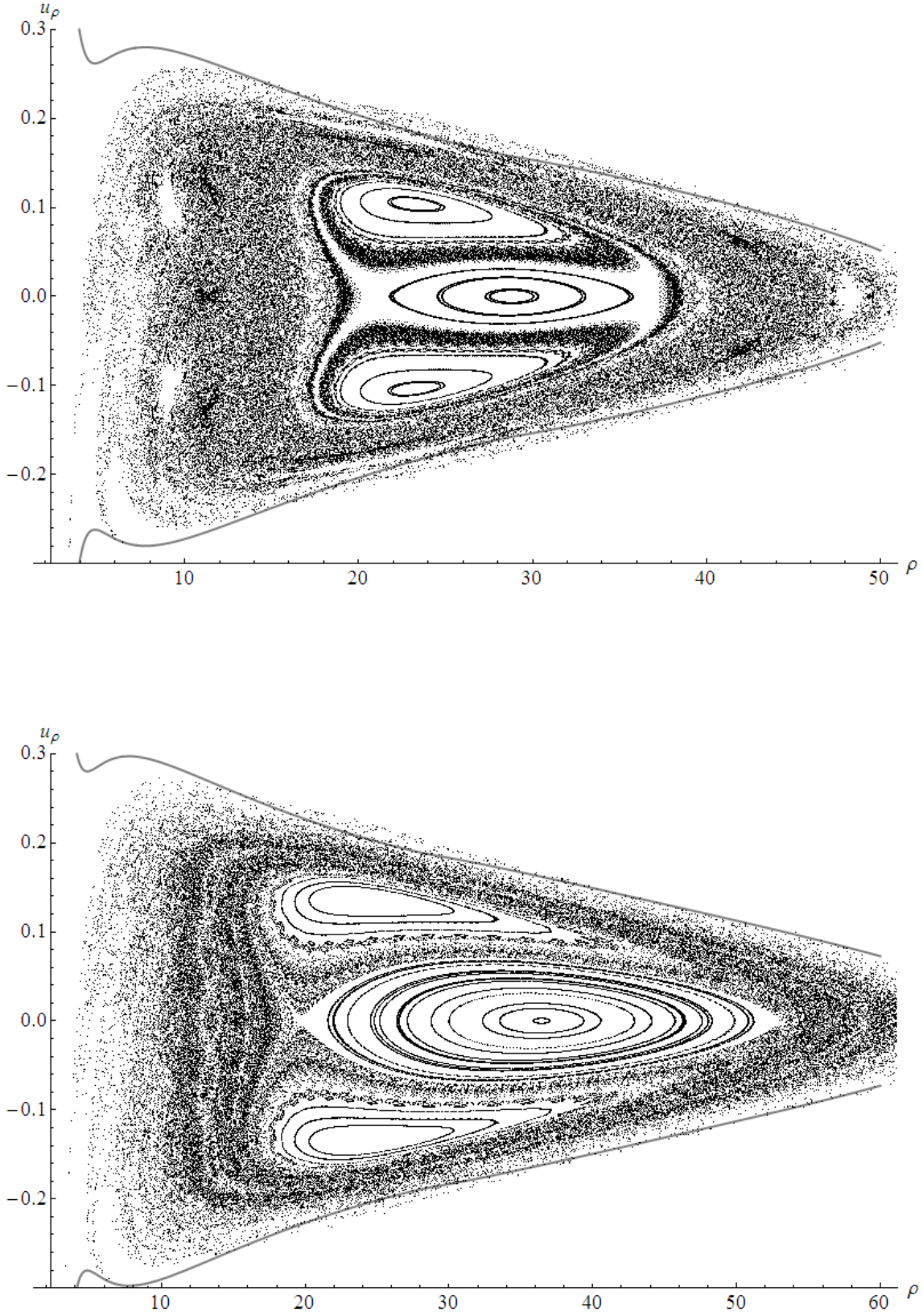

Figure 4.6: Surfaces of section for the first iMM disc superposition as in figure 4.2 for $\mathcal{E} = -0.025, -0.02$ respectively.

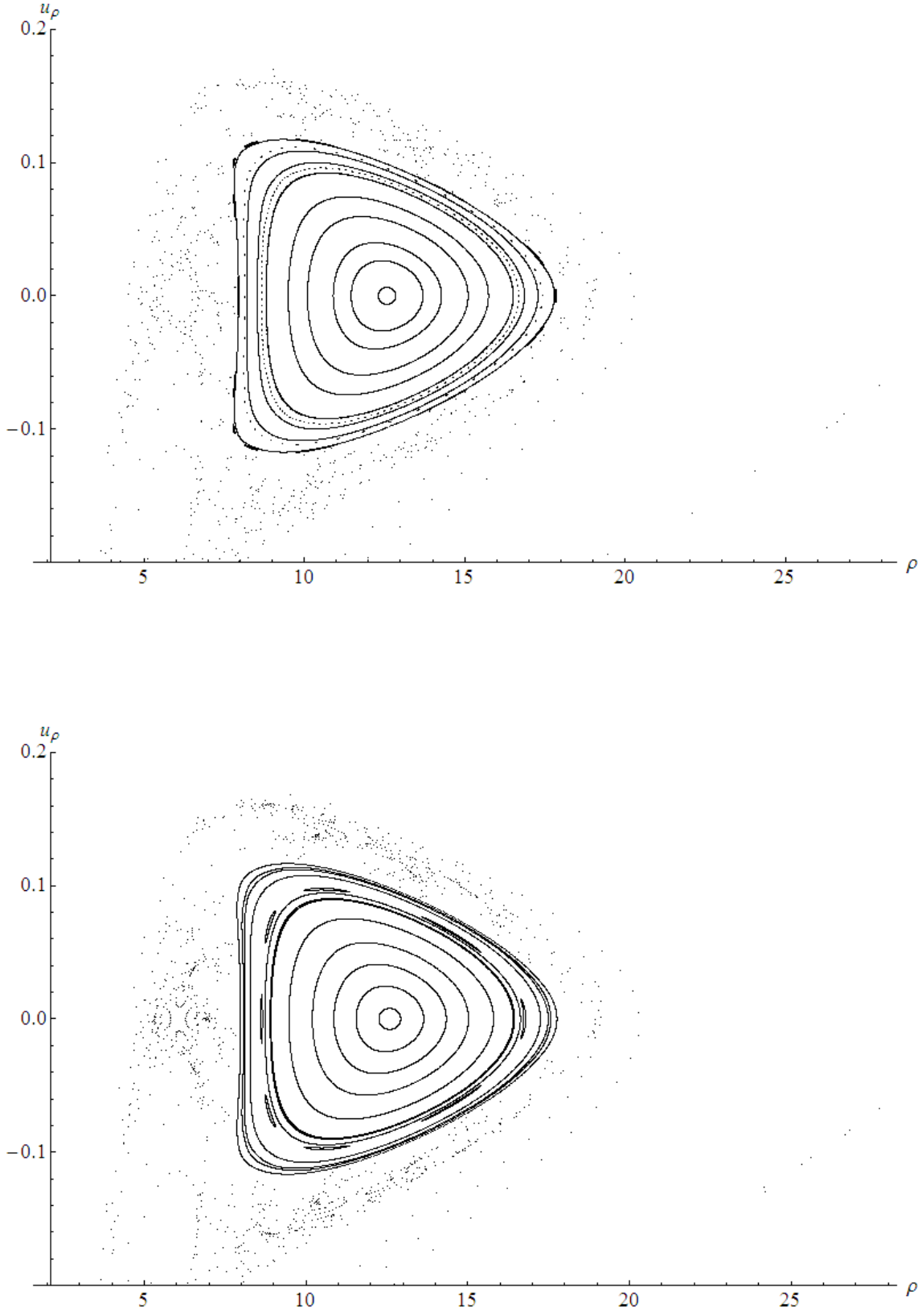

Figure 4.7: Surfaces of section at $z = 0$ for the first iMM disc superposition with parameter values $\mathcal{M} = 0.5$, $b = 20$, $\mathcal{E} = -0.04635$ and $\ell = 0.65$, 1.0 respectively.

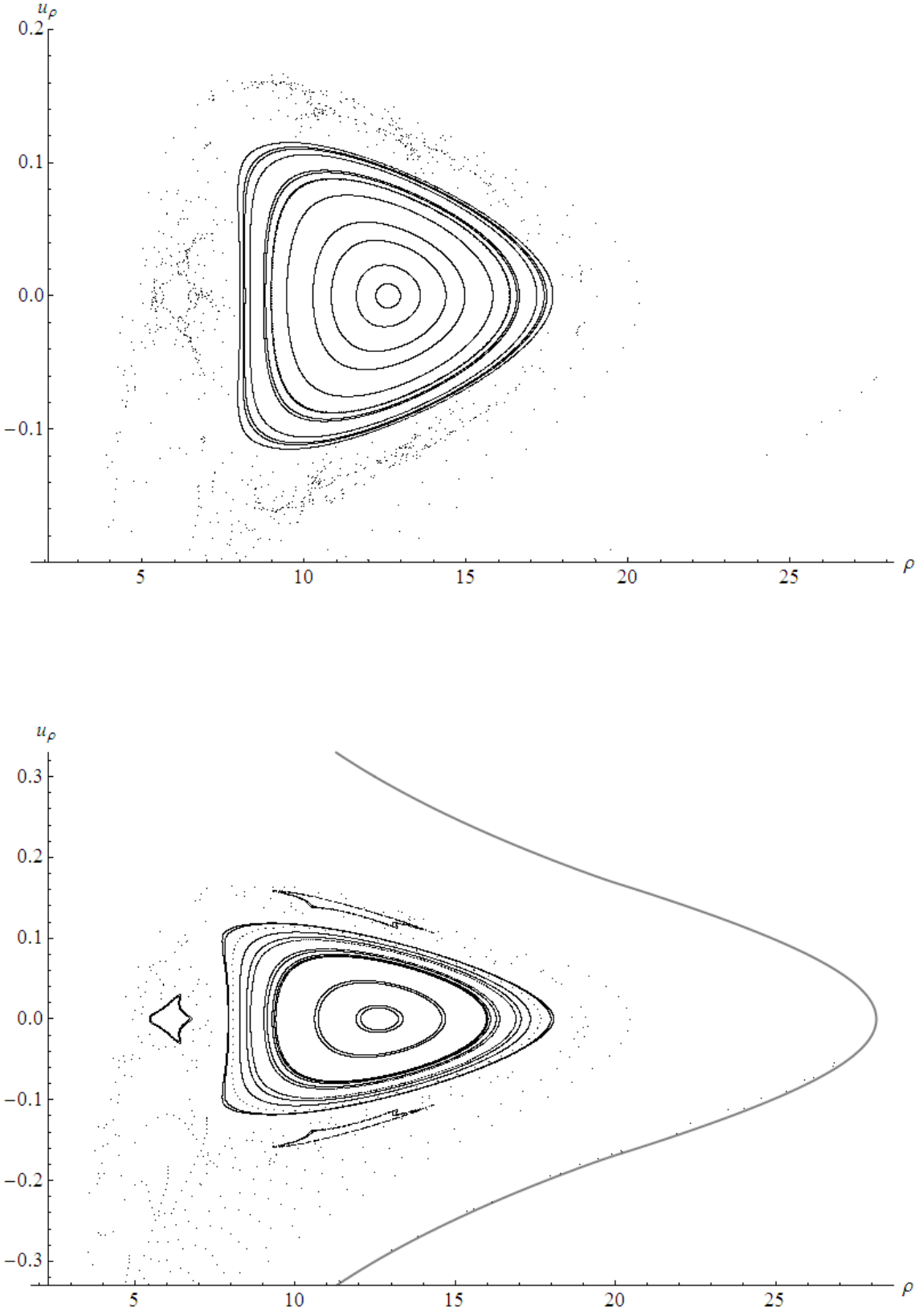

Figure 4.8: Surfaces of section for the first iMM disc superposition as in figure 4.7 for $\ell = 1.30$, 2.0 respectively.

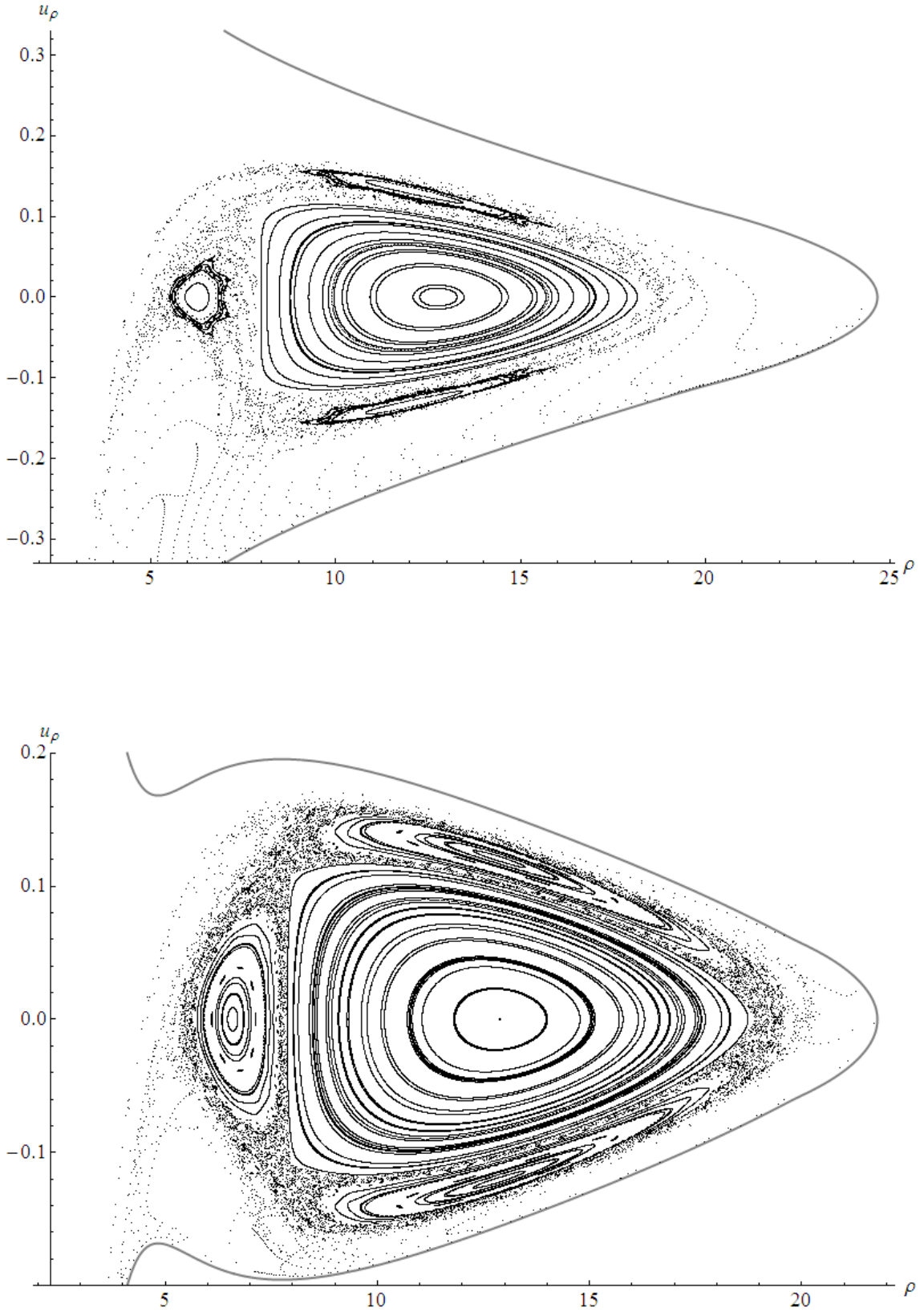

Figure 4.9: Surfaces of section for the first iMM disc superposition as in figure 4.7 for $\ell = 3.25$, 3.75 respectively.

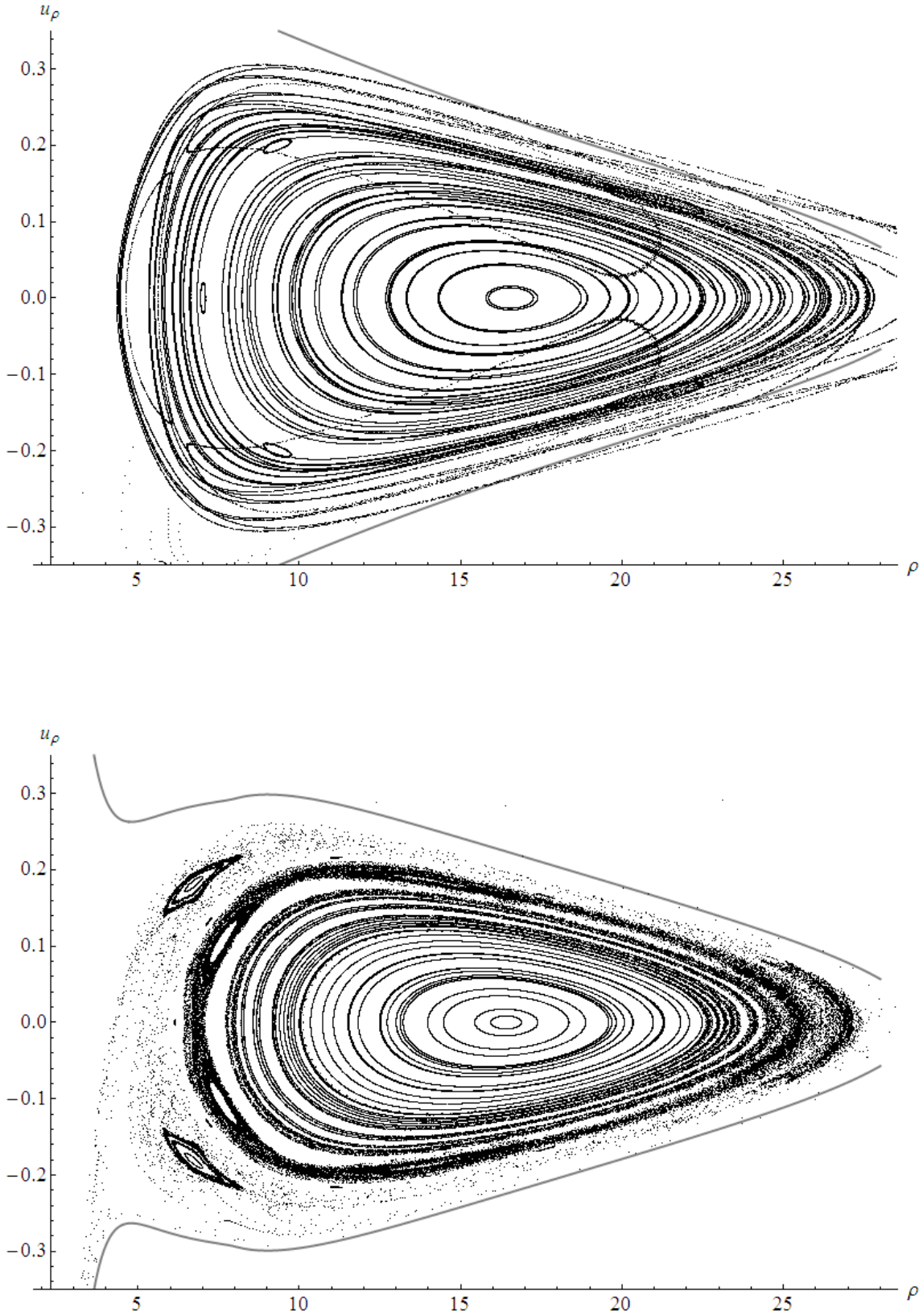

Figure 4.10: Surfaces of section at $z = 0$ for the first iMM disc superposition with parameter values $\mathcal{M} = 0.5$, $\ell = 3.75$, $\mathcal{E} = -0.045$ and $b = 3$, 8 respectively.

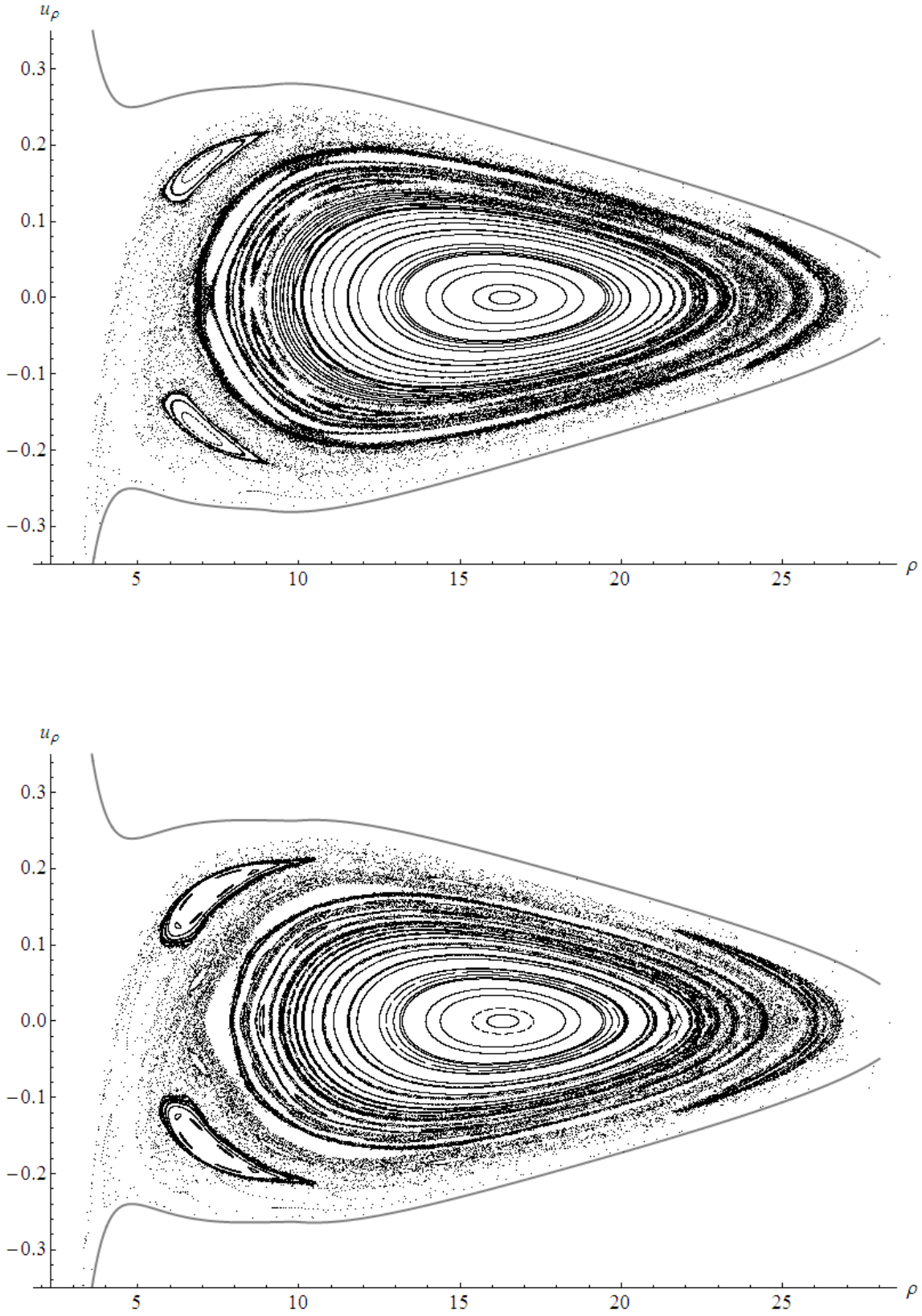

Figure 4.11: Surfaces of section for the first iMM disc superposition as in figure 4.10 for $b = 9$, 10 respectively.

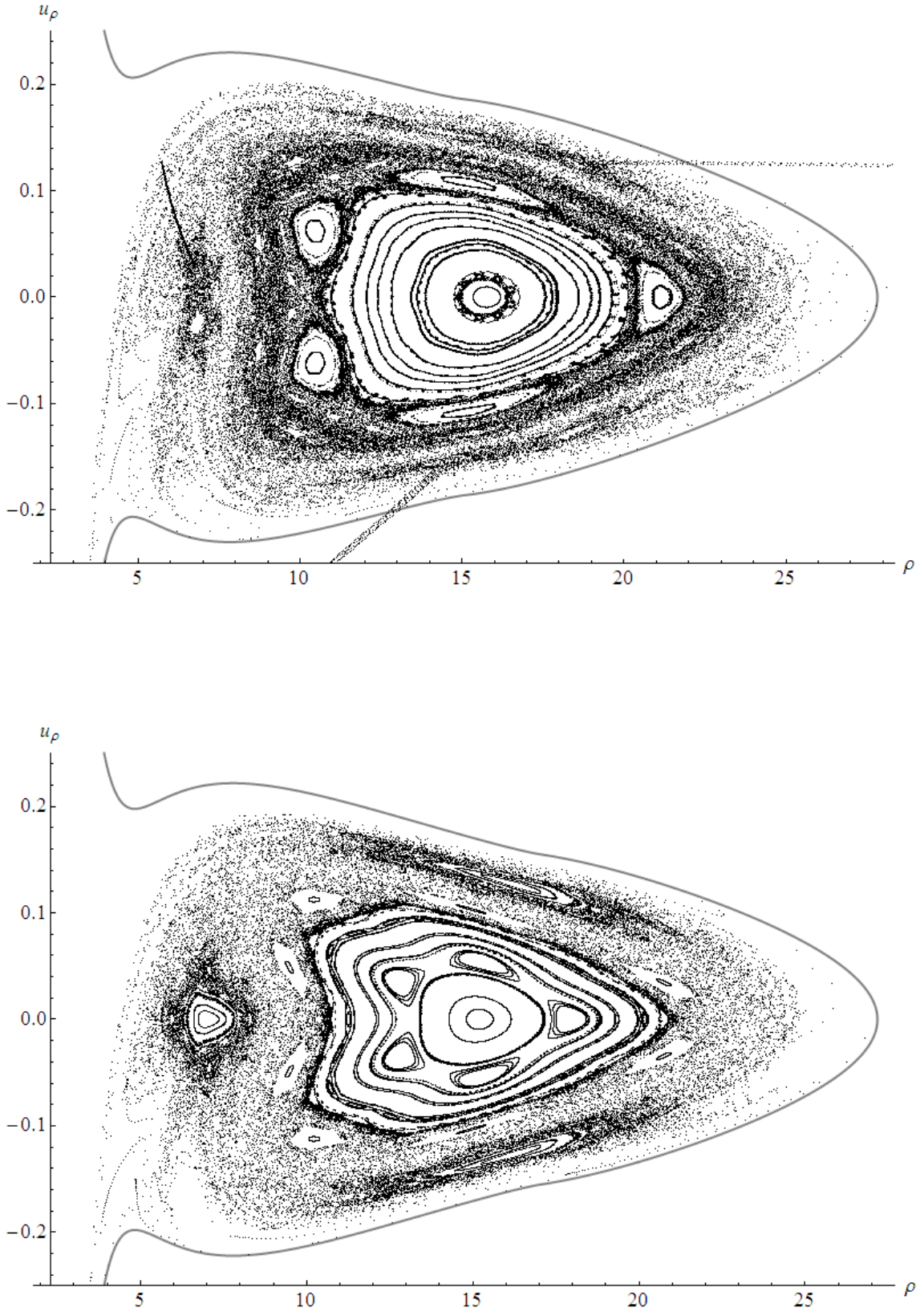

Figure 4.12: Surfaces of section for the first iMM disc superposition as in figure 4.10 for $b = 15$, 17 respectively.

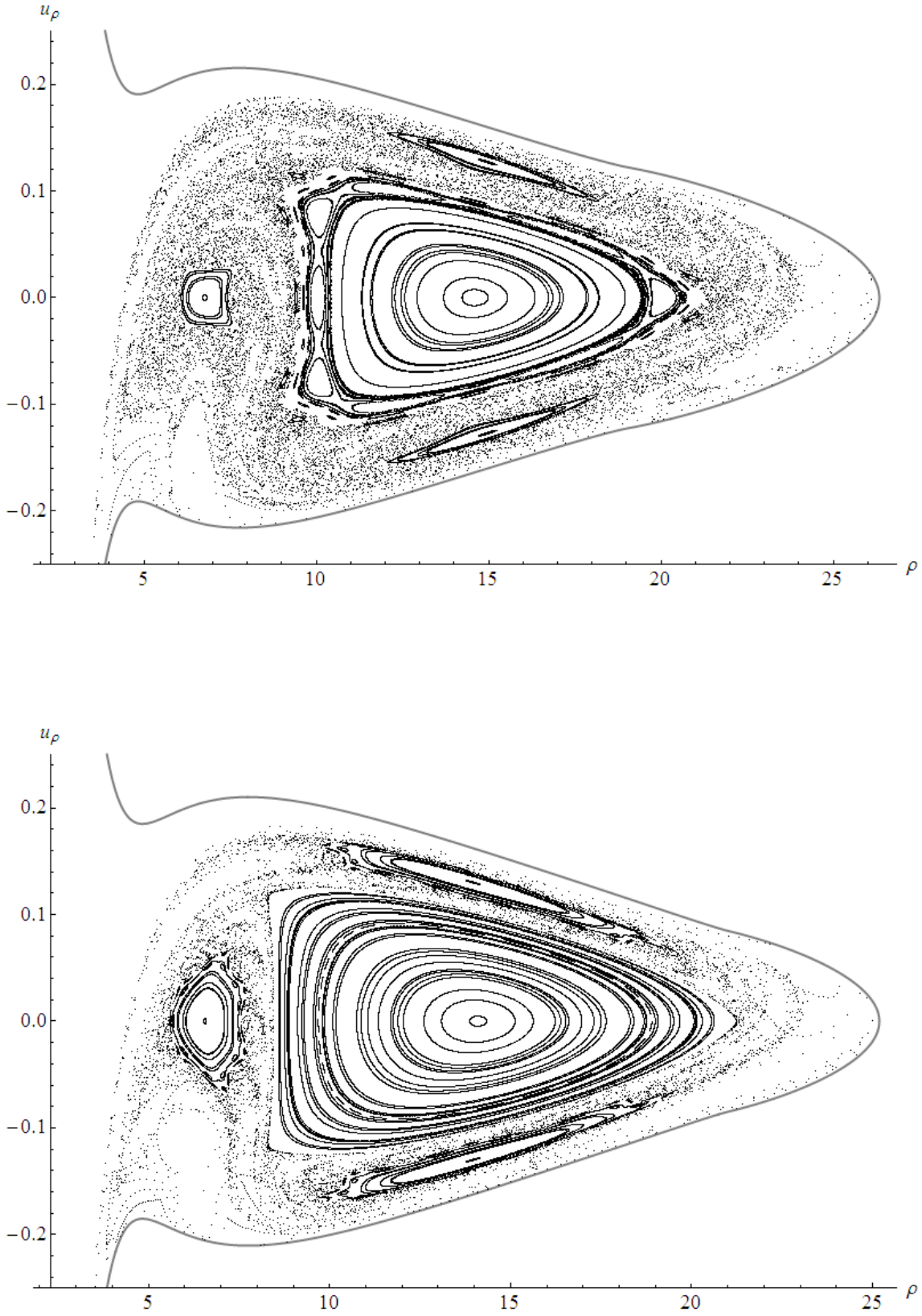

Figure 4.13: Surfaces of section for the first iMM disc superposition as in figure 4.10 for $b = 19$, 21 respectively.

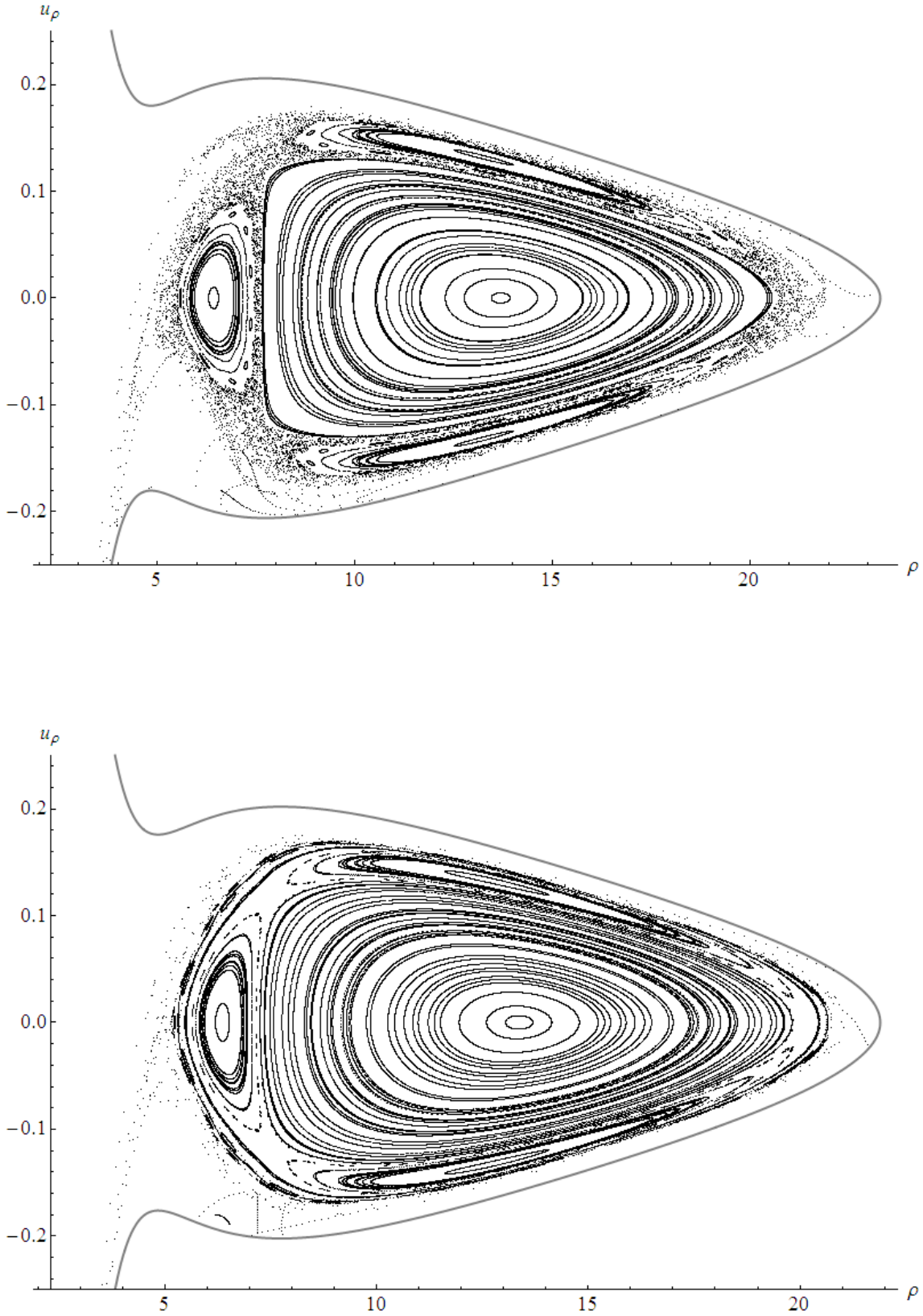

Figure 4.14: Surfaces of section for the first iMM disc superposition as in figure 4.10 for $b = 23$, 25 respectively.

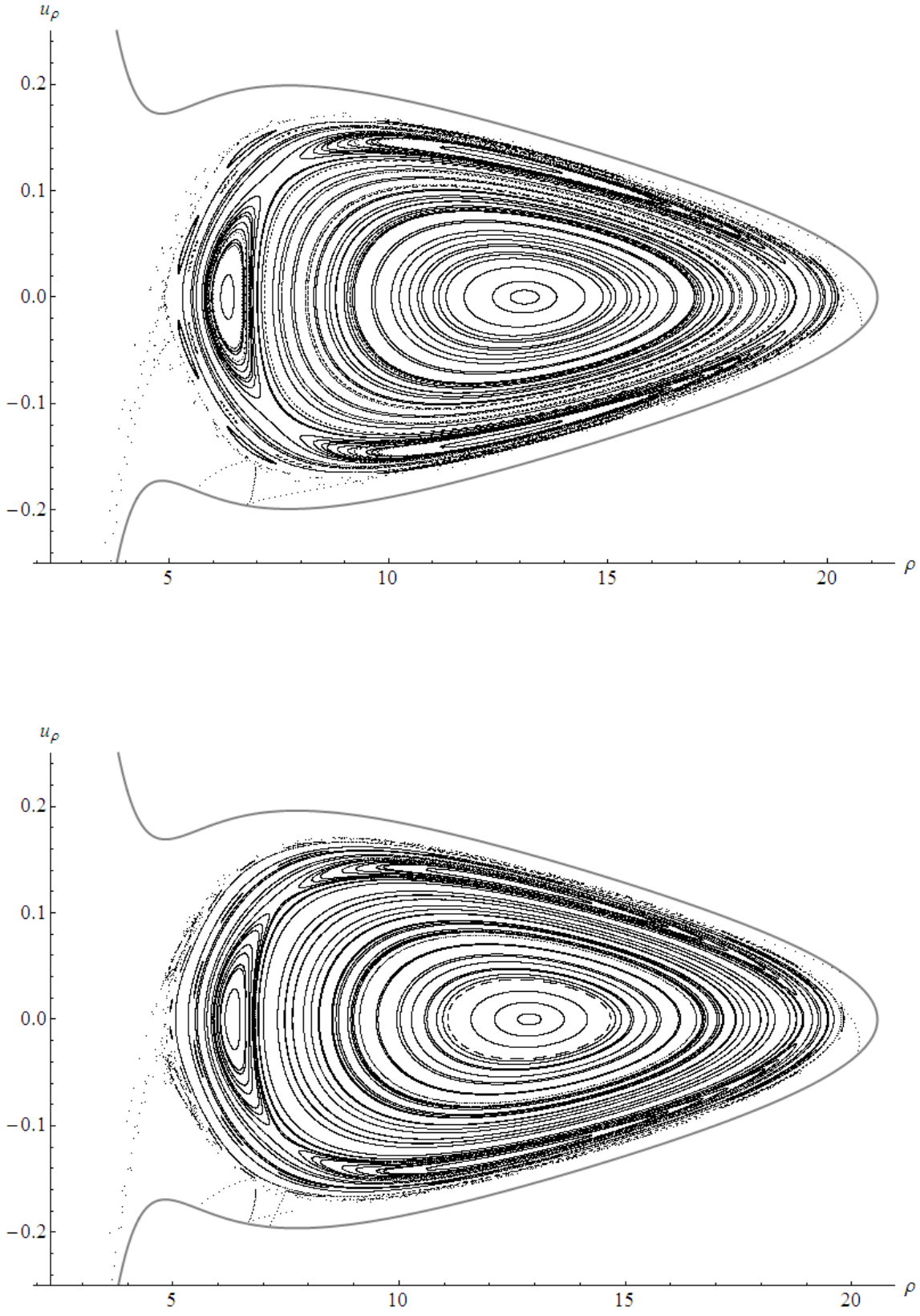

Figure 4.15: Surfaces of section for the first iMM disc superposition as in figure 4.10 for $b = 27$, 29 respectively.

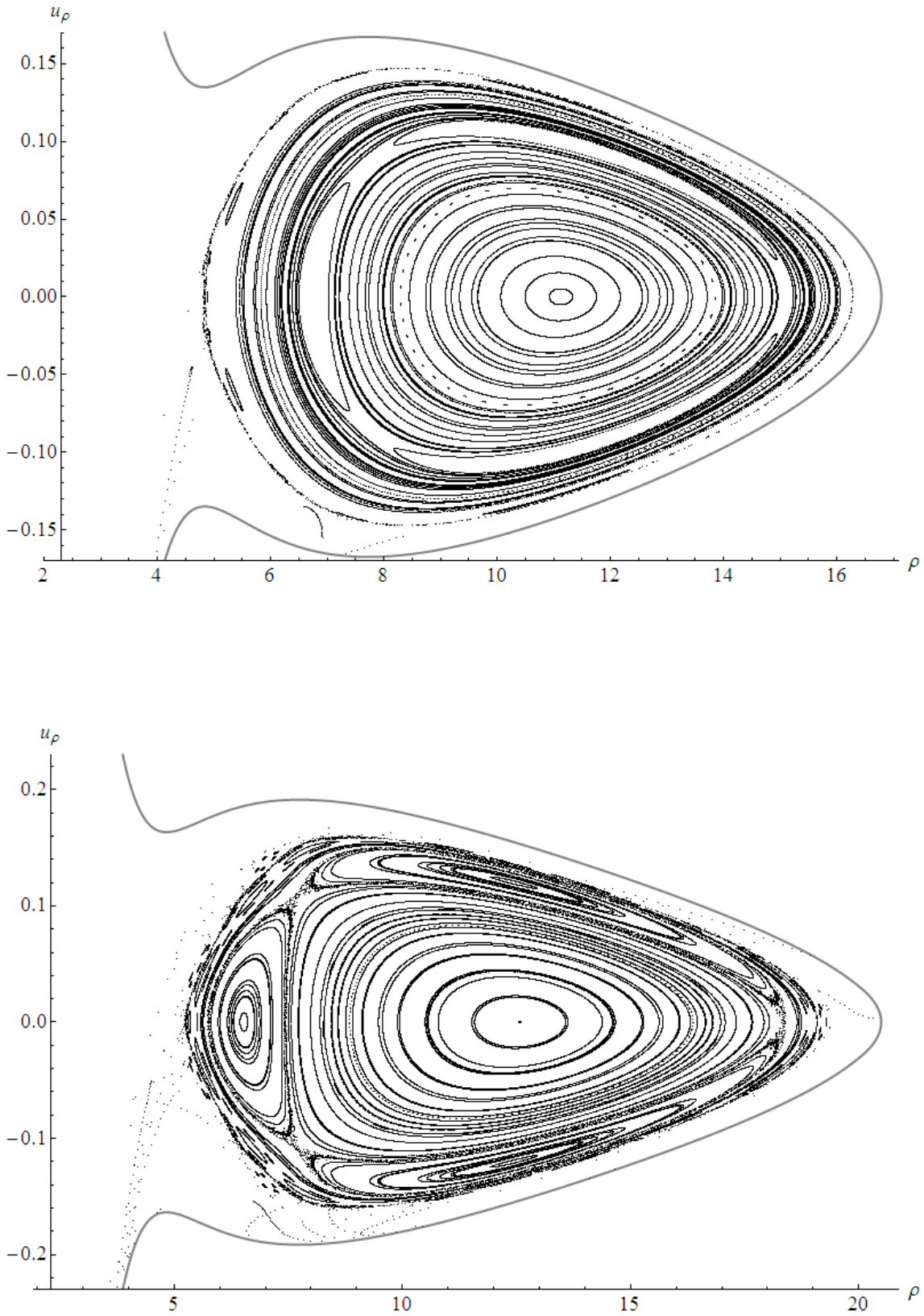

Figure 4.16: Surfaces of section at $z = 0$ for the first iMM disc superposition with parameter values $b = 20$, $\ell = 3.75$, $\mathcal{E} = -0.045$ and $\mathcal{M} = 0.1$, 0.3 respectively.

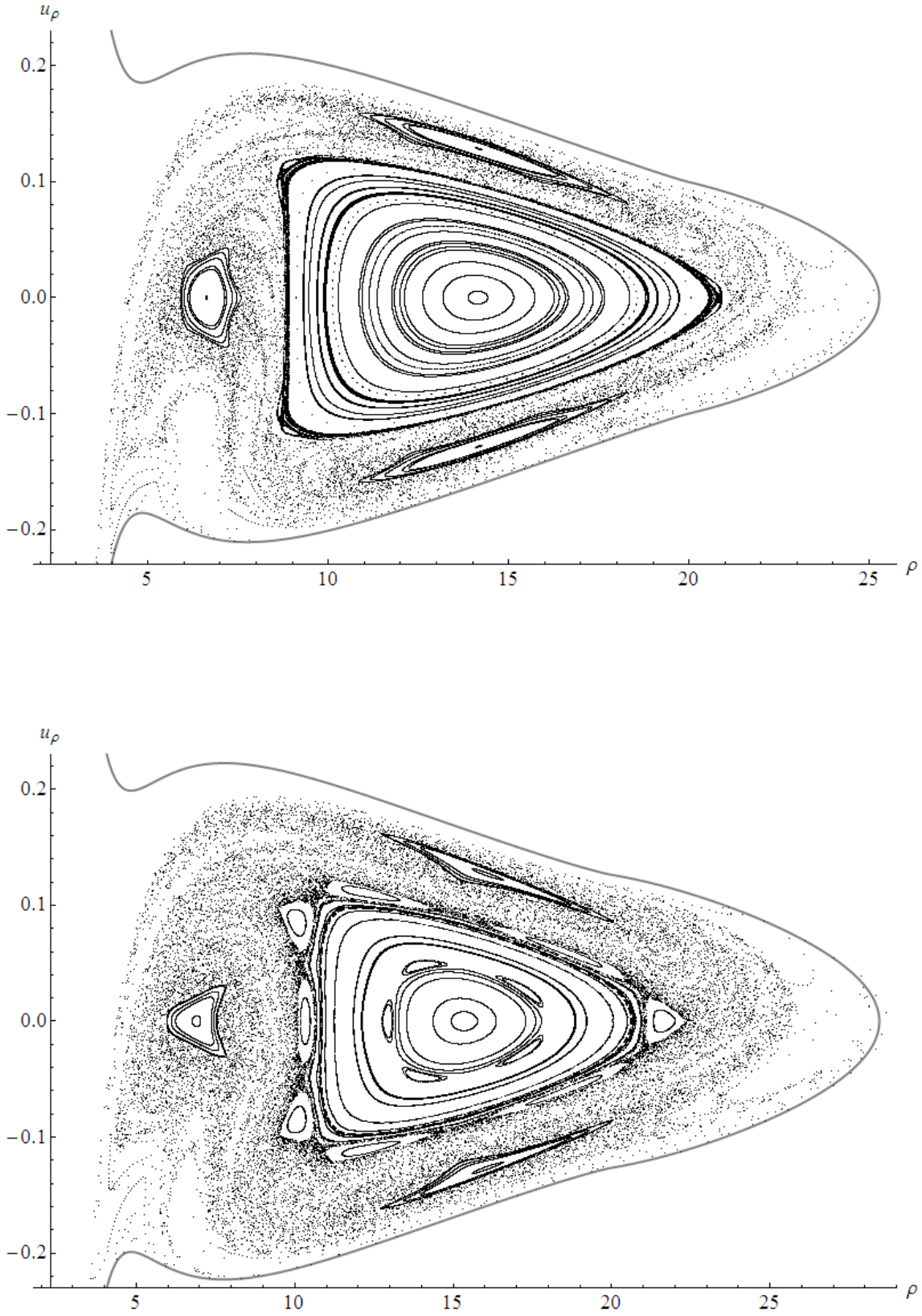

Figure 4.17: Surfaces of section for the first iMM disc superposition as in figure 4.16 for $\mathcal{M} = 0.48$, 0.6 respectively.

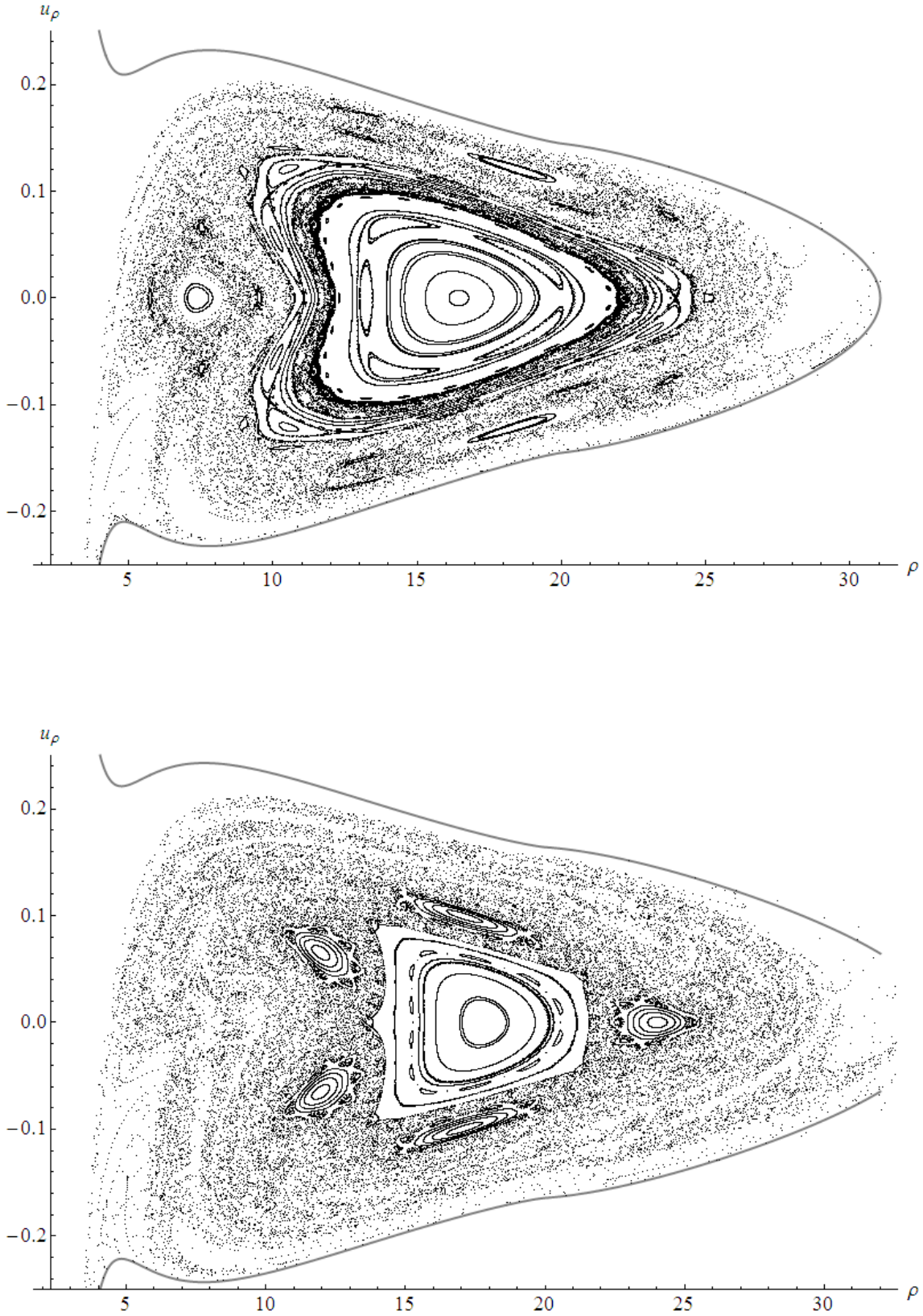

Figure 4.18: Surfaces of section for the first iMM disc superposition as in figure 4.16 for $\mathcal{M} = 0.6$, 0.7 respectively.

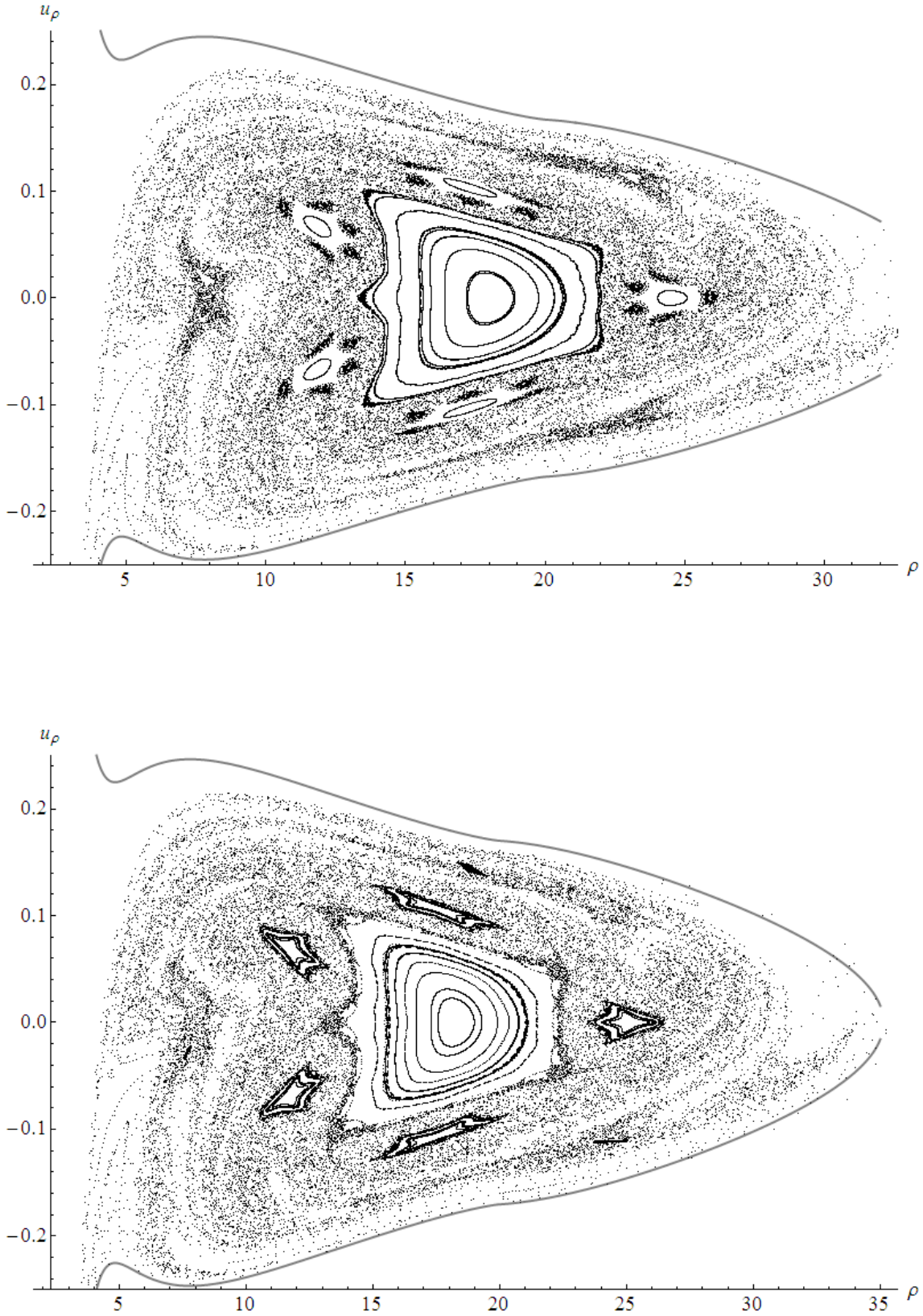

Figure 4.19: Surfaces of section for the first iMM disc superposition as in figure 4.16 for $\mathcal{M} = 0.82$, 0.84 respectively.

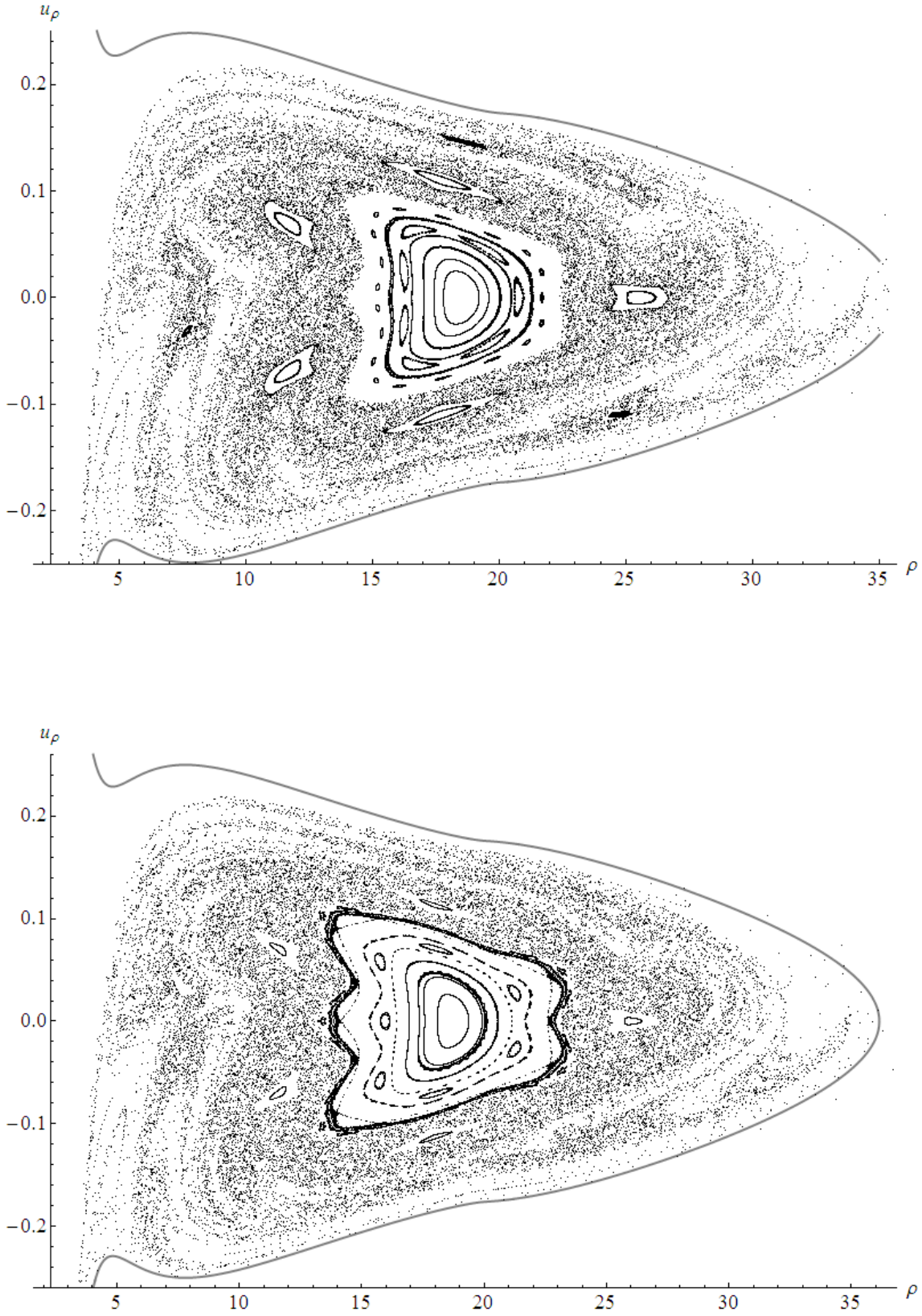

Figure 4.20: Surfaces of section for the first iMM disc superposition as in figure 4.16 for $\mathcal{M} = 0.86$, 0.88 respectively.

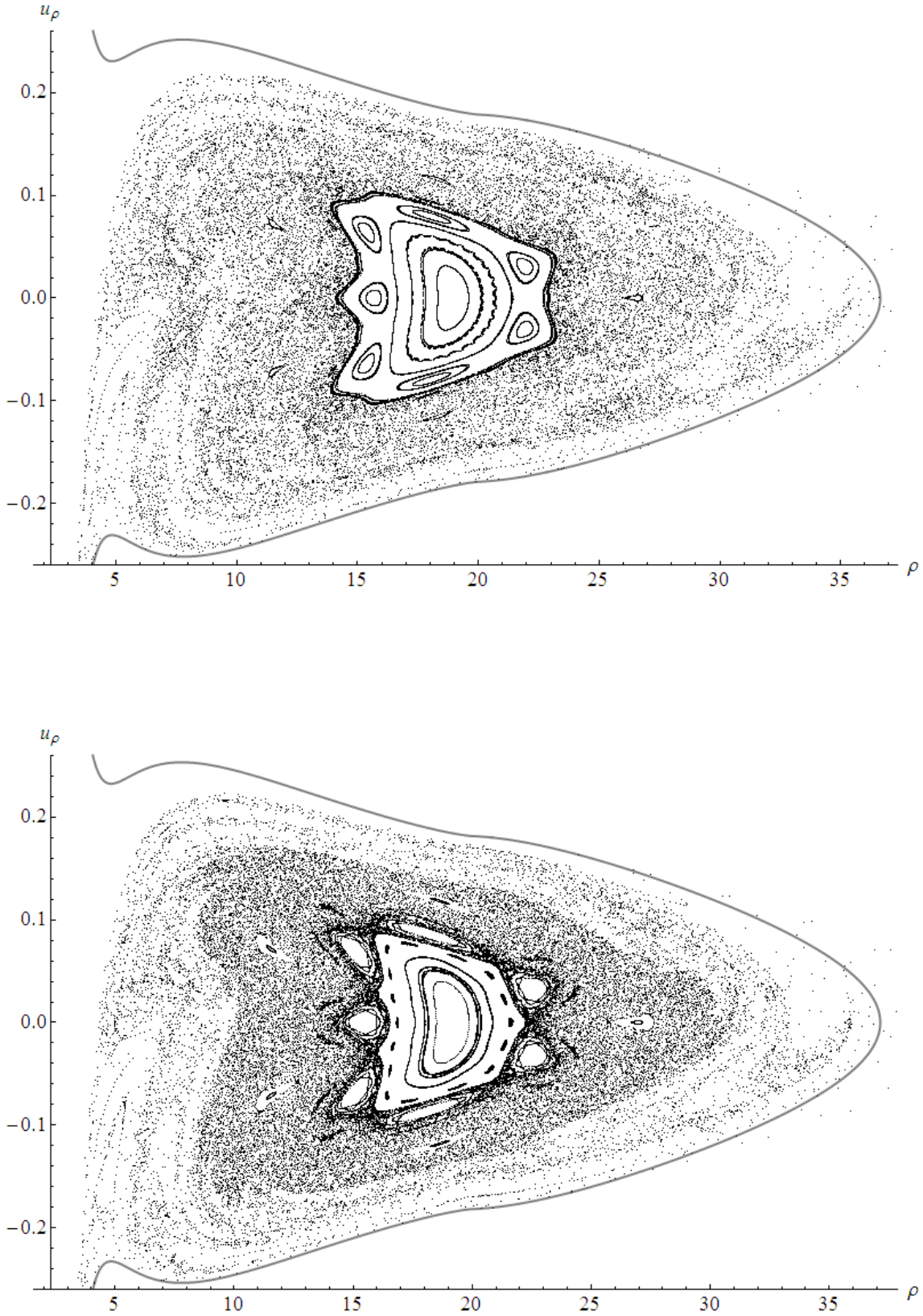

Figure 4.21: Surfaces of section for the first iMM disc superposition as in figure 4.16 for $\mathcal{M} = 0.90$, 0.92 respectively.

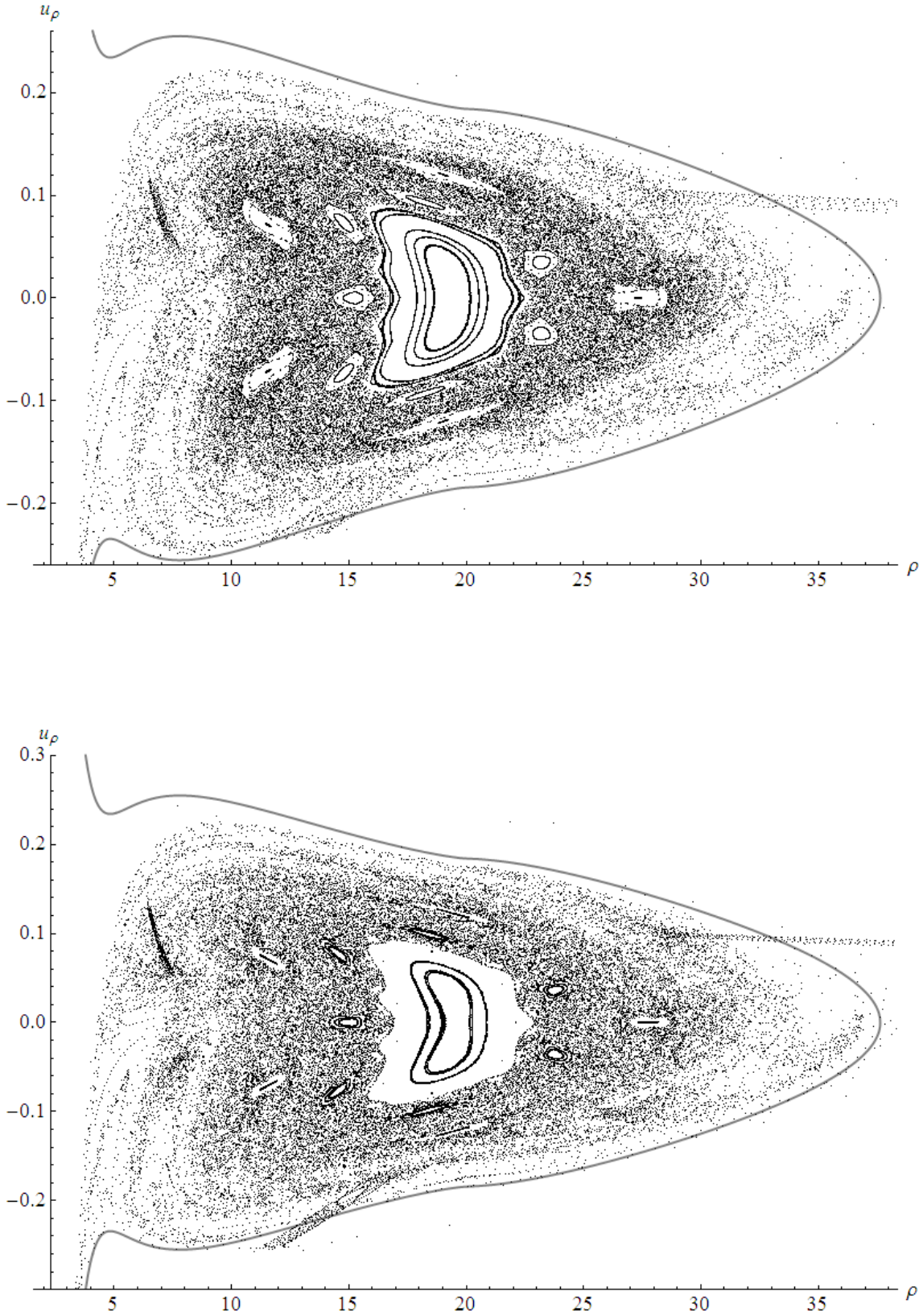

Figure 4.22: Surfaces of section for the first iMM disc superposition as in figure 4.16 for $\mathcal{M} = 0.94$, 0.96 respectively.

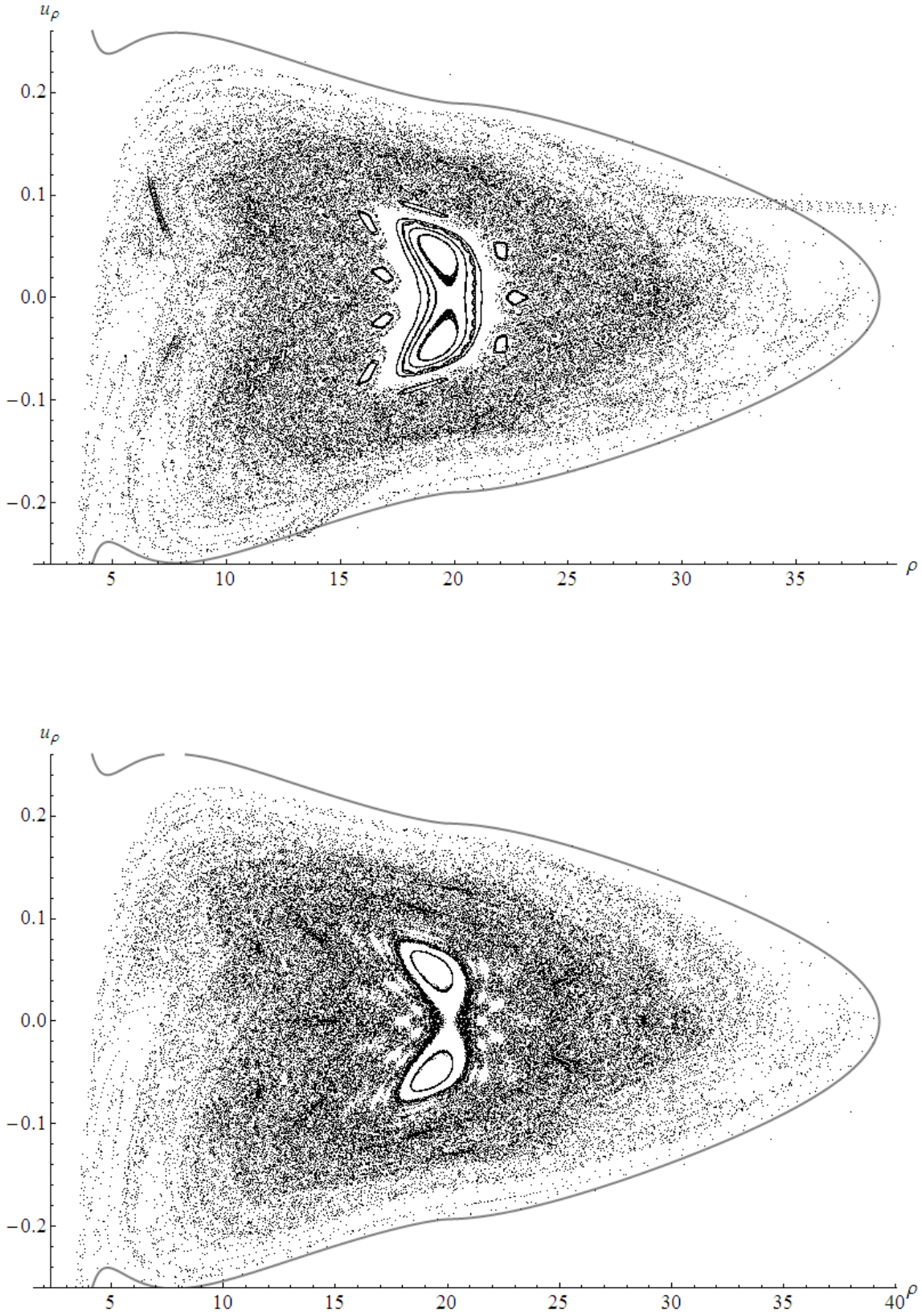

Figure 4.23: Surfaces of section for the first iMM disc superposition as in figure 4.16 for $\mathcal{M} = 0.98$, 1.0 respectively.

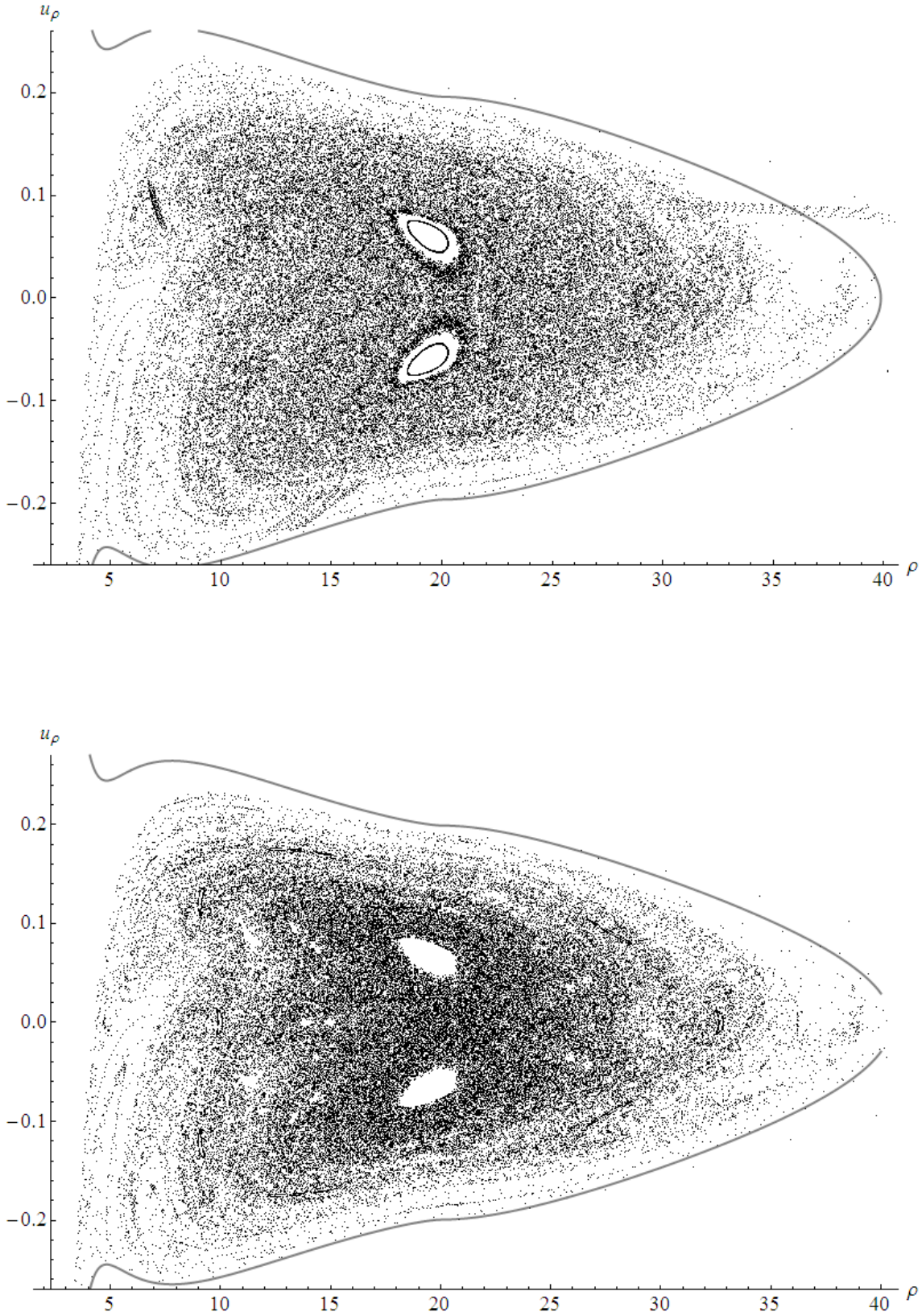

Figure 4.24: Surfaces of section for the first iMM disc superposition as in figure 4.16 for $\mathcal{M} = 1.025$, 1.05 respectively.

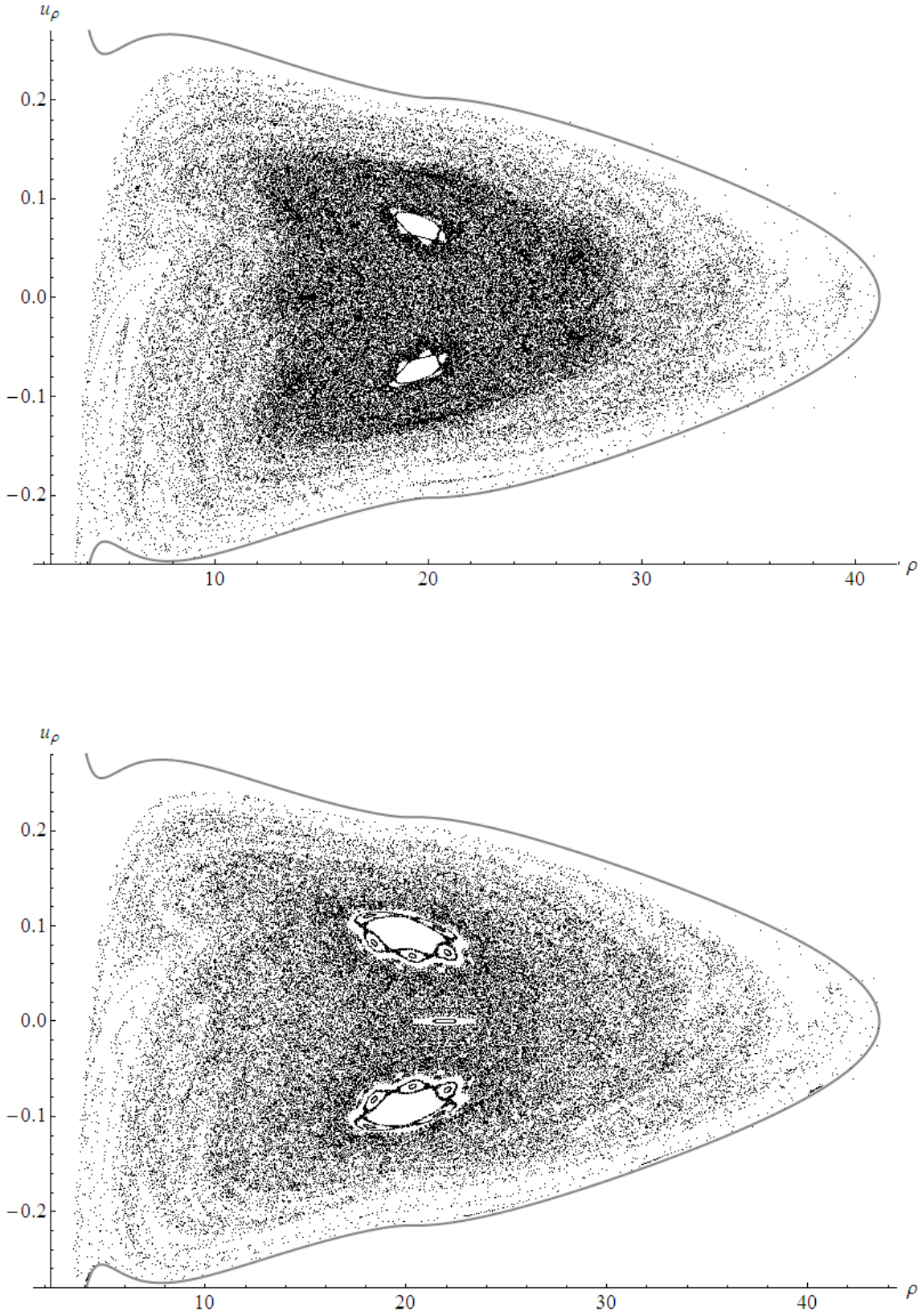

Figure 4.25: Surfaces of section for the first iMM disc superposition as in figure 4.16 for $\mathcal{M} = 1.075$, 1.1 respectively.

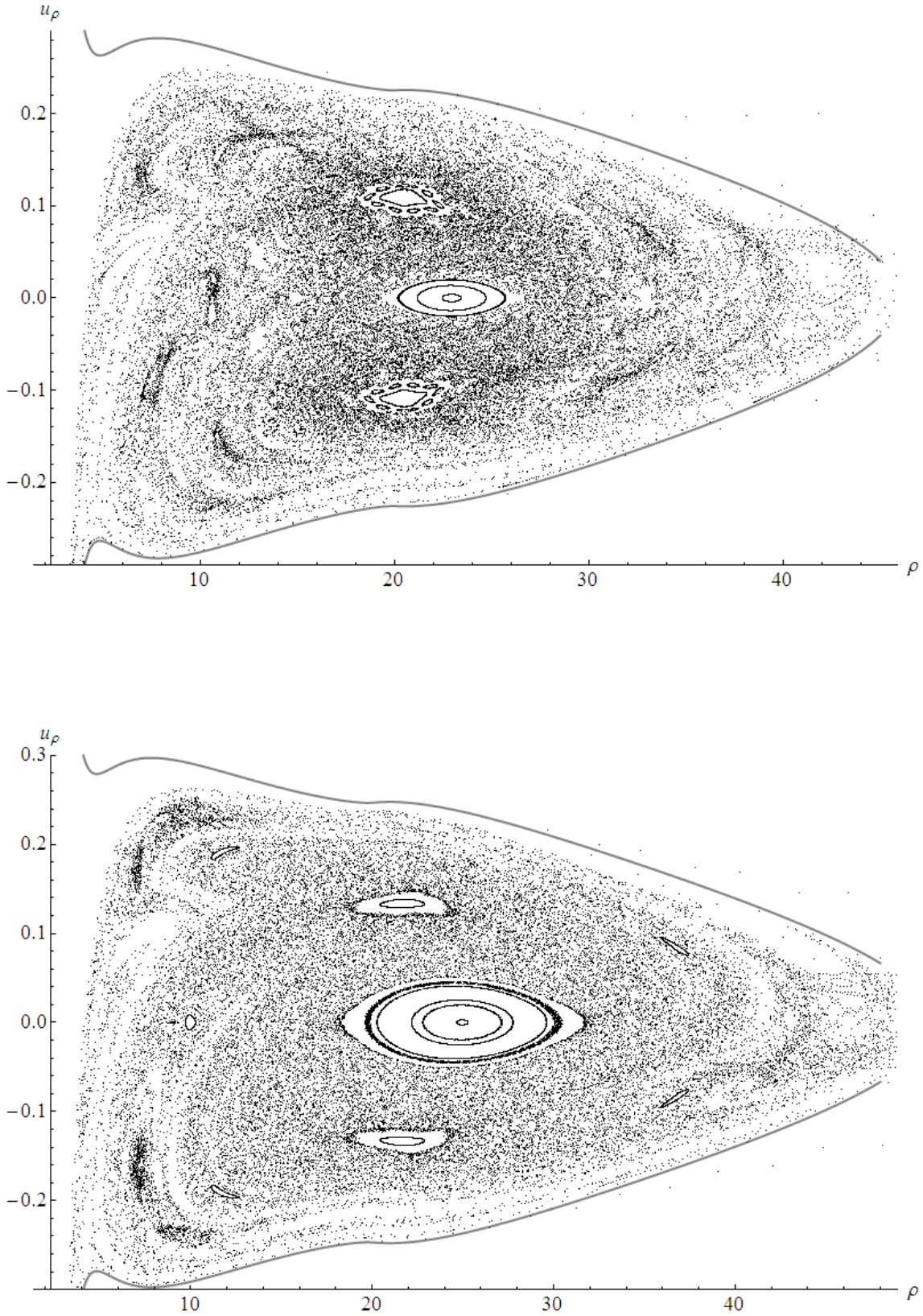

Figure 4.26: Surfaces of section for the first iMM disc superposition as in figure 4.16 for $\mathcal{M} = 1.2$, 1.3 respectively.

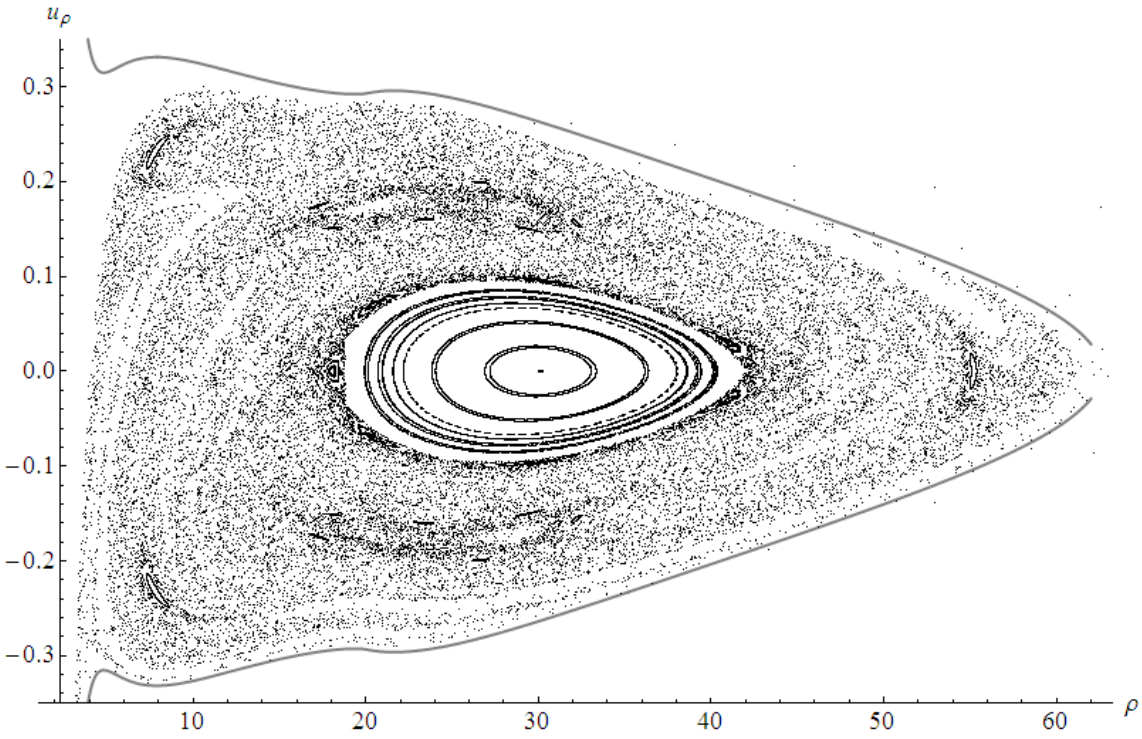

Figure 4.27: Surface of section for the first iMM disc superposition as in figure 4.16 for $\mathcal{M} = 1.5$.

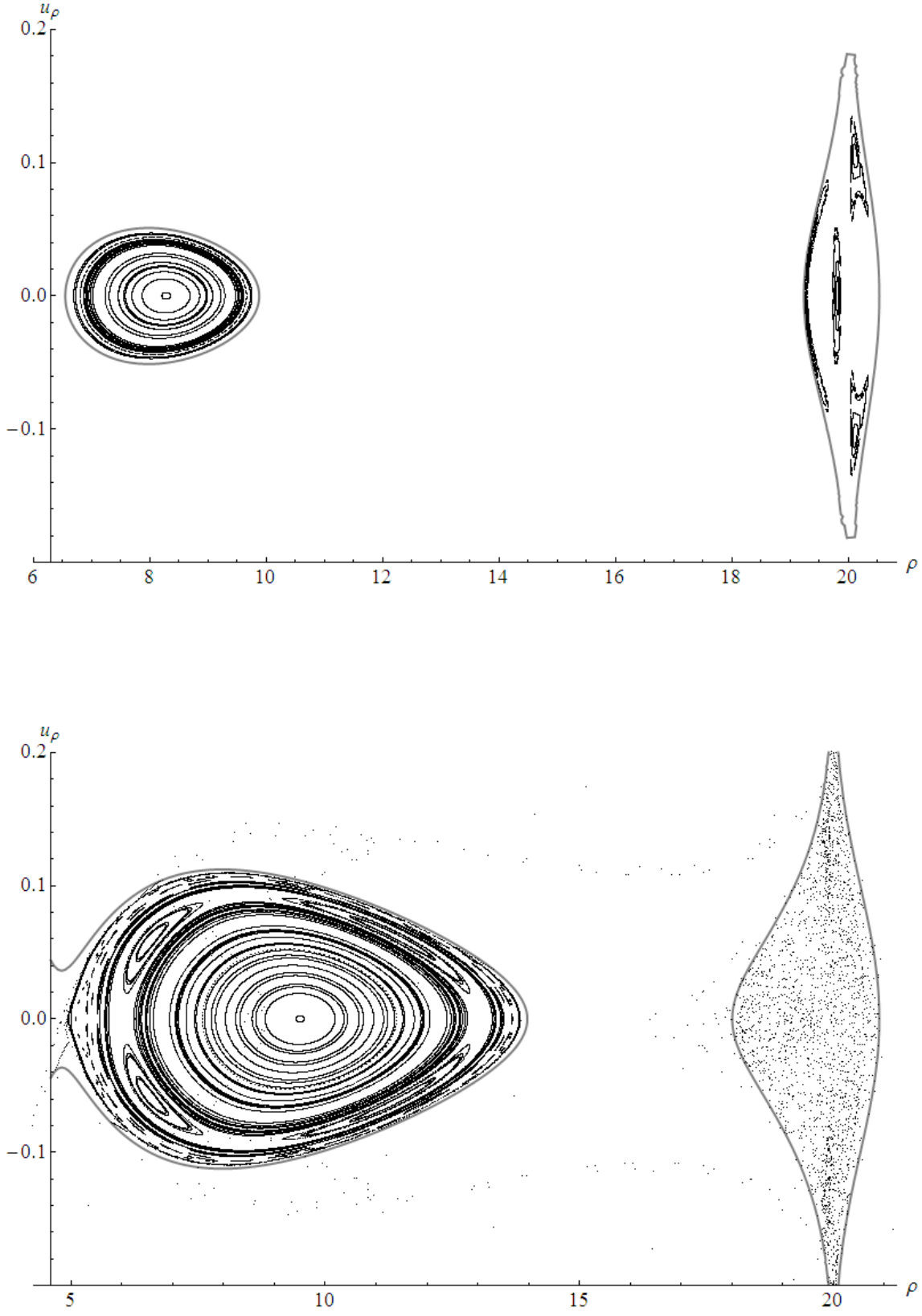

Figure 4.28: Surfaces of section at $z = 0$ for the BW ring superposition with parameter values $\mathcal{M} = 0.5$, $b = 20$, $\ell = 3.75$ and $\mathcal{E} = -0.085, -0.08$ respectively.

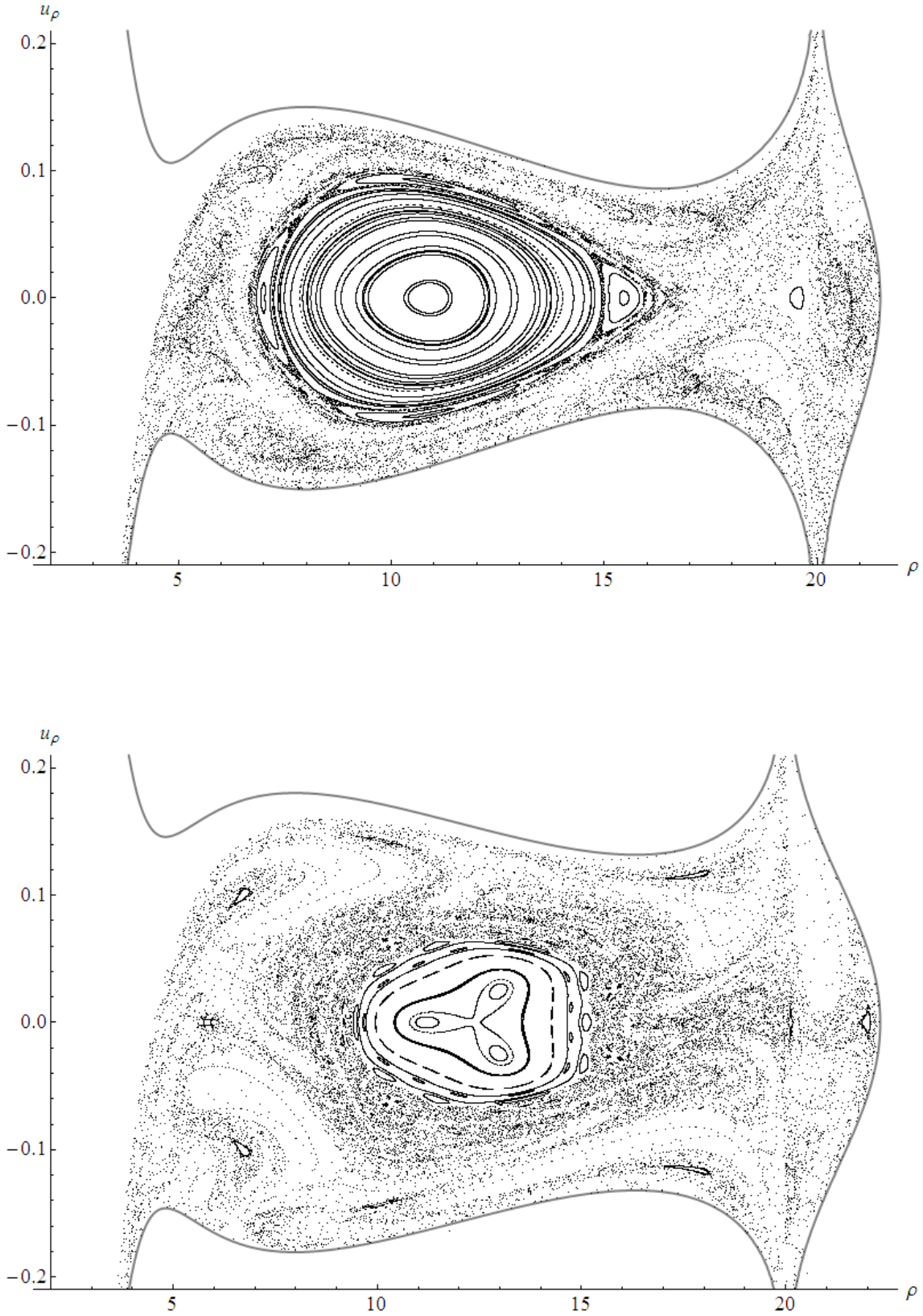

Figure 4.29: Surfaces of section for the BW ring superposition as in figure 4.28 for $\mathcal{E} = -0.075, -0.07$ respectively.

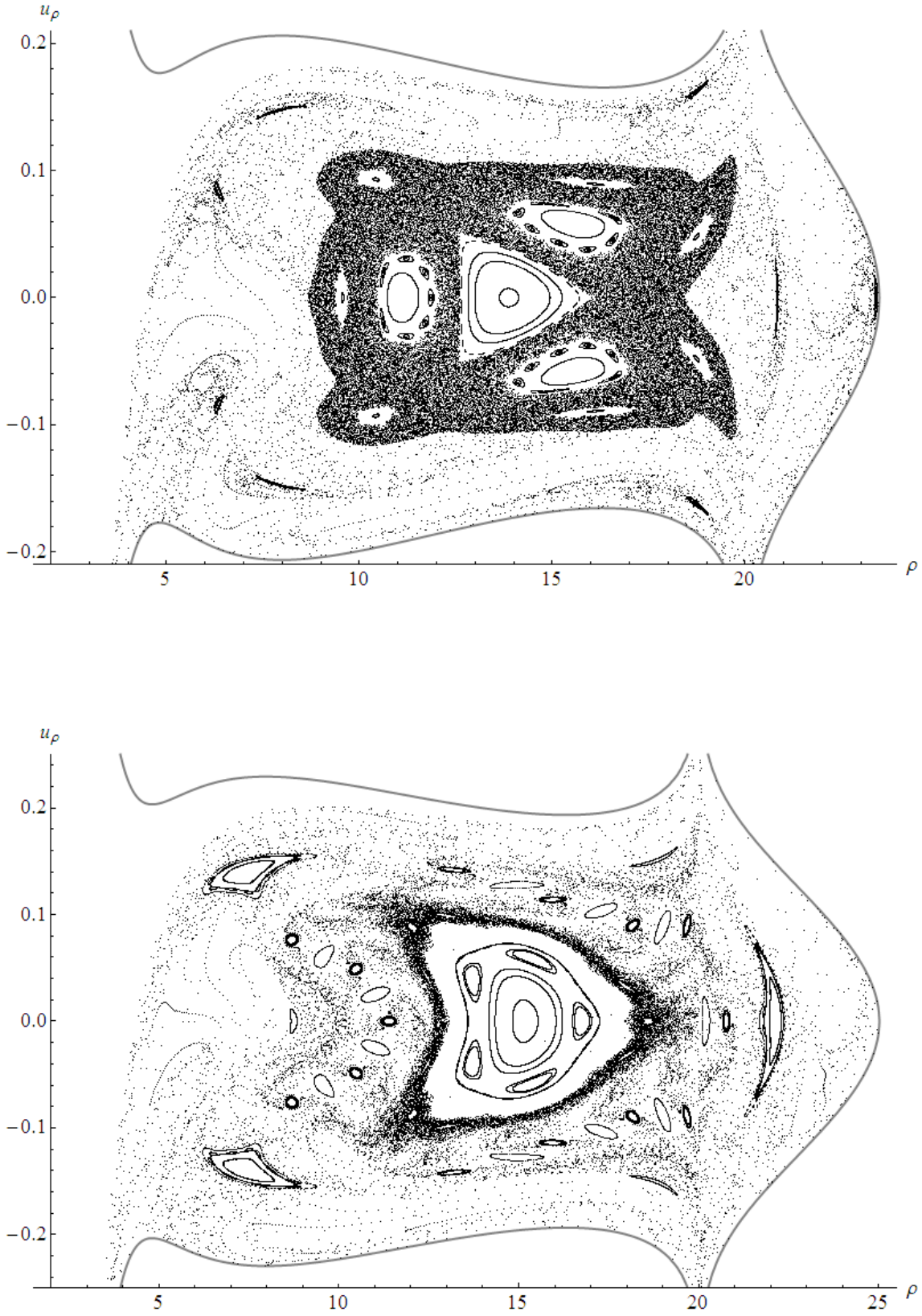

Figure 4.30: Surfaces of section for the BW ring superposition as in figure 4.28 for $\mathcal{E} = -0.065, -0.06$ respectively.

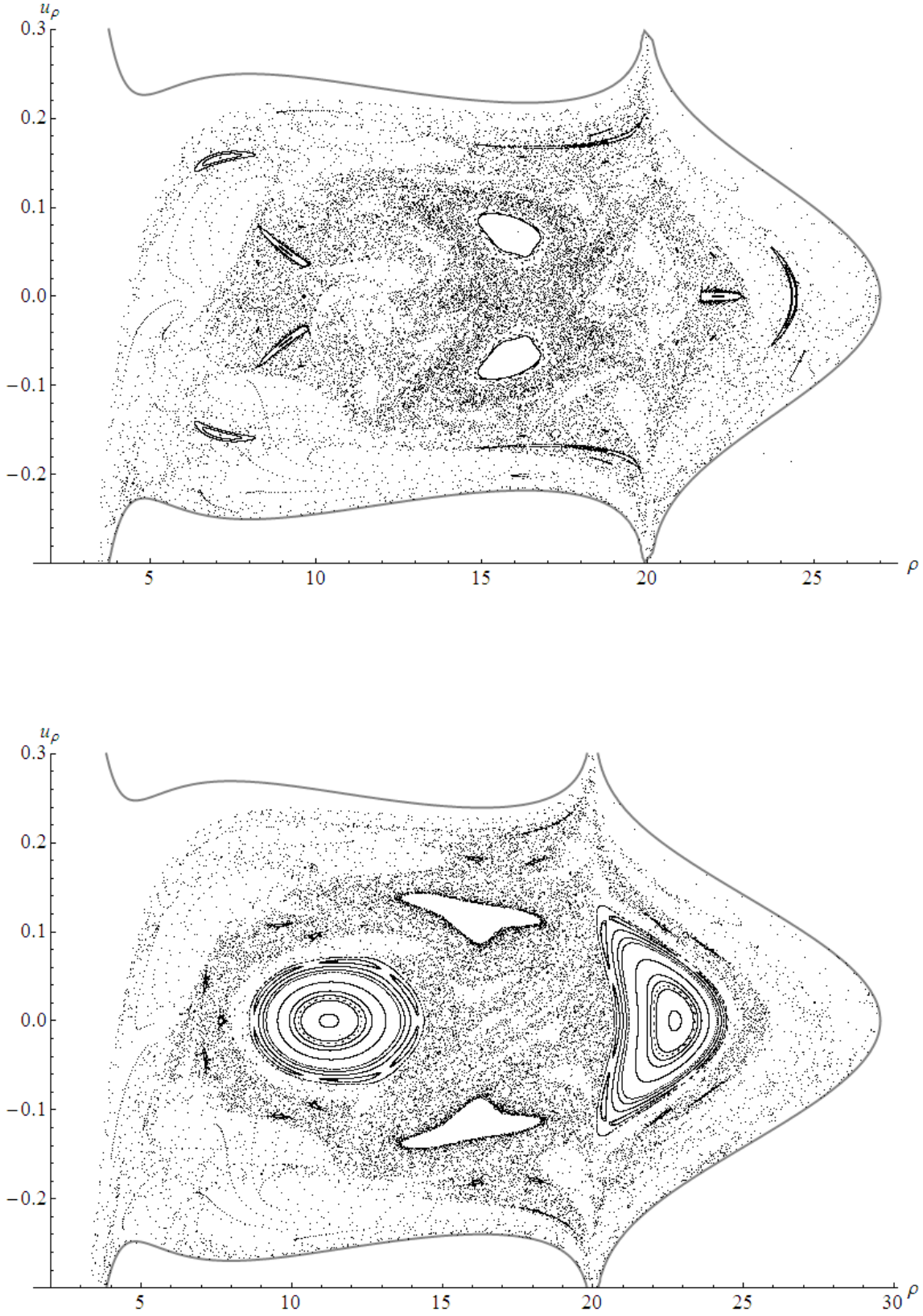

Figure 4.31: Surfaces of section for the BW ring superposition as in figure 4.28 for $\mathcal{E} = -0.055, -0.05$ respectively.

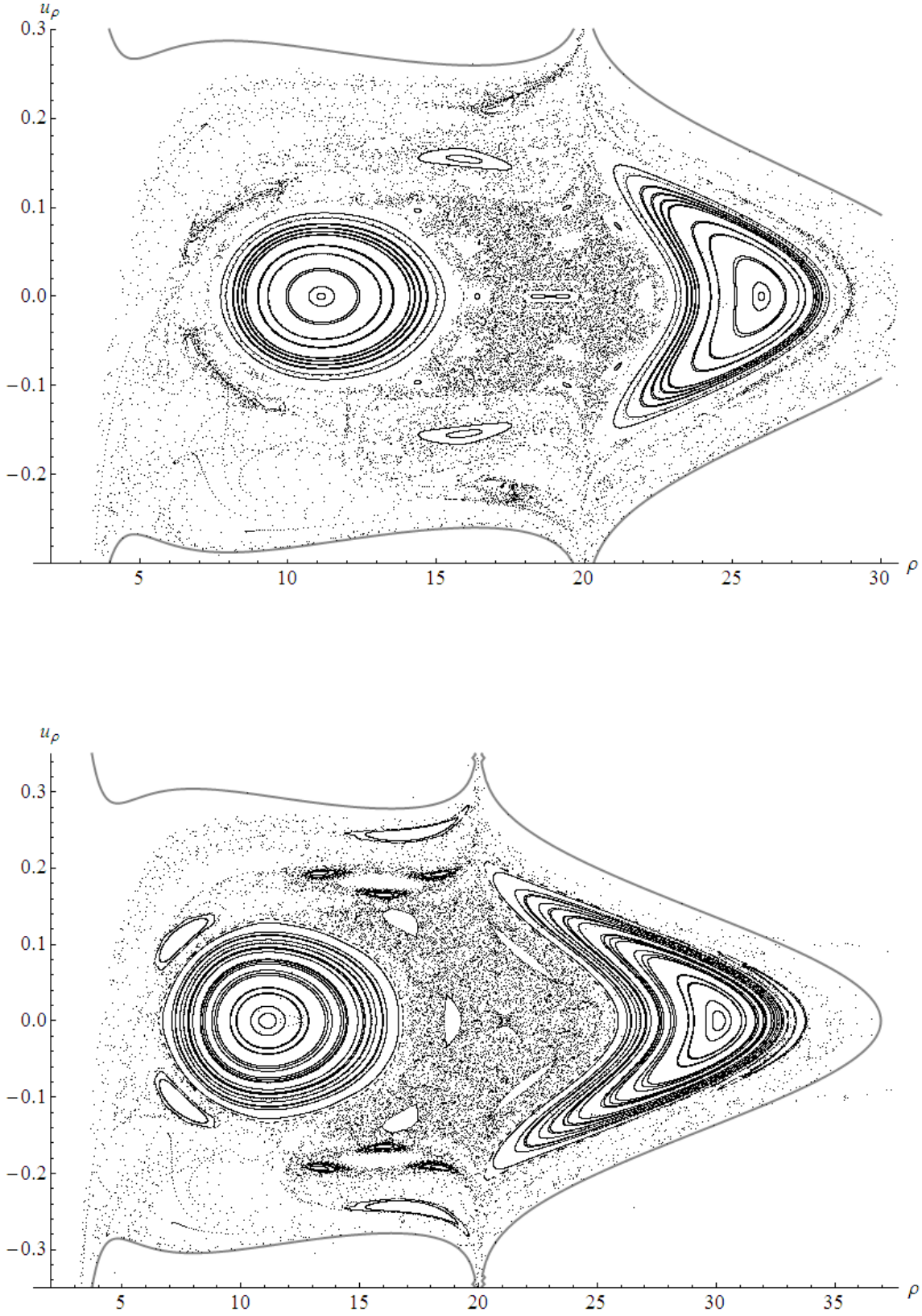

Figure 4.32: Surfaces of section for the BW ring superposition as in figure 4.28 for $\mathcal{E} = -0.045, -0.04$ respectively.

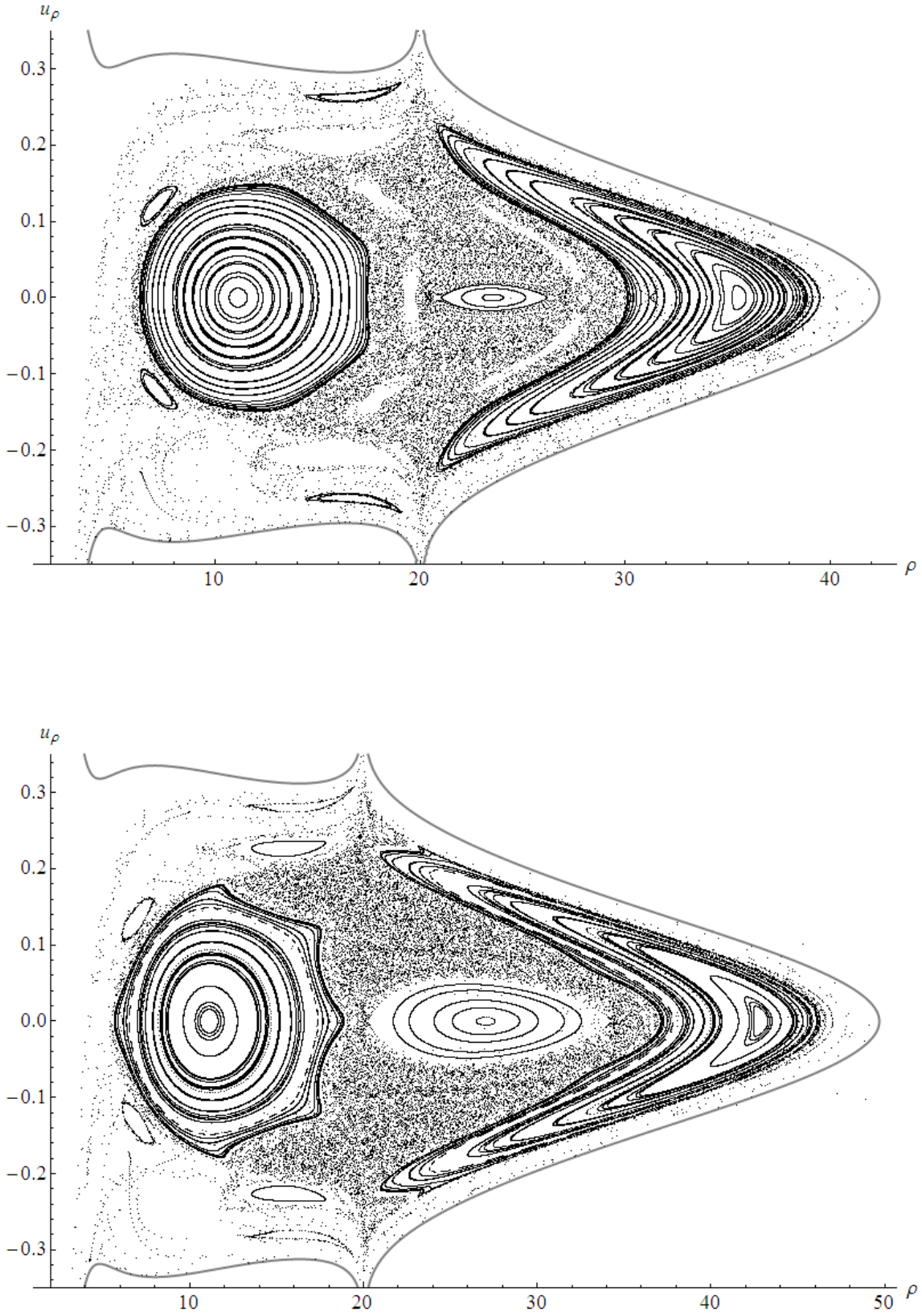

Figure 4.33: Surfaces of section for the BW ring superposition as in figure 4.28 for $\mathcal{E} = -0.035, -0.03$ respectively.

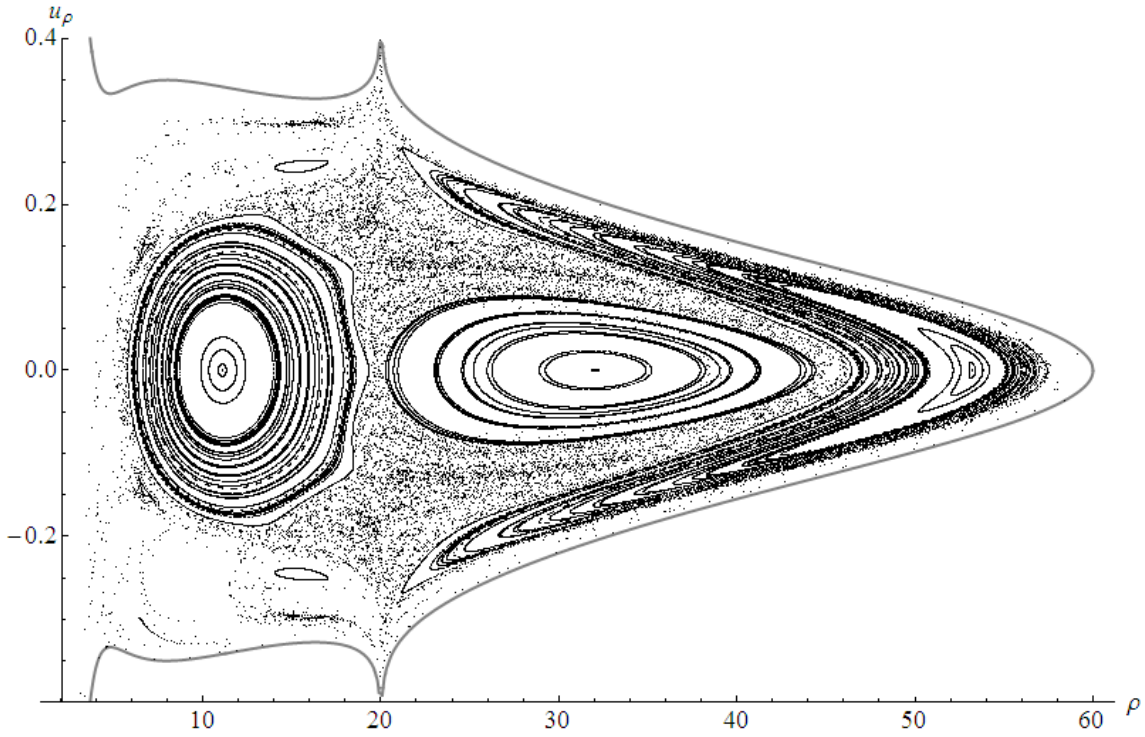

Figure 4.34: Surface of section for the BW ring superposition as in figure 4.28 for $\mathcal{E} = -0.025$.

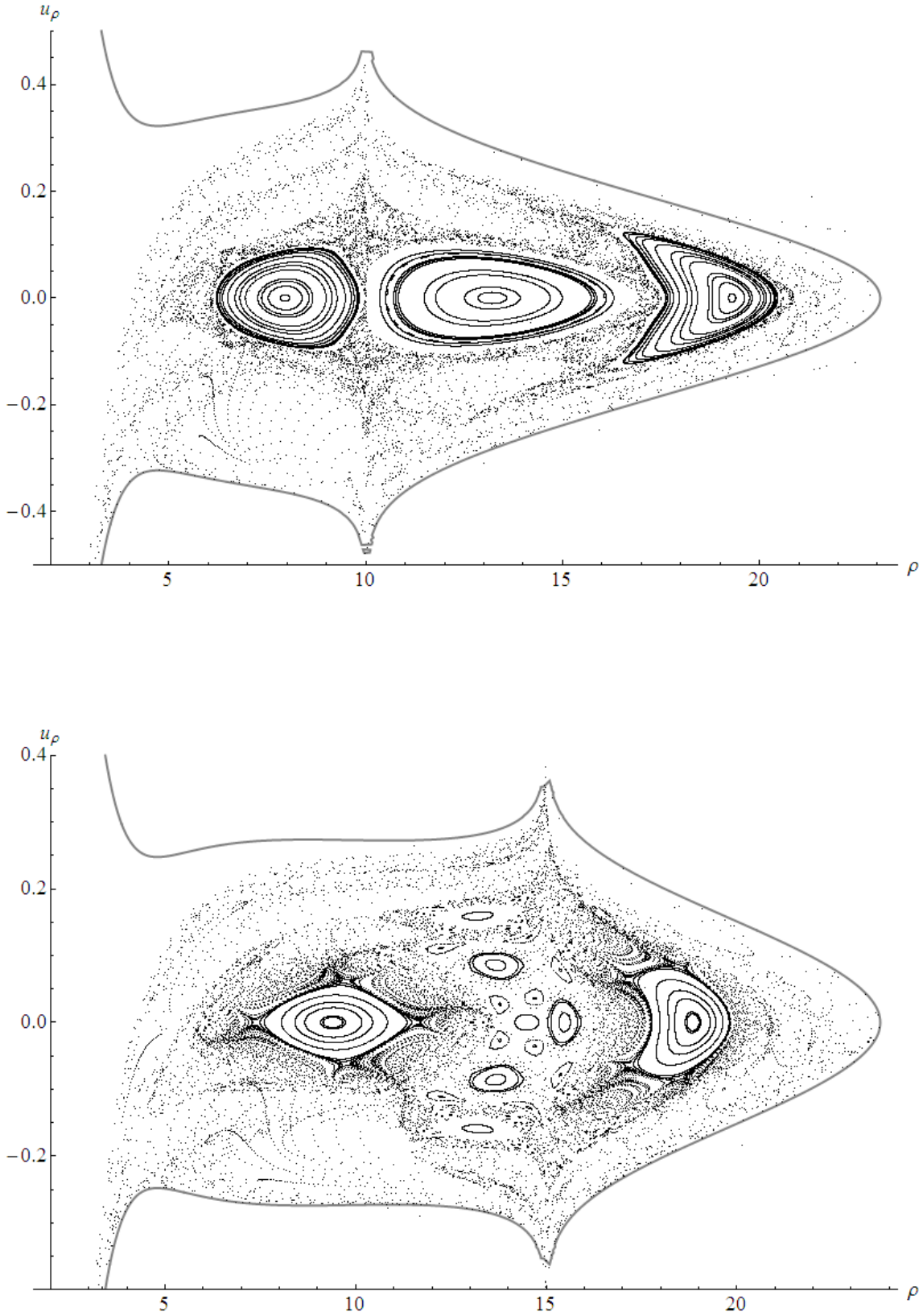

Figure 4.35: Surfaces of section at $z = 0$ for the BW ring superposition with parameter values $\mathcal{M} = 0.5$, $\mathcal{E} = -0.06$, $\ell = 3.75$ and $b = 10$, 15 respectively.

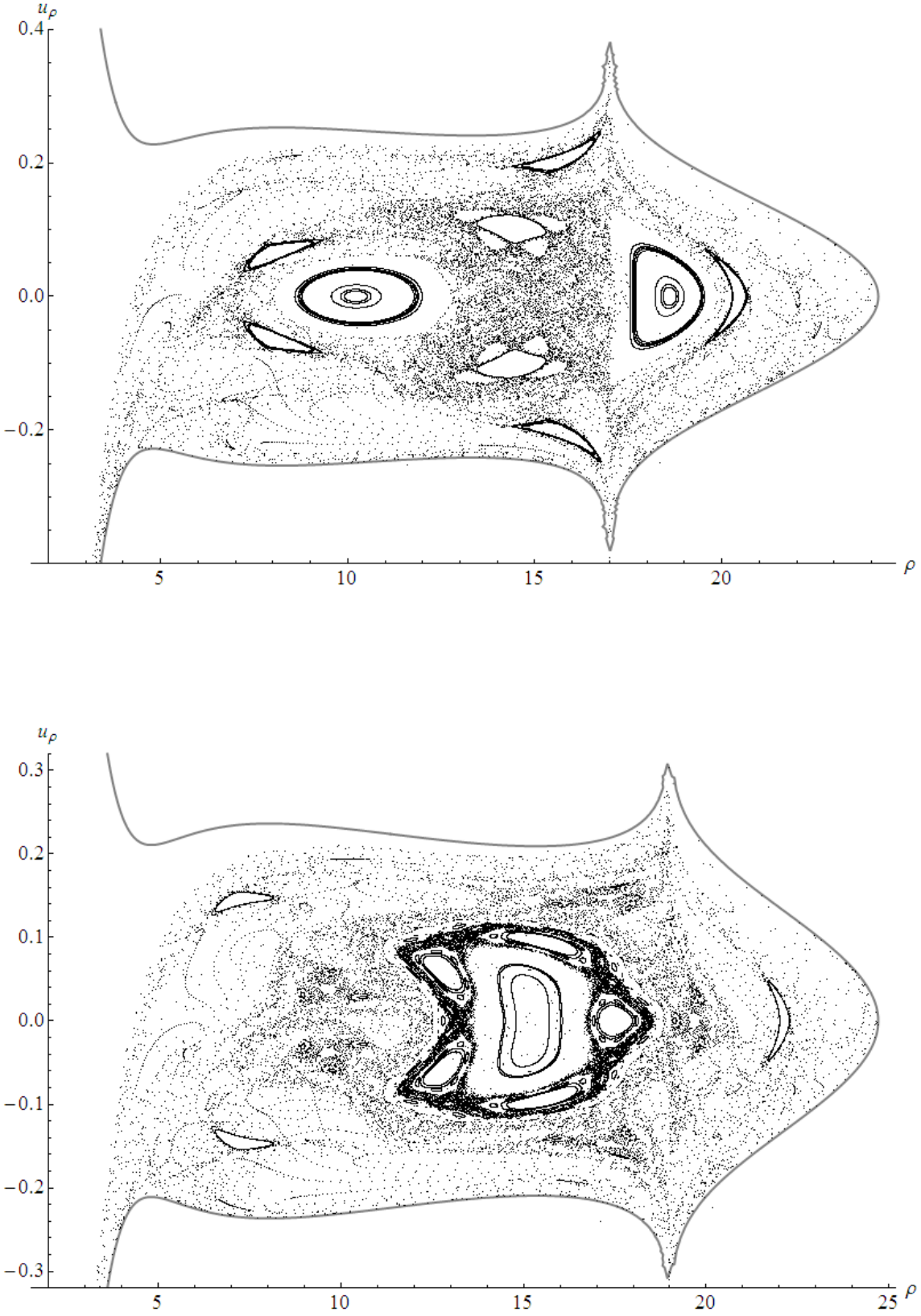

Figure 4.36: Surfaces of section for the BW ring superposition as in figure 4.35 for $b = 17$, 19 respectively.

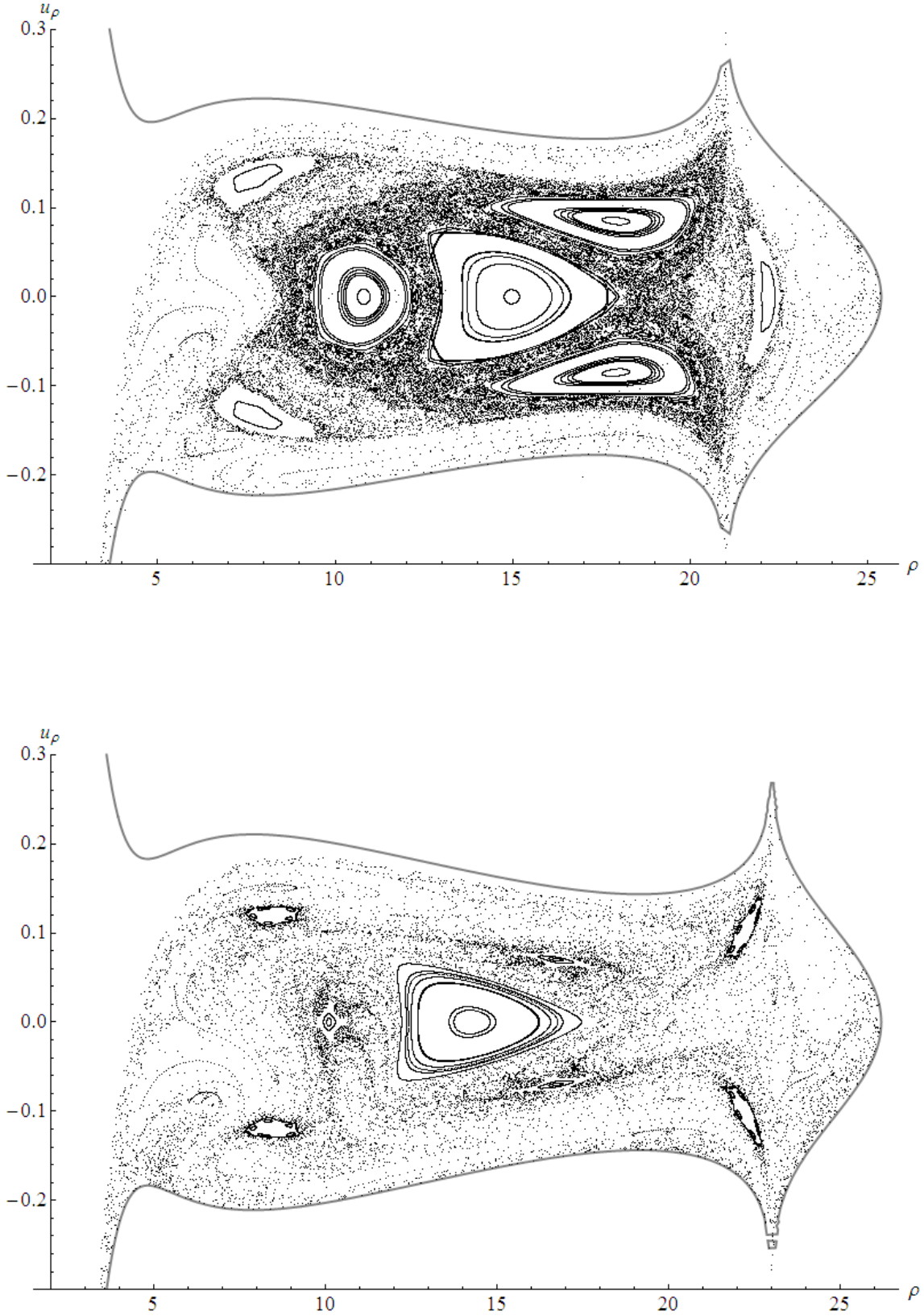

Figure 4.37: Surfaces of section for the BW ring superposition as in figure 4.35 for $b = 21$, 23 respectively.

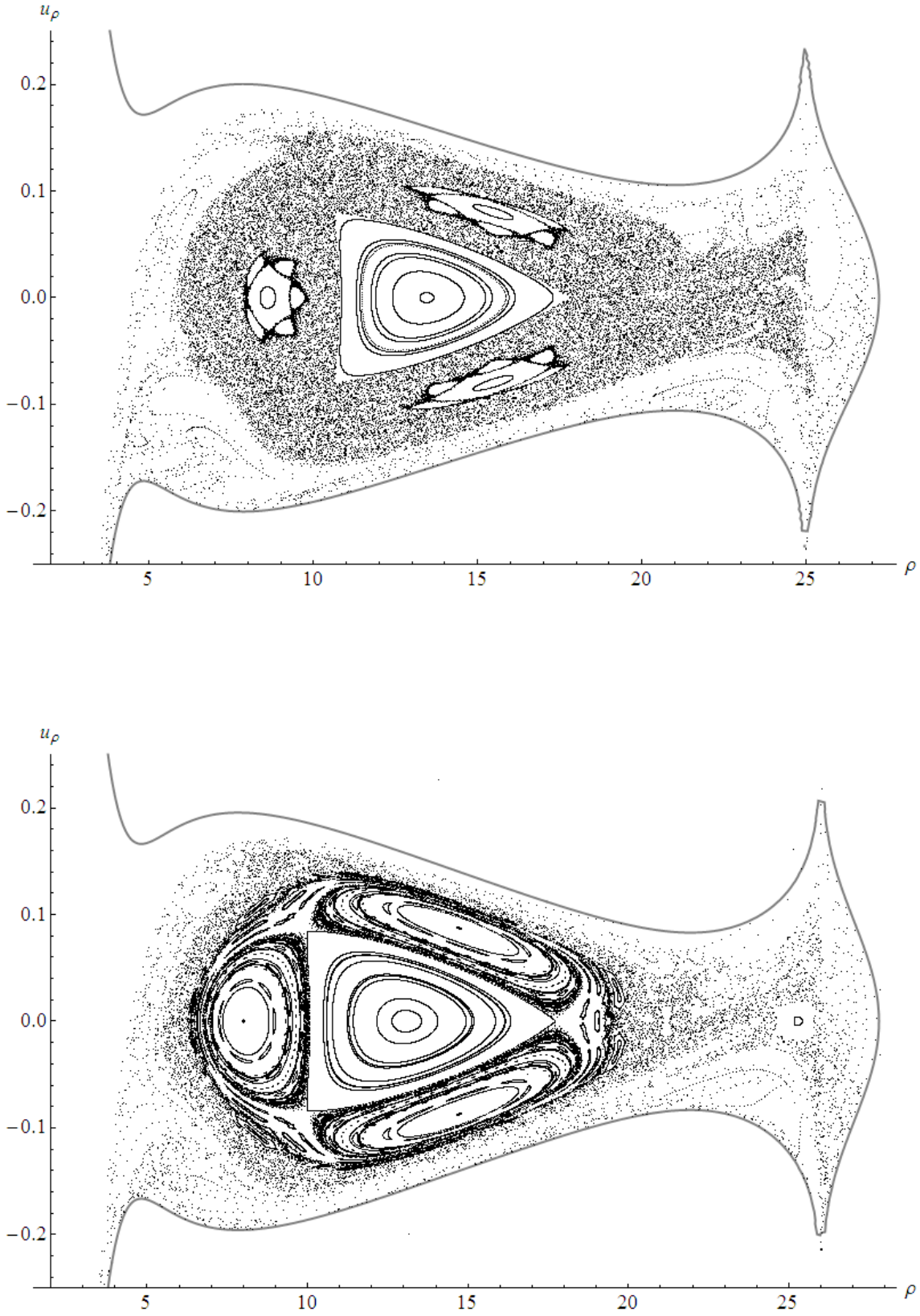

Figure 4.38: Surfaces of section for the BW ring superposition as in figure 4.35 for $b = 25$, 26 respectively.

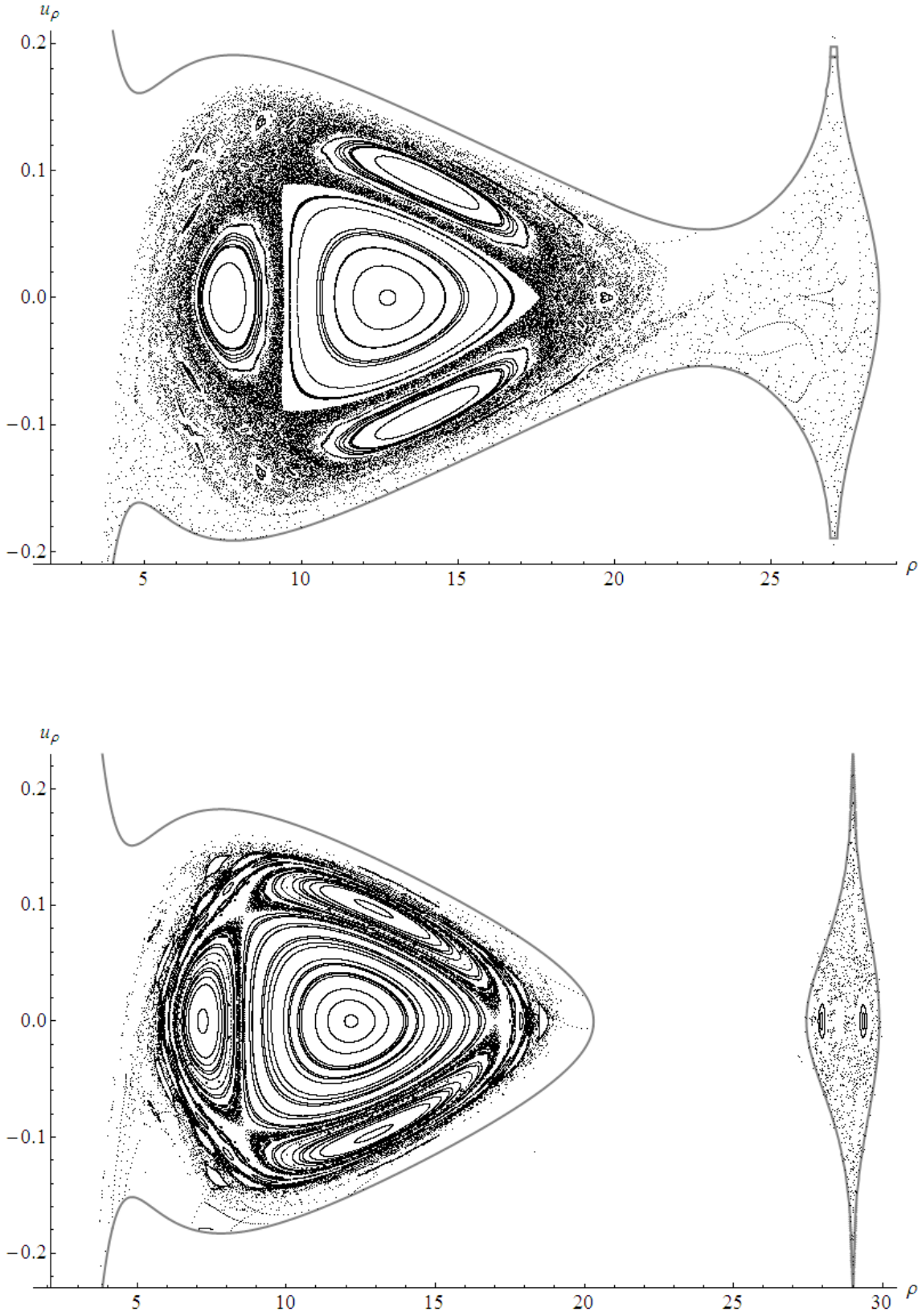

Figure 4.39: Surfaces of section for the BW ring superposition as in figure 4.35 for $b = 27$, 29 respectively.

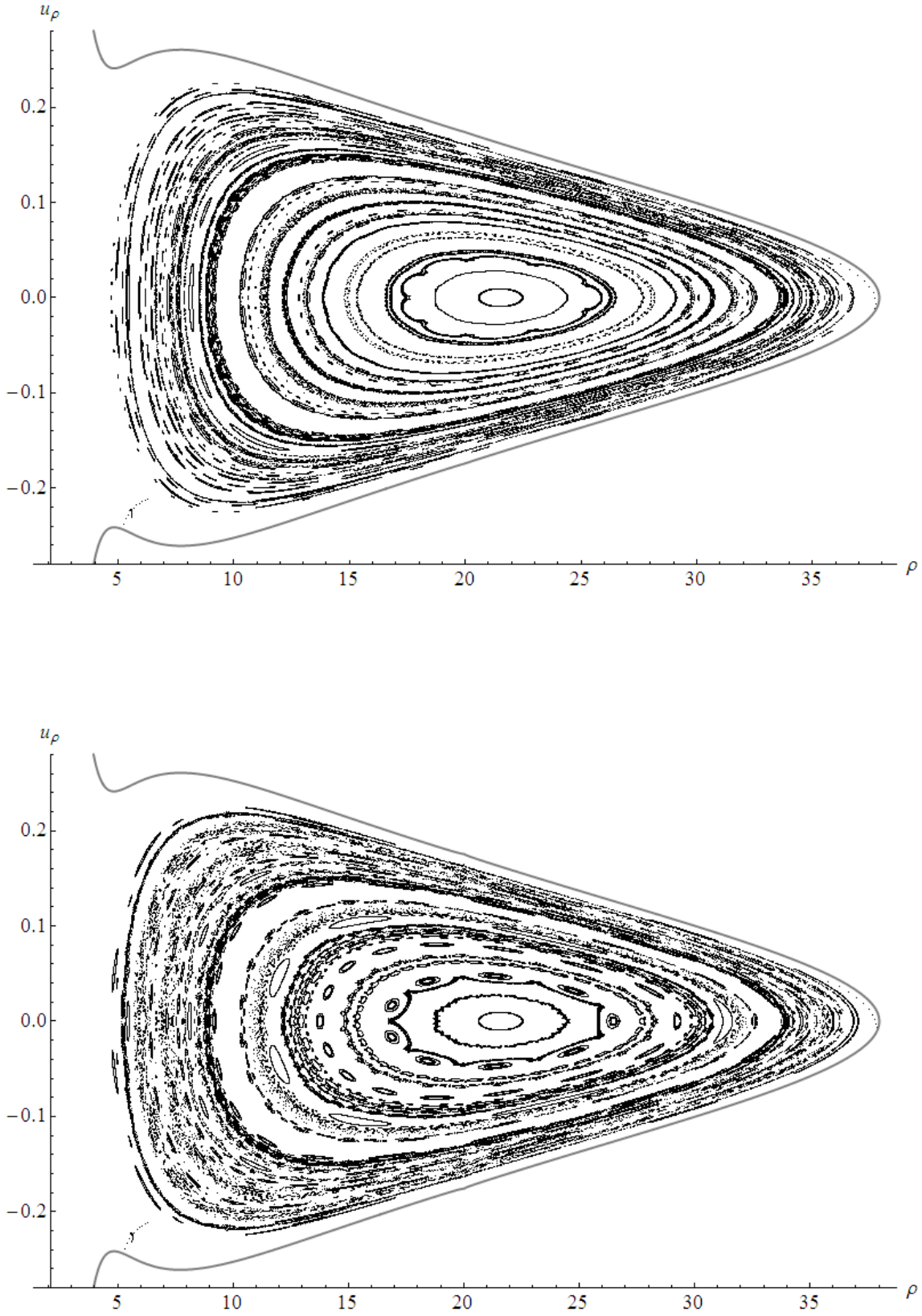

Figure 4.40: Surfaces of section at $z = 0$ for the BW ring superposition with parameter values $b = 20$, $\mathcal{E} = -0.023$, $\ell = 3.75$ and $\mathcal{M} = 0.001$, 0.003 respectively.

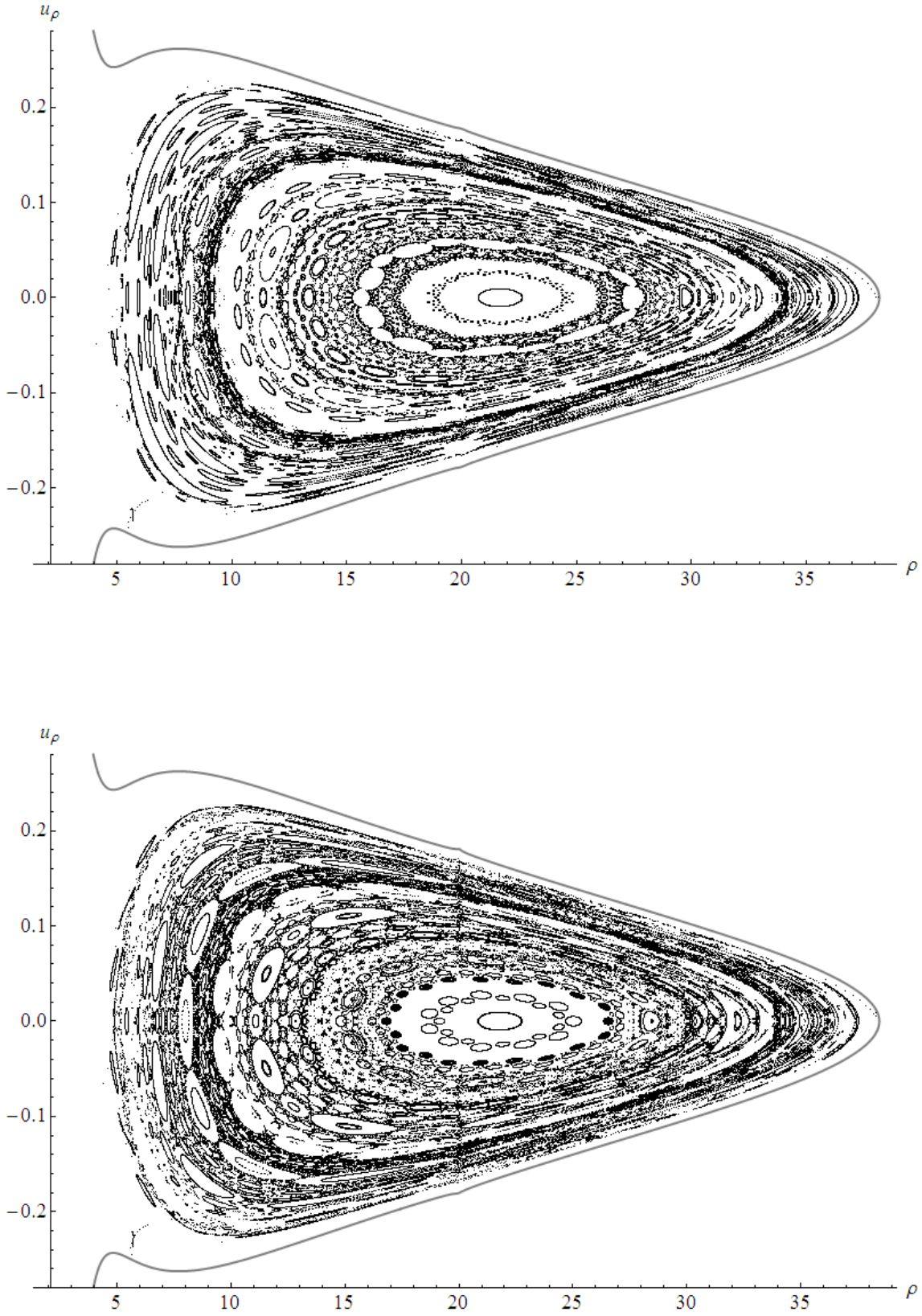

Figure 4.41: Surfaces of section for the BW ring superposition as in figure 4.40 for $\mathcal{M} = 0.006$, 0.01 respectively.

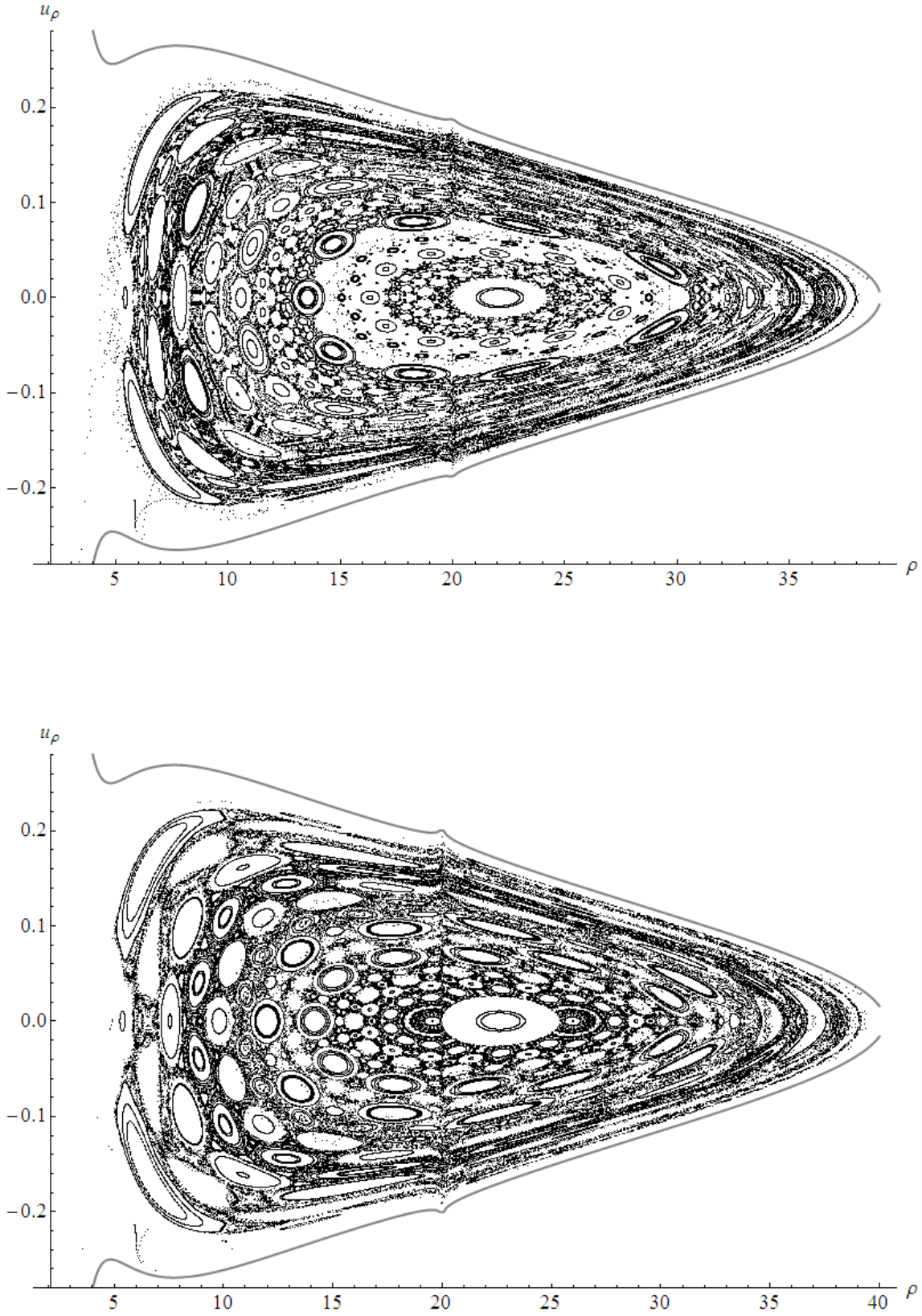

Figure 4.42: Surfaces of section for the BW ring superposition as in figure 4.40 for $\mathcal{M} = 0.02$, 0.04 respectively.

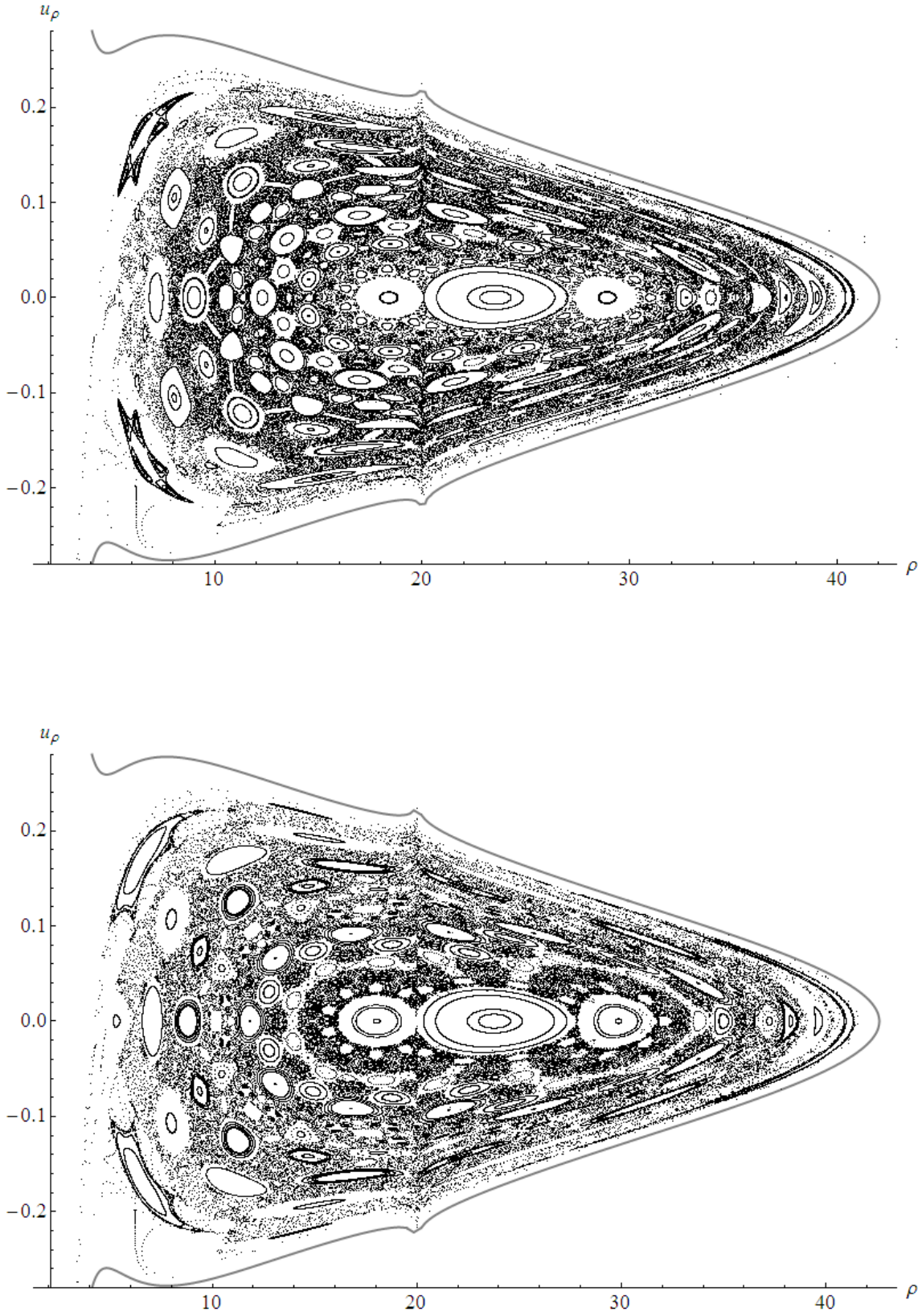

Figure 4.43: Surfaces of section for the BW ring superposition as in figure 4.40 for $\mathcal{M} = 0.07$, 0.08 respectively.

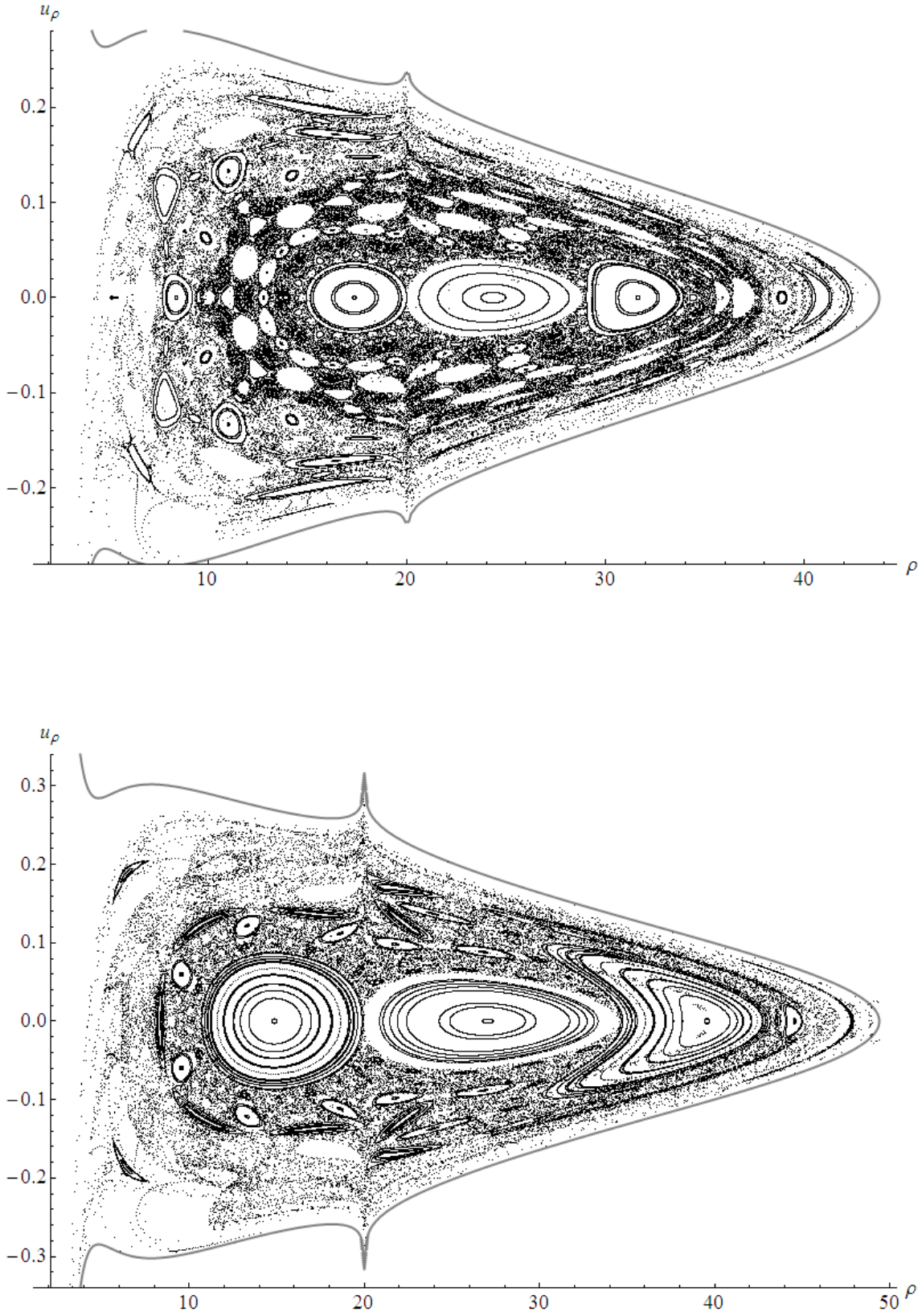

Figure 4.44: Surfaces of section for the BW ring superposition as in figure 4.40 for $\mathcal{M} = 0.1$, 0.2 respectively.

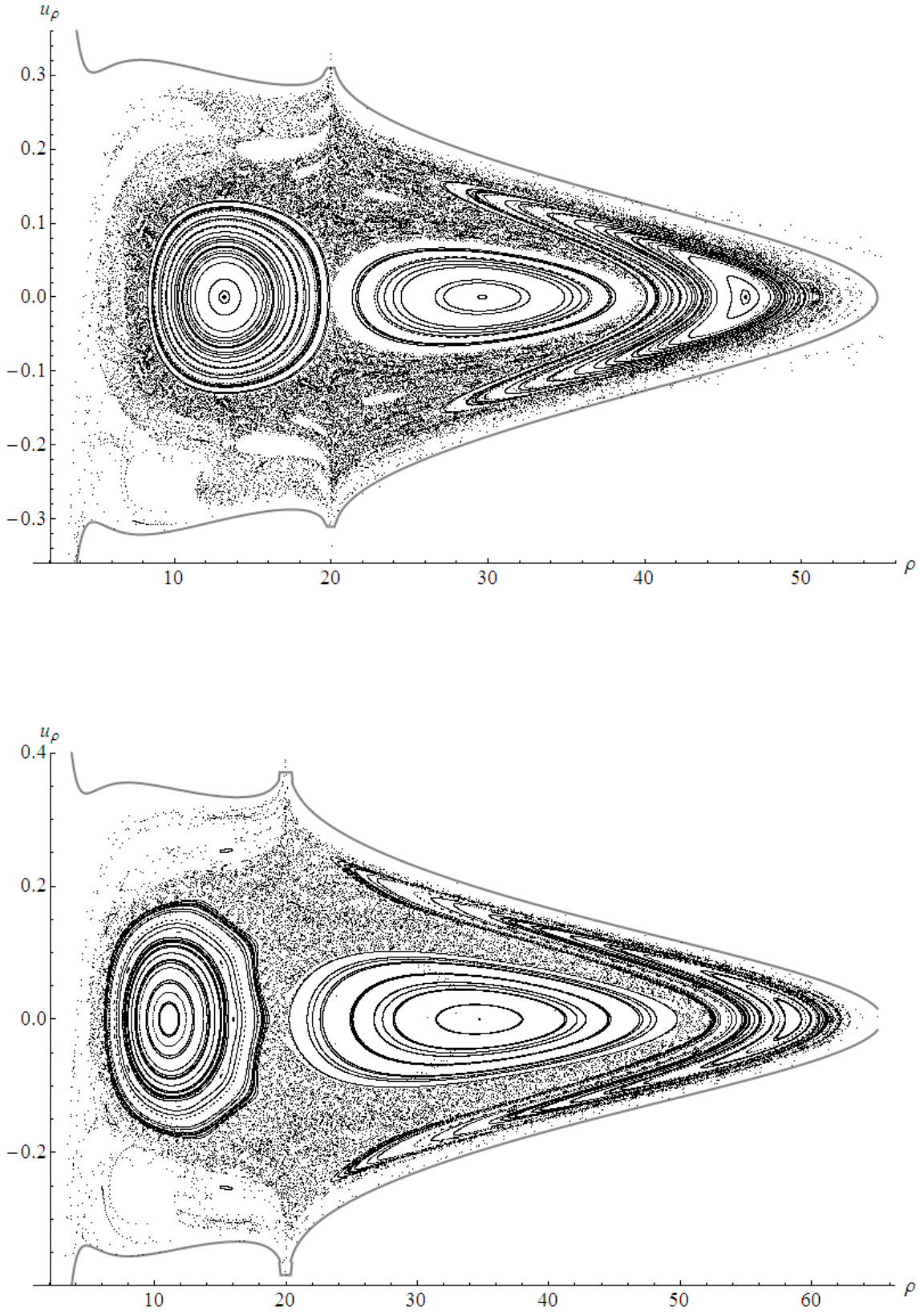

Figure 4.45: Surfaces of section for the BW ring superposition as in figure 4.40 for $\mathcal{M} = 0.3$, 0.5 respectively.

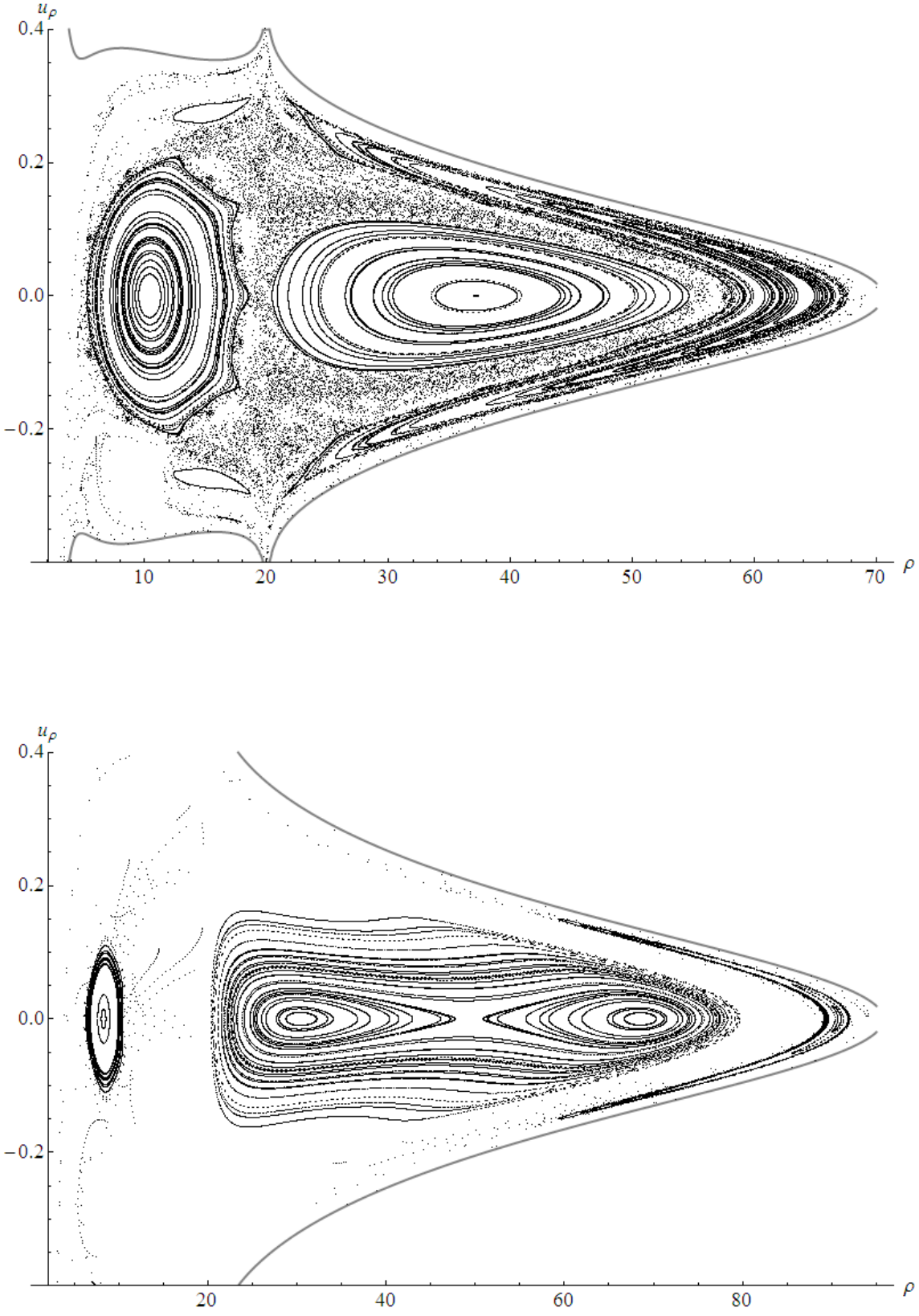

Figure 4.46: Surfaces of section for the BW ring superposition as in figure 4.40 for $\mathcal{M} = 0.6$, 1.1 respectively.

Concluding Remarks

Some of the confidence in the presented results could be undermined by the numerical errors, perhaps the main imperfection of this work. The strength of the chosen symplectic algorithm however ensured that the strongly regular regions are *always* computed at the verge of machine precision ($10^{-12} - 10^{-15}$ relative energy error). Such are for example the centers of major regular islands. Smaller islands and edges of the larger ones on the other hand tend to slightly blur in certain contexts.

An improvement of this bachelor thesis could be a truly systematic study of the dynamics, not only a copy of parameters from Suková (2009) with higher number representation ensuring greater accuracy, and more implementation work invested in the time-derivative fields precise evaluations. It is also a question whether an overly ardent study of fine dynamics in pseudo-Newtonian potentials is truly needed with the relativistic formulations becoming more and more accessible and also required for a full grasp of the astrophysical problems.

An ambitious extension of the work would be an elaborate quantitative comparison of some kind. Developing algorithms tracing the evolution of individual invariant structures seems rather ambitious, but a kind of overall statistical evaluation might be realistic.

Physicists studying Hamiltonian chaos often state the need of "new statistical mechanics" reflecting chaos. In the case of perturbed black-hole fields the scattering into the black-hole with scattering into infinity could present an exotic equilibrium ensemble of "surviving" particles possibly presenting a challenge for the apparatus of classical statistical mechanics.

Nevertheless, we have not given greater attention to the precise dynamics of the phase space under parameter variation such as island spawning, complexification, resonance overlap, stickiness, transport etc. Such a study is of better sense in the context of highly realistic models with physically strongly motivated sets of parameters, or, on the other hand, in the case of numerically very simple toy models allowing a very accurate and detailed study of the general chaotic phenomena.

The conclusion of our study is clear - the motion in pseudo-Newtonian superpositions highly resembles through Poincaré surfaces of section the motion in the fully relativistic formulation. But the most notable failures in the correspondence expose the principal incommensurability of the two theories.

However, most of the correspondence suggests a possible recipe for simplifying Hamiltonian dynamical systems in general. By finding a simpler Hamiltonian which reproduces principal stable and unstable orbits and sets of initial conditions

leading to similar scattering outcomes, we could probably get a dynamical system acting similarly under perturbation in the fashion of the pseudo-Newtonian vs. relativistic correspondence. This is nonetheless a quite unsubstantiated conjecture.

Bibliography

Alligood K., Sauer T., Yorke J., 1996, Chaos: An Introduction to Dynamical Systems, Textbooks in Mathematical Sciences, Springer

Arnol'd V., 1989, Mathematical Methods of Classical Mechanics, Graduate Texts in Mathematics, Springer

Arnol'd V., Kozlov V., Neishtadt A., 1993, Dynamical Systems III: Mathematical Aspects of Classical and Celestial Mechanics, Encyclopaedia of mathematical sciences, Springer-Verlag

Artemova I. V., Björnsson G., Novikov I. D., 1996, Modified Newtonian Potentials for the Description of Relativistic Effects in Accretion Disks around Black Holes, ApJ, 461, 565

Bach R., Weyl H., 2012, Republication of: New solutions to einstein's equations of gravitation. b. explicit determination of static, axially symmetric fields, Gen. Rel. Grav., 44, 817

Benettin G., Galgani L., Giorgilli A., 1980, Further results on universal properties in conservative dynamical systems, Lett. Nuovo Cim. Ser. 2, 29, 163

Birkhoff G. D., 1917, Dynamical systems with two degrees of freedom, Trans. Am. Math. Soc., 18, pp. 199

Blanes S., Moan P. C., 2002, Practical symplectic partitioned runge–kutta and runge–kutta–nyström methods, J. Comput. Appl. Math., 142, 313

Bolsinov A. V., Jovanovic B., 2003, Integrable geodesic flows on Riemannian manifolds: Construction and Obstructions, ArXiv Mathematical Physics e-prints

Bombelli L., Calzetta E., 1992, Chaos around a black hole, Class. Quantum Grav., 9, 2573

Campbell L., Garnett W., 2010, The Life of James Clerk Maxwell: With a Selection from His Correspondence and Occasional Writings and a Sketch of His Contributions to Science, Cambridge Library Collection - Physical Sciences, Cambridge University Press

Contopoulos G., 2010, Order and Chaos in Dynamical Astronomy, Astronomy and Astrophysics Library, Springer

Cvitanović P., Artuso R., Mainieri R., Tanner G., Vattay G., 2012, Chaos: Classical and Quantum, Niels Bohr Institute, Copenhagen, [Stable version 14, Dec 31st, 2012]

Dettmann C. P., Frankel N. E., Cornish N. J., 1995, Chaos and fractals around black holes., Fractals, 3, 161

Gaidashev D., Johnson T., Martens M., 2012, Rigidity for infinitely renormalizable area-preserving maps, ArXiv e-prints

Gleick J., 1997, Chaos: Making a new science, Random House

Grebogi C., Kostelich E., Ott E., Yorke J. A., 1987, Multi-dimensioned intertwined basin boundaries: Basin structure of the kicked double rotor, Physica D, 25, 347

Guckenheimer J., Holmes P., 1990, Nonlinear oscillations, dynamical systems, and bifurcations of vector fields, Applied mathematical sciences, Springer-Verlag

Guéron E., Letelier P. S., 2001, Chaos in pseudo-Newtonian black holes with halos, A&A, 368, 716

Hairer E., 2006, Cambridge University Press

Hairer E., Lubich C., Wanner G., 2006, Geometric Numerical Integration: Structure-Preserving Algorithms for Ordinary Differential Equations, Springer Series in Computational Mathematics, Springer-Verlag Berlin and Heidelberg GmbH & Company KG

Haller G., 1999, Chaos Near Resonance: Methods and Applications, Applied Mathematical Sciences, 138, Springer-Verlag

Helgason S., 1962, Differential geometry and symmetric spaces, Pure and Applied Mathematics, Elsevier Science

Kiuchi K., Koyama H., Maeda K.-I., 2007, Gravitational wave signals from a chaotic system: A point mass with a disk, Phys. Rev. D, 76, 024018

Letelier P. S., Vieira W. M., 1997, Chaos in black holes surrounded by gravitational waves, Class. Quantum Grav., 14, 1249

Lorenz E. N., 1963, Deterministic Nonperiodic Flow., J. Atmosph. Sci., 20, 130

MacKay R., 1987, Hyperbolic cantori have dimension zero, J. Phys. A, 20, L559

MacKay R., Meiss J., Percival I., 1984, Transport in hamiltonian systems, Physica D, 13, 55

Meiss J. D., 1992, Symplectic maps, variational principles, and transport, Rev. Mod. Phys., 64, 795

Montesinos Armijo M., 2012, Review: Accretion Disk Theory, ArXiv e-prints

Morgan T., Morgan L., 1969, The gravitational field of a disk, Phys. Rev., 183, 1097

Novikov I. D., Thorne K. S., 1973, in Black Holes (Les Astres Occlus), Dewitt C., Dewitt B. S., eds., pp. 343–450

Nowak M. A., Wagoner R. V., 1991, Diskoseismology: Probing accretion disks. I - Trapped adiabatic oscillations, ApJ., 378, 656

O'Neill E., 1938, The Complete Greek Drama, vol. 2., Random House, New York

Oseledets V., 2008, Oseledets theorem, Scholarpedia, 3, 1846

Ott E., Sauer T., Yorke J., 1994, Coping with Chaos, Wiley Series in Nonlinear Science, Wiley

Paczyńsky B., Wiita P. J., 1980, Thick accretion disks and supercritical luminosities, A&A, 88, 23

Palmer K. J., 2009, Shadowing lemma for flows, 4, 7918

Podolský J., Kofroň D., 2007, Chaotic motion in Kundt spacetimes, Class. Quantum Grav., 24, 3413

Poincaré H., 1899, Les méthodes nouvelles de la mécanique céleste, Les méthodes nouvelles de la mécanique céleste No. sv. 3, Gauthier-Villars et fils

Saa A., Venegeroles R., 1999, Chaos around the superposition of a black-hole and a thin disk, Phys. Lett. A, 259, 201

Semerák O., Karas V., 1999, Pseudo-Newtonian models of a rotating black hole field, A&A, 343, 325

Semerák O., Suková P., 2010, Free motion around black holes with discs or rings: between integrability and chaos - I, MNRAS, 404, 545

Semerák O., Suková P., 2012, Free motion around black holes with discs or rings: between integrability and chaos - II, MNRAS, 425, 2455

Semerák O., 2004, Exact power-law discs around static black holes, Class. Quantum Grav., 21, 2203

Seyrich J., Lukes-Gerakopoulos G., 2012, Symmetric integrator for nonintegrable Hamiltonian relativistic systems, Phys. Rev. D, 86, 124013

Shakura N. I., Sunyaev R. A., 1973, Black holes in binary systems. Observational appearance., A&A, 24, 337

Silva I. P. C. e., 2010, On the Gannon-Lee singularity theorem in higher dimensions, Class. Quantum Grav., 27, 155016

Smale S., 1967, Differentiable dynamical systems, Bull. Am. Math. Soc., 73, 747

Steklain A. F., Letelier P. S., 2006, Newtonian and pseudo-Newtonian Hill problem, Phys. Lett. A, 352, 398

Stephani H., Kramer D., Maccallum M., Hoenselaers C., Herlt E., 2003, Exact Solutions of Einstein's Field Equations, Cambridge Monographs on Mathematical Physics, Cambridge : Cambridge University Press

Suková P., 2009, Chaotic motion around black holes, Master's thesis, Charles University, Czech republic

Tejeda E., Rosswog S., 2013, An accurate Newtonian description of particle motion around a Schwarzschild black hole, MNRAS

Vieira W. M., Letelier P. S., 1999, Relativistic and Newtonian Core-Shell Models: Analytical and Numerical Results, ApJ, 513, 383

Weyl H., 2012, Republication of: 3. on the theory of gravitation, Gen. Rel. Grav., 44, 779

Wikipedia, 2013, Phase portrait of a simple pendulum

Wu X., Zhang H., 2006, Chaotic Dynamics in a Superposed Weyl Spacetime, ApJ, 652, 1466

Zaslavskii G., 2007, The physics of chaos in Hamiltonian systems, Imperial College Press